THE DEVELOPMENT OF EXOGENOUS ANTICONVULSANTS AND
ENDOGENOUS URACIL-BASED ANTIEPILEPTIC AGENTS

by

Sarah Ward

Submitted in partial fulfillment of the requirements
for the degree of Master of Science

at

Dalhousie University
Halifax, Nova Scotia, Canada
August 2011

DALHOUSIE UNIVERSITY

DEPARTMENT OF CHEMISTRY

The undersigned hereby certify that they have read and recommend to the Faculty of Graduate Studies for acceptance a thesis entitled "THE DEVELOPMENT OF EXOGENOUS ANTICONVULSANTS AND ENDOGENOUS URACIL-BASED ANTIEPILEPTIC AGENTS" by Sarah Ward in partial fulfilment of the requirements for the degree of Master of Science.

Dated: August 19, 2011

Supervisor: _____

Readers: _____

_____

_____

DALHOUSIE UNIVERSITY

DATE: August 19, 2011

AUTHOR: Sarah Ward

TITLE: THE DEVELOPMENT OF EXOGENOUS ANTICONVULSANTS AND
              ENDOGENOUS URACIL-BASED ANTIEPILEPTIC AGENTS

DEPARTMENT OR SCHOOL: Department of Chemistry

DEGREE: MSc   CONVOCATION: October   YEAR: 2011

_____
Signature of Author

DEDICATION

To those who live with epilepsy every day, especially KW—your perseverance and optimism have touched my life in a way I will never forget!

TABLE OF CONTENTS

LIST OF TABLES

LIST OF FIGURES

LIST OF SCHEMES

ABSTRACT

Epilepsy is a common neurological disorder for which the development of new and improved therapies is essential. Thus, the central theme of this thesis pertains to the design and synthesis of putative antiepileptic drugs.

A substructure search was performed on a database of exogenous compounds to find those that contain a known sodium channel pharmacophore. The anticonvulsant activity of several compounds identified by this search was evaluated, resulting in the recognition of multiple molecular classes from which new anticonvulsant scaffolds could be derived.

A series of analogues derived from uracil (an endogenous molecule) were synthesized and evaluated for anticonvulsant activity. Several of these analogues displayed promising activity and minimal toxicity, further supporting the theory that uracils could serve as potent, non-toxic, broad-range antiepileptic drugs capable of targeting both ictogenesis and epileptogenesis. A uracil QSAR model was also developed that could be used in the future to guide further analogue synthesis.

LIST OF ABBREVIATIONS USED

6 Hz	Six-Hertz psychomotor
AED	Antiepileptic drug
ADME	Absorption, distribution, metabolism, and excretion
AIBN	Azoisobutyronitrile
AMPA	γ-amino-3-hydroxy-5-methyl-4-isoxazolepropionate
ASP	Anticonvulsant Screening Project
BBB	Blood-brain barrier
BOM	Benzyloxymethyl
BSA	Bis(trimethylsilyl)acetamide
CBZ	Carbamazepine
CNS	Central nervous system
DBU	1,8-Diazabicyclo[5.4.0]-undec-7-ene
DCM	Dichloromethane
DMF	Dimethylformamide
DMSO	Dimethylsulfoxide
EC_{50}	Half-maximal effective concentration
EtOH	Ethanol
GABA	γ-aminobutyric acid
GAT	GABA transporters
HMDS	1,1,1,3,3,3-hexamethyldisilizane
HTPS	High-throughput screening
IC_{50}	Half-maximal inhibitory concentration

i.p.	Intraperitoneal
MeOH	Methanol
MES	Maximal electroshock
MTM	Methylthiomethyl
NMR	Nuclear magnetic resonance
NOESY	Nuclear Overhauser enhancement spectroscopy
NIH	The National Institutes of Health
NMDA	*N*-Methyl-D-aspartate
PMB	*p*-Methoxybenzyl
PTZ	Pentylenetetraole (or metrazol)
QSAR	Quantitative structure-activity relationship study
SAR	Structure-activity relationship study
ScMET	Subcutaneous metrazol
SE	Status epilepticus
SEM	2-(Trimethylsilyl)ethoxymethyl
SRS	Spontaneous recurrent seizure
SUDEP	Sudden unexpected death in epilepsy
TLC	Thin layer chromatography
TMS	Tetramethylsilane
TMSCl	Trimethylsilyl chloride
UPG	Uracil protecting-group
UV	Ultraviolet
VPA	Valproic acid

ACKNOWLEDGEMENTS

This thesis would not have been possible without the help and support of many individuals. I am extremely grateful to all of my colleagues, friends, and family for everything they have done.

First and foremost, I would like to thank my supervisor, Dr. Don Weaver, for providing me with an incredibly interesting and meaningful research topic. His knowledge and advice have been essential for the completion of this project, and his humour and enthusiasm have made for a memorable, entertaining, and enjoyable experience. I feel very fortunate to have worked with such a dedicated researcher and physician.

Secondly, I would like to express my gratitude to all of the members of the Weaver research group, especially Mark, Fan, Shengguo, Arun, Chris, Gord, Katharine, Erin, Autumn, Felix, Rose, Karla, and Maneesha; their input and assistance has contributed greatly to my research, and I will never forget their kindness and friendship.

Furthermore, I would like to acknowledge Dr. Xaio Feng for providing mass spectrometry data, Dr. Stanley Cameron for his x-ray crystallographic analyses, NIH for conducting all in vivo biological testing, and ChanTest for running in vitro sodium channel binding assays. I would also like to thank NSERC and Dalhousie University for funding.

Lastly I want to express my gratitude to my family and friends for their love, encouragement, and unwavering confidence in my abilities.

Thank you all very much!

Chapter 1: Introduction

1.1   Epilepsy Overview

1.1.1   The Definition and Etymology of Epilepsy

Epilepsy is regarded as a symptom of pathological excitatory processes in the brain, rather than a disease in itself, and is commonly defined as a group of chronic neurological disorders characterized by recurrent and unprovoked seizures [1]. The word "epilepsy" is derived from the Greek prefix *epi*, meaning "upon", and the Greek verb *labein*, meaning "to take", "to grasp" or "to seize". Therefore, *epilepsy* literally means "to be seized" or "to be taken hold of", demonstrating the once-popular belief that seizures were a form of demonic possession or punishment from the Gods [2].

1.1.2   Nervous Tissue and the Pathology of Epilepsy

The underlying pathology of epilepsy involves aberrant hyperexcitability of cells in the central nervous system (CNS). Therefore, an understanding of epilepsy at the cellular level requires a basic knowledge of the anatomy and physiology of nervous tissue.

The CNS, which consists of the spinal cord and brain, is protected by the blood-brain barrier (BBB)—a layer of tightly connected endothelial cells that surround the capillaries in the CNS. This barrier serves as a filter, preventing unwanted material found in the circulating blood from contaminating the cerebrospinal fluid. Individual nerve cells, known as neurons, are some of the longest cells in the human body and are responsible for transmitting information throughout the body. In the CNS, nerve cells process sensory data and coordinate appropriate motor responses. Neurons vary in shape

and structure, but typically consist of a large cell body with numerous branching projections called dendrites, and a long slender projection called an axon (figure 1). While dendrites are responsible for receiving information, the axon relays information on to other cells by sending electrical impulses down its length. These electric pulses—also referred to as action potentials—occur as a propagating change in the neuron's transmembrane potential, which is created by an electrochemical gradient and the movement of ions across the cell membrane [3].
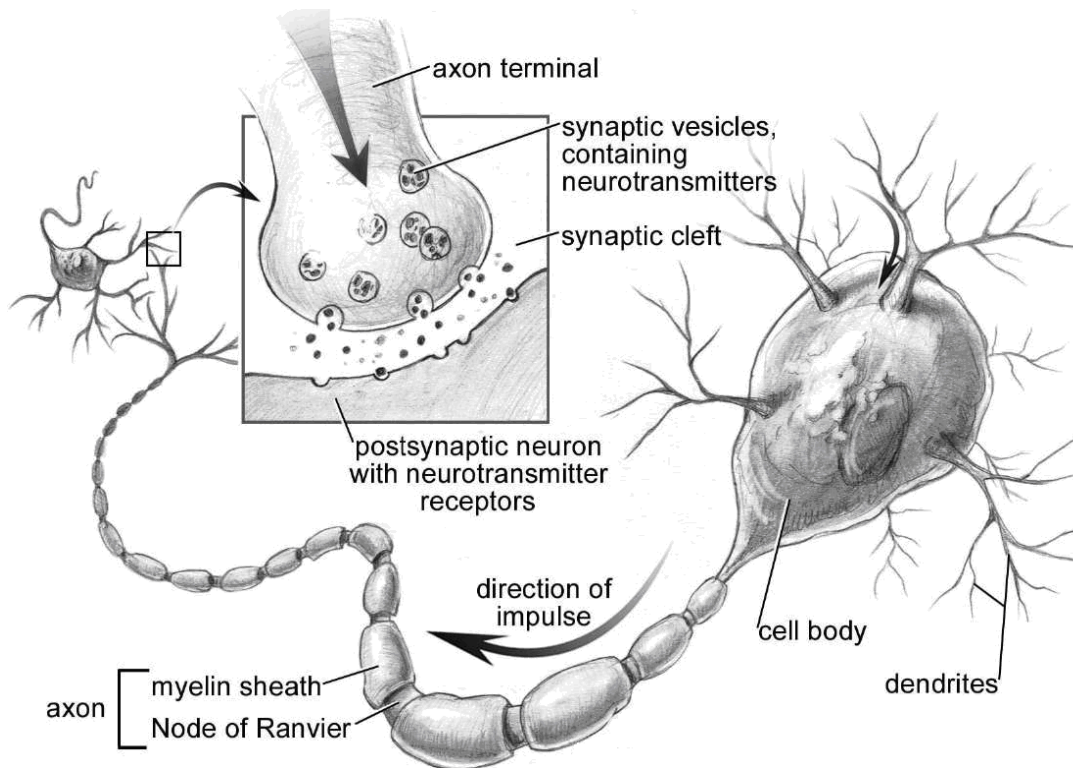
Figure 1: The neuron and the chemical synapse [4]

The junction where a neuron passes a signal on to another cell is called a synapse (figure 1). In a chemical synapse, the arrival of an action potential from the presynaptic neuron triggers the release of chemical messengers known as neurotransmitters into the synaptic cleft. After the neurotransmitters interact with the postsynaptic cell to elicit the desired response, they are then broken down by degradative enzymes, or taken back up

by the synaptic terminal and stored until the arrival of a subsequent action potential. Depending on the type of receptor in the postsynaptic cell, a neurotransmitter can have either an excitatory or inhibitory effect [3].

A seizure results when neurons in the brain fire abnormally or excessively. The initiation and dissemination of a seizure, or "ictogenesis" [5], is triggered by neurons that are susceptible to paroxysmal electrical activity. Collections of these hyperexcitable neurons, called epileptic foci, are found primarily in the cerebral cortex (figure 2).
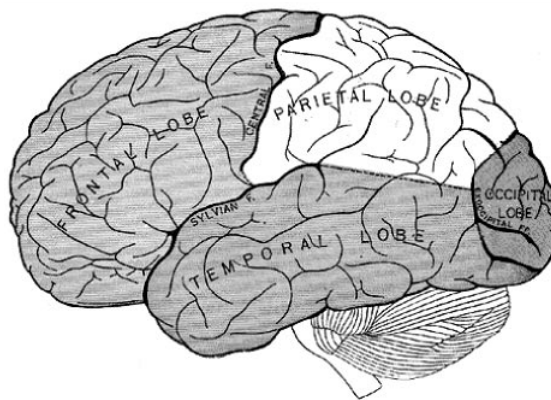
Figure 2: Lobes of the cerebral cortex [6]

Epileptic foci can be localized to one area of the cortex or part of an interconnected epileptic web involving larger portions of the brain. When seizure foci become hyper-excited, the aberrant electrical activity may stay confined to the site of origin, or it can spread outward to neighbouring neurons and affect other areas of the brain. While seizures can originate from the frontal, occipital, and parietal lobes of the cortex, temporal lobe epilepsy is the most common form of the disorder, occurring in 40-60 % of patients with epilepsy [7]. One can graphically record epileptic neuronal activity in an electroencephalogram by placing electrodes on the outer surface of the skull or directly on the brain.

1.1.3 Seizure Types

The physical manifestation of a seizure varies widely, depending on the extent of the cortex involved and the neuroanatomical region affected; consciousness may or may not be lost, muscles may lose their tone or contract in a variety of ways, and symptoms such as hallucinations, false emotions, or uncontrolled vocalizations may occur. Due to their complicated nature, seizures are difficult to categorize, but the generally accepted classification system (the International Classification of Epileptic Seizures) states that there are three broad types: partial seizures, generalized seizures, and unclassified epileptic seizures [8, 9].

1.1.3.1 Partial Seizures

Partial seizures, also known as focal or local seizures, arise when ictogenesis is restricted to part of one cerebral hemisphere. Based on whether or not consciousness is maintained, partial seizures can be subdivided into two groups: simple partial seizures and complex partial seizures. In simple partial seizures, consciousness is not impaired and a variety of motor signs (e.g., twitching, an arrest of speech), special-sensory symptoms (e.g., tingling sensations, buzzing noises), autonomic symptoms (e.g., sweating, flushing), and psychic symptoms (e.g, distortion of time, déjà-vu) may be experienced. In contrast, complex partial seizures do involve an impairment of consciousness. They are often accompanied by various psychomotor automatisms (e.g., picking at clothing, walking, chewing) and can have simple partial onset. Both simple and complex partial seizures are capable of evolving to secondarily generalized seizures.

1.1.3.2   Generalized Seizures

Generalized seizures arise when ictogenesis involves both cerebral hemispheres, and as a result, they are often accompanied by an impairment of consciousness. There are six subtypes of generalized seizures: absence, myoclonic, clonic, tonic, tonic-clonic, and atonic (astatic) seizures. A combination of these generalized seizure-types can occur during any given epileptic episode.

Absence seizures are characterized by a brief spell of decreased responsiveness or altered consciousness, typically lasting from 5-10 seconds. Clinical manifestations often include a blank facial expression, rhythmic eye blinking or other automatisms, increased or decreased postural tone and other mild motor symptoms, or various autonomic symptoms. Absence seizures can be further broken down into typical and atypical absence seizures. In comparison to typical absence seizures, atypical absence seizures have more pronounced motor symptoms, a less intense suppression of mental functions, and an onset and/or cessation that is not as sudden.

Myoclonic seizures involve sudden involuntary muscle contractions. These myoclonic jerks most often affect the flexor muscles of the upper extremities. Consciousness is normally maintained.

Clonic seizures consist of a more prolonged and rapidly successive myoclonus. These spasms are often asymmetric, but the entire body may be involved. Consciousness is lost.

Tonic seizures are characterized by an abrupt increase in muscle tone, resulting in a stiffening of the body, as well as flexion or extension of the extremities. Consciousness is usually impaired during the episode. Recovery may be swift or involve a prolonged state of disorientation or coma.

Generalized tonic-clonic seizures, also known as grand mal seizures, are the most recognizable of all seizure types, and the most severe. Tonic-clonic seizures begin with a complete loss of consciousness, followed by a tonic phase (rigid stretching and contorting) and then a clonic phase (rhythmic convulsions), and ultimately end in a state of flaccidity. Incontinence may occur during the event, as well as various autonomic symptoms, including perspiration, salivation, and increased blood pressure. Patients typically awake from the episode in a confused and drowsy state that lasts for minutes or hours, and often suffer from postictal headaches or muscle aches.

Atonic seizures involve a loss of muscle tone, which is often preceded by a subtle or severe myoclonic jerk. Patients do not lose consciousness, but they will fall to the ground if standing, as the lack of body tone causes a buckling of the knees and the slumping forward of the head and trunk.

1.1.3.3 Unclassified Epileptic Seizures and Status Epilepticus

Unclassified epileptic seizures are those that cannot be identified because they defy the accepted classification system. Although not every epileptic seizure can be placed into an appropriate category, unclassifiable seizures are relatively rare, accounting for less than 1.5% of seizures [10].

It should be noted that when a patient experiences prolonged seizure activity, he or she is said to have entered a state of status epilepticus (SE). By definition, one has entered SE after 30 mintutes or more of continuous seizure activity or consecutive seizure activity without recovery between attacks [11]. However, a seizure that has not ceased after 5 minutes is treated as SE, and is considered a medical emergency because prolonged aberrant neuronal firing can lead to significant brain damage or death [12].

Although SE most frequently arises from generalized tonic-clonic seizures, any seizure type—even those that are non-epileptic—can lead to SE.

1.1.4 Causes of Epilepsy

The cause of epilepsy is unknown in over half of afflicted patients, and the underlying mechanisms of the development of epilepsy—a process referred to as epileptogenesis—have yet to be clearly identified. However, the generation of seizure disorders in humans has been connected to various phenomena.

Any event that triggers acute convulsions may lead to the development of epilepsy if status epilepticus is attained, as prolonged seizure activity can result in brain damage that may lead to abnormal epileptic firing patterns. For instance, several illicit drugs, including cocaine and phencyclidine (PCP), can trigger major seizures and may lead to the development of epilepsy. Metabolic abnormalities, such as hyperglycemia, hypoglycemia, hypocalcemia or hypomagnesemia, are also capable of inducing convulsions. Thus, etiologies of epilepsy can include kidney failure, chronic alcoholism, diabetes mellitus, and many other medical conditions.

Cerebral palsy and a number of neurodegenerative diseases, such as Sturge-Weber syndrome, are frequently accompanied by epileptic seizures. Individuals who have had cerebrovascular complications, such as cerebral anoxia or stroke, can develop recurrent seizures as a result of compromised blood flow in the brain. Brain tumors and other intracranial lesions are a common cause of chronic seizure disorders in individuals aged 20 years or older. One of the leading causes of epilepsy in all age groups is CNS infection.

Finally, it has been shown that one can be genetically predisposed to acquiring epilepsy, which may account for why many of the aforementioned causes only lead to the development of the disorder in some cases. To date, eleven human epilepsy genes have been discovered [13], including various ion channel and neurotransmitter gene mutations [14].

1.2 Antiepileptic Drug Discovery

1.2.1 The History of Anticonvulsant Drug Discovery

Throughout the years, antiepileptic drug (AED) discovery has progressed from centuries of ignorance and ineffective treatments, to a period of discovery by serendipity and random screening, and finally, to the modern era of rational drug design.

Prior to the mid 1800s, effective anticonvulsant treatment was virtually nonexistent. Although the link between head trauma and epilepsy was recognized in ancient times, as well as the role of heredity, it was still commonly thought that seizures were caused by supernatural forces. Thus, epileptic disorders were treated using fairly ludicrous "remedies", such as purgatives, enemas, gladiator blood, dog urine, or human bile [15, 16].

The first genuine anticonvulsant, potassium bromide, was serendipitously discovered in 1857. At this time, it was thought that excessive sexuality was the cause of catamenial epilepsy, a seizure disorder linked to the menstrual cycle. Sir Charles Locock, obstetrician to Queen Victoria, attempted to diminish the libido of a group of epileptic patients by administering potassium bromide, which was known for its hypnotic effects. Although Locock's rationale was incorrect, bromide solutions were effective in preventing seizures. Consequently, the inorganic bromides became the primary

antiepileptic therapy for the next 55 years, despite their tendency to cause dermatitis and psychosis. Due to their high toxicity, the bromides are generally not used today, although they are still occasionally prescribed in certain cases of porphyria [17].

In 1912, Alfred Hauptmann accidentally discovered the anticonvulsant activity of phenobarbital, a barbiturate already on the market as a sedative. During his residency in psychiatry, Hauptmann was often kept awake at night by the epileptic attacks of nearby patients. In hopes of keeping them quiet while he slept, he gave the drug to the patients as a tranquilizer and observed that the frequency of their seizures was significantly reduced, even throughout the following day. Due to its higher efficacy and lower toxicity, phenobarbital quickly replaced bromide therapy, becoming the first known organic, small-molecule AED [18].
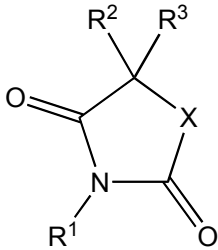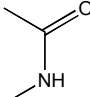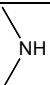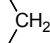
The next major breakthrough in the history of antiepileptic drug discovery occurred in the late 1930s when Putnam and Merritt successfully employed random screening to find a non-sedative anticonvulsant. Knowing that phenobarbital—the only barbiturate with anti-seizure activity—contained a phenyl group, Putnam and Merritt tested an assortment of phenyl-containing compounds in an electroshock-induced cat model of epilepsy. This lead to the identification of phenytoin, a hydantoin with high anti-ictogenic activity and fairly low toxicity [17].

Putnam and Merritt's achievement revealed that animal models of epilepsy could be used to find putative AEDs and prompted an increased focus on research in this area. In vivo screening experiments permitted the discovery of several new anti-seizure agents, including the oxazolidinedione known as trimethadione. Trimethadione, an anti-absence medication, was introduced in 1946 as the first anticonvulsant specific for the treatment

9

of one seizure type [19]. In search of a less toxic alternative to trimethadione, a major

screening of succinimides was conducted, resulting in the release of phensuximide and

methsuximide, as well as today's drug of choice for the prevention of absence seizures:

ethosuximide.

The organic anticonvulsant classes mentioned thus far—the barbiturates,

hydantoins, oxazolidinediones, and succinimides—all contain a common structural

feature: the cyclic ureide moiety, as shown in table 1:

Table 1: Molecular classes containing the cyclic ureide moiety

Cyclic Ureide Moiety	—X—	Molecular Class
		Barbiturates
		Hydantoins
		Oxazolidinediones
		Succinimides

The cyclic ureides were the most prevalent form of antiepileptic medication until the mid

1960s. At this point, the search for additional AEDs of this type was becoming

exhausted; in fact, ethosuximide was the last of the cyclic ureides to ever be put on the

market in the United States [17]. Fortunately, however, luck prevailed again when the

anti-seizure properties of valproic acid (VPA), carbamazepine (CBZ), and the

benzodiazepines were discovered. VPA was identified in 1963, when Pierre Eymard, a

research student at the University of Lyon, had a series of khellin and coumarin

analogues screened for anticonvulsant activity. Due to their insoluble nature, the

compounds were dissolved in VPA prior to evaluation. When all of Eymard's compounds

seemed to display activity, the connection to the solvent was made. The sodium salt of VPA then underwent clinical testing and was marketed as early as 1967 in some countries. The benzodiazepines (such as diazepam or clonazepam) and CBZ were both originally investigated as putative therapeutics for psychosis, but were later identified as anticonvulsants when subjected to random screening [18].

VPA, CBZ, the benzodiazepines, and the cyclic ureides are collectively referred to as the "first generation" drugs [20]. Despite their serendipitous discovery, many of these drugs are still regularly used today. Indeed, the most commonly prescribed AED worldwide is phenobarbital [21], and phenytoin is the most frequently used AED in the United States [18]. The discovery and study of the first-generation anticonvulsants greatly improved our understanding of epilepsy at the molecular level, and ultimately led to the modern and more strategic approach of rational antiepileptic drug design.

Although much still remains unknown, our insight into the pathological mechanisms of ictogenesis and our knowledge of drug-receptor interactions has permitted the development of several new anticonvulsants. The past three decades have seen the introduction of over 15 AEDs, including two carbamazepine-like compounds (oxcarbazepine and eslicarbazepine acetate), as well as a number of drugs belonging to novel anticonvulsant classes, such as topiramate, felbamate, levetiracetam, zonisamide, lamotrigine, gabapentin, pregabalin, vigabatrin, tiagabine, lacosamide, stiripentol, and rufinamide [22, 23, 24].

The structures of all anticonvulsants mentioned thus far can be found in figures 3 and 4. Additionally, each anticonvulsant, along with its commercial name, intended use, and American release date, can be found in table 2 [25, 26, 27].
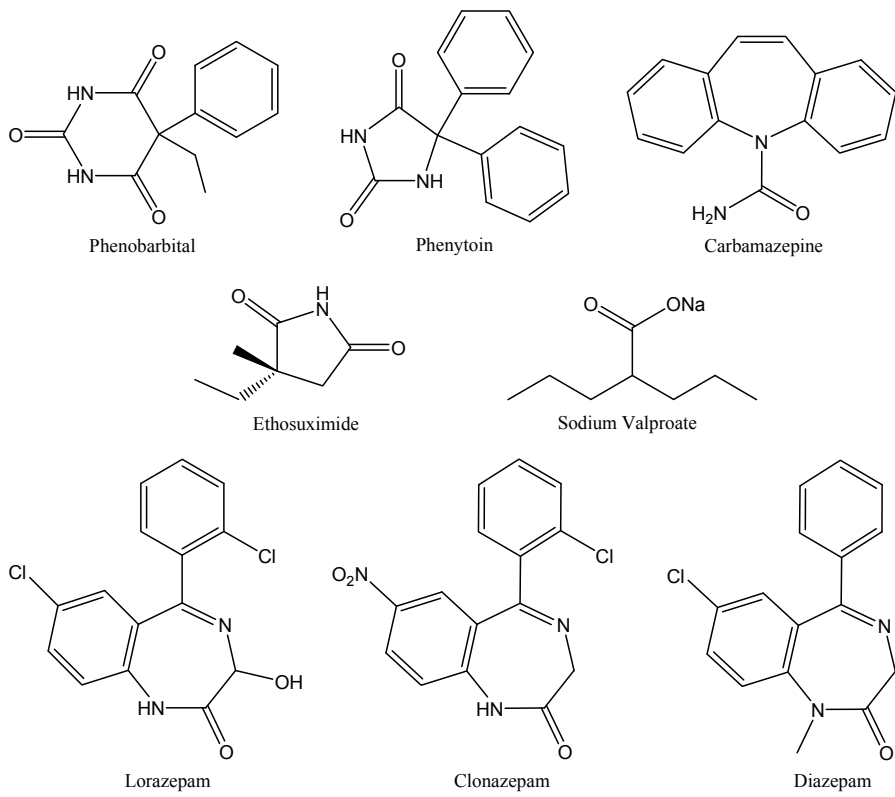
Figure 3: First generation anticonvulsant drugs
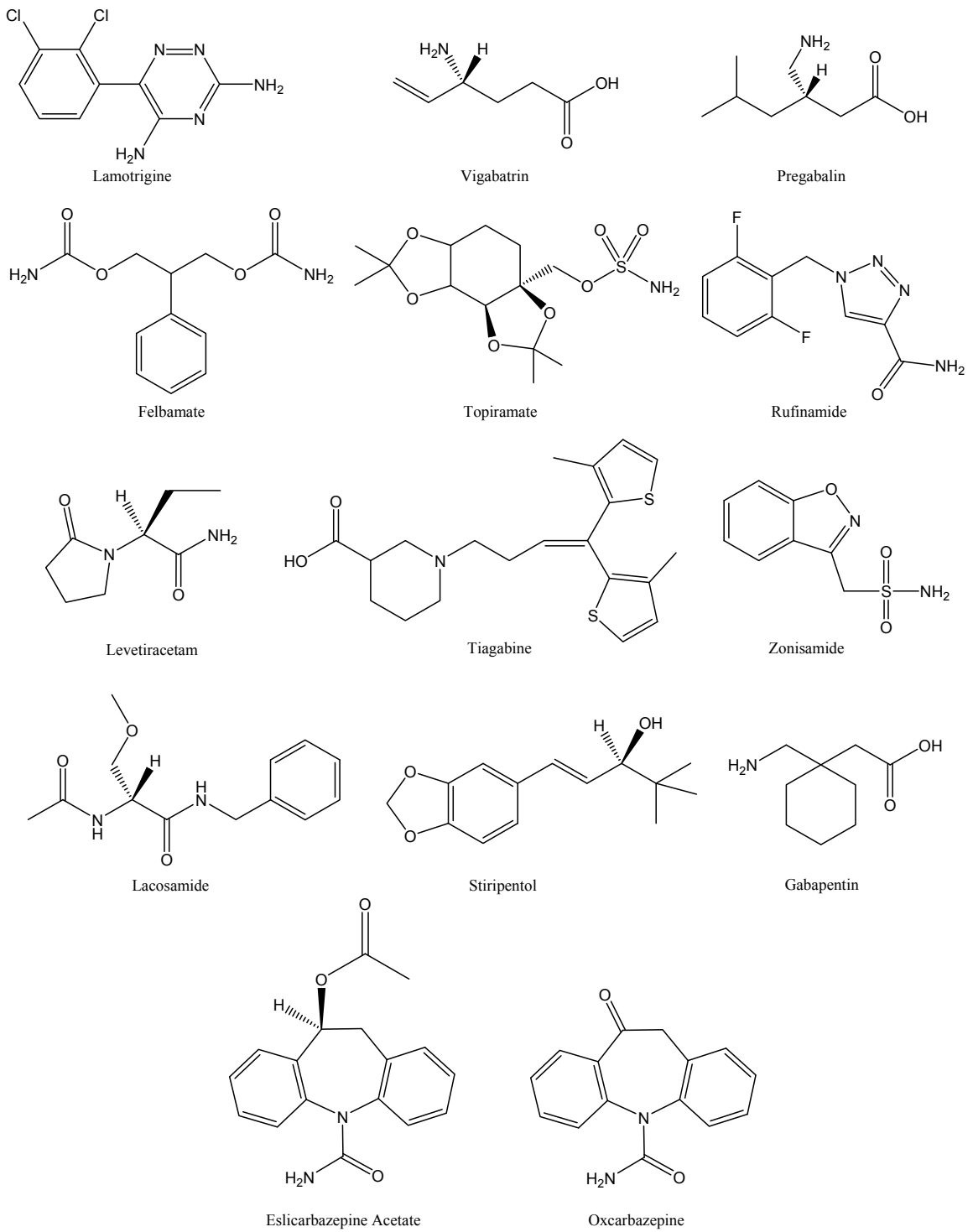
Figure 4: Newer anticonvulsant drugs

Table 2: Current anticonvulsant drugs (*Withdrawn from market; φEuropean release, not available in USA)

Drug	Commercial Name	Target Seizure Type(s)	Date (USA)
Carbamazepine	Tegretol	Partial seizures, generalized tonic-clonic seizures	1974
Ethosuximide	Zarontin	Absence seizures	1960
Phenytoin	Dilantin	Partial seizures, generalized tonic-clonic seizures	1938
Phenobarbital	Luminal	Broad spectrum	1912
Sodium Valproate	Epival	Broad spectrum	1978
Diazepam		Status epilepticus	1963
Clonazepam	Frisium	Broad spectrum	1975
Gabapentin	Neurontin	Partial seizures (adjunctive therapy)	1993
Lamotrigine	Lamictal	Partial seizures (adjunctive therapy)	1994
Felbamate	Felbatol	Severe partial seizures, and drug-resistant seizures associated with Lennox-Gastaut Syndrome	*1993
Topiramate	Topamax	Partial seizures (adjunctive therapy)	1996
Oxcarbazepine	Trileptal	Partial seizures, generalized tonic-clonic seizures	1999
Vigabatrin	Sabril	Partial seizures, generalized tonic-clonic seizures	2009
Levetiracetam	Keppra	Broad spectrum	1999
Tiagabine	Gabitril	Partial seizures, generalized tonic-clonic seizures	1997
Rufinamide	Inovelon	Partial seizures, generalized tonic-clonic seizures	2008
Zonisamide	Zonegran	Partial seizures, generalized tonic-clonic seizures	2000
Lacosamide	Vimpat	Partial seizures, generalized tonic-clonic seizures	2008
Pregabalin	Lyrica	Partial seizures, generalized tonic-clonic seizures	2004
Eslicarbazepine Acetate	Zebinix	Partial seizures, generalized tonic-clonic seizures	2009
Stiripentol	Diacomit	Partial seizures, generalized tonic-clonic seizures	φ2007

1.2.2 The Modern Approach: Rational Antiepileptic Drug Design

Modern AED discovery focuses primarily on rational drug design—an approach

to drug development that requires an understanding of the pathophysiology of a given

disease or disorder and the macromolecular receptor sites involved. Such knowledge permits the scientific engineering of chemical entities that will bind and disrupt the functioning of specific molecular targets, ultimately preventing the abnormal biological process of interest.

Upon the identification of potential disease-related molecular targets, the process of rational drug design can begin. The stepwise procedure for this modern approach to drug discovery [28, 29] is outlined in figure 5:

1. Discovery of lead compound

-High-throughput screening
-Biological sources
-Mechanistic design

⇩

2. Optimization of lead compound

-Pharmacodynamic optimization
-Pharmacokinetic optimization
-Pharmaceutical optimization

⇩

3. Toxicological study of optimized compound

-Minimal toxicity demonstrated in animals

⇩

4. Clinical Trials

-Phase I
-Phase II
-Phase III
-Phase 1V

Figure 5: The modern approach to drug discovery

The entire process of drug discovery—from lead identification to marketing—takes approximately 8-12 years [28]. A graphical representation of the estimated duration of each stage in the development of a drug is shown in figure 6:
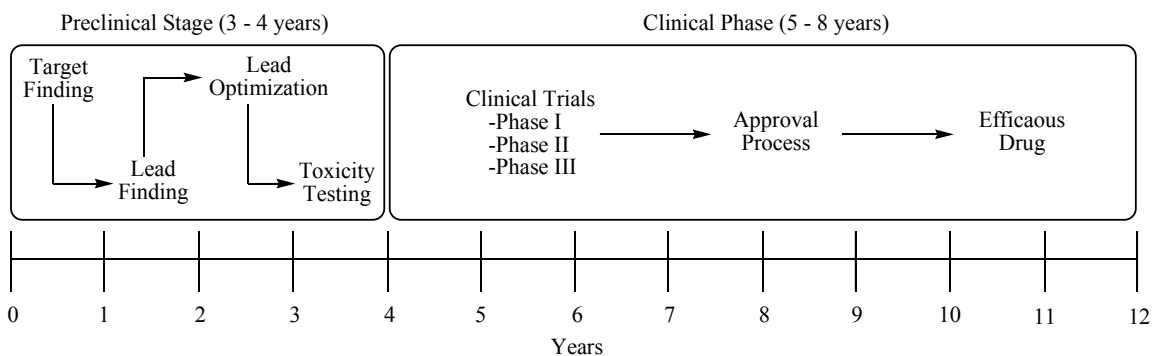
Figure 6: An approximate timeline for the process of drug discovery

1.2.2.1   Discovery of a Lead Compound

A lead compound is a chemical substance that demonstrates affinity for the desired target and serves as a structural starting point in the search to find a promising clinical drug candidate. In rational drug design, strategic chemical modifications of the lead compound are performed in attempts to find analogues with improved biological activity. The discovery of a lead compound can be achieved in a variety of different ways, including the following commonly used techniques: high-throughput screening (HTPS), the investigation of biological sources, and mechanistic design.

HTPS is the process whereby large libraries of compounds are screened against a biological target using in silico methods or rapid in vitro assays. A lead compound can be discovered through the random screening of diverse libraries, but a more systematic approach is also possible by screening focused libraries, such as those consisting only of known drug platforms. HTPS is more commonly employed in big pharmaceutical companies, rather than in academia where resources and funding are more limited. This technique is also not feasible for epilepsy research because reliable in vitro assays for epilepsy are scarce; antiepileptic efficacy testing is predominantly carried out using in

16

vivo animal models, which are too labour-intensive, time-consuming, and expensive for HTPS.

A lead compound can also be identified through the investigation of biological sources. Bioactive agents found in various herbal remedies or indigenous medicines often serve as promising lead compounds. While ethnopharmacology can be used as a tool in antiepileptic drug research, the more commonly employed technique is mechanistic design.

The mechanistic design of a lead compound involves purposefully engineering a molecule that will interrupt a pathological process by interacting with known molecular targets. Hence, it is necessary to understand the underlying mechanisms of the disease or disorder. Our ever-expanding knowledge pertaining to pathology of epilepsy has allowed for the identification of several antiepileptic drug targets. The majority of these druggable targets are only involved in seizure activation; no targets have been concretely linked to epileptogenesis, although it is believed that regulation of the *N*-methyl-D-aspartate (NMDA) receptor (vide infra) is involved [30]. It should be noted that current anti-seizure agents typically affect more than one molecular target, and it is likely that having multiple modes of action will result in higher efficacy [31].

Mechanistic anticonvulsant drug design traditionally places emphasis on three main modes of action: i) modulation of voltage-gated ion channels, ii) enhancement of GABA-mediated inhibition and iii) diminution of glutamate-mediated excitation.

1.2.2.1.1   Modulation of Voltage-Gated Ion Channels

Neuronal action potentials are controlled by the influx and efflux of ions through voltage-gated ion channels. Thus, molecular targets of interest with respect to

17

anticonvulsant drug development are sodium (Na+), calcium (Ca2+) and potassium (K+) channels. Genetic mutations involving any of these ion channel types have been linked to various epileptic syndromes [32].

An action potential is propagated down the length of an axon by the sequential opening of sodium channels. This results in an influx of positively charged sodium ions, which depolarizes the cell membrane from its resting potential of approximately -70 mV to +30 mV. At +30 mV, the channel enters a state of inactivation and cannot be reopened until resting potentials are restored [3]. Any molecule that disrupts the flow of ions through sodium channels can prevent the generation of an action potential and potentially serve as an anticonvulsant. Many currently available sodium channel blockers, such as carbamazepine and phenytoin, exert their effects by binding to the inactivated conformation of the channel, which prolongs the inactivated state and prevents the high-frequency firing characteristic of epilepsy in a use-dependent manner [30].

Voltage-gated potassium channels are also important targets for anti-seizure drugs, as they are partially responsible for the repolarization of neurons after the generation of an action potential. Extracellular potassium ion concentrations are approximately 40 times lower than intracellular neuronal concentrations [33]. Thus, the opening of potassium channels results in a net efflux of positively charged potassium ions, leading to hyperpolarization. Under normal circumstances, potassium channels would close after hyperpolarization is achieved and resting levels of intra- and extracellular ion concentrations would be restored through active transport [3]. However, if potassium channels remain open, repolarization will not be able to occur and the neuron will remain hyperpolarized. This will dampen the excitability of the neuron, as the threshold potential

18

required to trigger an action potential would be more difficult to reach from lowered starting potentials. Therefore, any compound that activates potassium channels may possess anticonvulsant properties [33].

Lastly, high-voltage-activated N- and P/Q-type calcium channels are necessary for synaptic neurotransmitter release and are thereby considered key possible targets for anticonvulsant drugs. Blockade of these ion channels will interrupt neurotransmitter release and thus impede the generation of an action potential, possibly giving rise to seizure prevention [30].

1.2.2.1.2 Enhancement of GABA-Mediated Inhibition

The primary inhibitory neurotransmitter of the CNS is γ-aminobutyric acid (GABA). GABA binds to three receptor types: $GABA_A$, $GABA_B$ and $GABA_C$ [34]. It is thought that the $GABA_A$ receptor plays the largest role in managing neuronal hyperexcitability and is the target for many established anticonvulsants. Activation of the $GABA_A$ receptor triggers the opening of ligand-gated chloride channels and results in the influx of negatively charged chloride ions. This hyperpolarizes the neuronal membrane and dampens the excitability of the neuron [30]. Therefore, the inhibition of neurons, and potentially the prevention of seizures, can be accomplished by introducing either $GABA_A$ receptor agonists or GABA prodrugs, which are agents that produce GABA as a metabolite after entering the brain. Unfortunately, the administration of GABA itself is not effective in preventing or stopping seizure activity, as its molecular properties render it incapable of crossing the BBB.

In addition to the modulation of GABA receptors, GABA-mediated inhibition can be enhanced by preventing the enzymatic breakdown of GABA, which begins as follows:

GABA   GABA tranaminase   Succinic semialdehyde
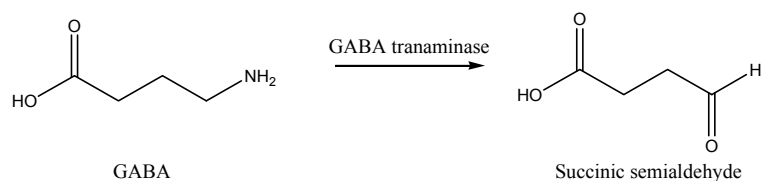
Scheme 1: The enzymatic breakdown of GABA

Therefore, the GABA transaminase enzyme is a potential molecular target for anticonvulsants, as its inhibition will increase cerebral concentrations of GABA and consequently decrease neuronal excitability.

Elevated levels of GABA can also be achieved by preventing its removal from extracellular space. After GABA is released, its reuptake into glial cells and neurons occurs by way of GABA transporters (GATs). The introduction of GAT antagonists or allosteric inhibitors will decrease neuronal excitability by increasing the amount of GABA available at the synaptic cleft [35].

1.2.2.1.3   **Diminution of Glutamate-Mediated Excitation**

Glutamate is the principal excitatory neurotransmitter of the CNS and hence plays a role in the generation of seizures. Glutamate binds to three receptor subtypes: the kainate, NMDA, and γ-amino-3-hydroxy-5-methyl-4-isoxazolepropionate (AMPA) receptors. All of these receptor types are possible molecular targets for antiepileptic drugs, as each is responsible for increasing neuronal excitability. Activation of the AMPA and kainate receptors activates ligand-gated sodium channels, and activation of the NMDA receptor—which requires a coagonist of either glycine or D-serine—opens both ligand-gated sodium and calcium channels [30, 32]. Thus, glutamate receptor antagonists would serve as putative anticonvulsants. Furthermore, the excitatory effects of the NMDA receptor could also be hindered by preventing the binding of its coagonists. For example,

glycine transporters, which regulate cerebral glycine concentrations by transporting glycine to and from glial cells, could be targeted.

Finally, antiepileptic therapeutics could also act on the synthetic pathway of glutamate, part of which involves the enzyme glutaminase [35]. Enzymatic inhibition of glutaminase would decrease cerebral concentrations of glutamate and in turn diminish glutamate-mediated excitation.

1.2.2.2   Optimization of the Lead Compound

A lead compound that targets one of the various receptors implicated in the disorder of interest must be modified to achieve optimal biological activity. This optimization process can be broken down into three parts: pharmacodynamic optimization, pharmacokinetic optimization, and pharmaceutical optimization.

1.2.2.2.1   Pharmacodynamic Optimization

The main objective of pharmacodynamic optimization is to improve the binding interactions between a drug molecule and its target receptor. This process involves synthesizing analogues of the lead compound and investigating how their structural differences affect biological activity. Analogue synthesis is achieved using a variety of structural modification techniques. One such technique is bioisosteric substitution—the replacement of one functional group with another that possesses similar physicochemical properties and is thus potentially capable of eliciting similar or more pronounced biological responses [36]. Several other techniques of structural modification [29] are listed in table 3:

Table 3: Techniques for analogue synthesis

Technique	Purpose
Homologation (extending alkyl chains)	To evaluate lipophilicity or fluidity
Structure pruning or the addition of bulk	To evaluate spatial requirements
Introduction of double bonds	To evaluate lipophilicity, rigidity, or stereochemical requirements
Varying ring structures	To evaluate lipophilicity, molecular geometry, or the effect of conformational restraint
Substituent variation	To evaluate electronic effects or pKa, aqueous solubility, and other physicochemical properties

The correlation between various structural modifications and biological activity is analyzed either using simple observation (a structure activity relationship study; SAR), or using computational methods (a quantitative SAR; QSAR). Information gathered from these studies is then used to synthesize additional analogues, and the process is repeated until the most promising structural modifications have been identified.

Unfortunately, it is not enough that a drug molecule binds to its target receptor with sufficient strength and selectivity; in order for a drug candidate to successfully reach its in vivo destination and survive the journey intact, pharmacokinetic and pharmaceutical optimization must also be performed.

1.2.2.2.2   Pharmacokinetic/Pharmaceutical Optimization, Lipinski's Rules, and the Concept of a Prodrug

Considerations of absorption, distribution, metabolism, and excretion (ADME) are the focus of both the pharmaceutical and pharmacokinetic phases of optimization. The pharmaceutical phase involves optimizing a drug's route of administration and its absorption into the bloodstream. Although many routes of administration exist, oral administration is most preferred due to high patient compliancy. Orally active drugs must withstand exposure to the metabolic enzymes found in saliva, gastric juices, and intestinal bile. Stability in the acidic conditions of the stomach (pH = 1.8-2.1) and basic conditions

of the duodenum (pH = 8.5-8.8) [3] is also required. Furthermore, orally administered drugs must posess the ability to traverse the intestinal membrane.

Pharmacokinetic optimization is aimed at achieving the safe and successful transport of a drug through the bloodstream and into the receptor microenvironment. This necessitates the molecular characteristics of both aqueous and lipid solubility, as well as liver metabolic stability and the resistance to kidney excretion. For CNS drugs, the ability to cross the BBB by passive diffusion or active transport is also required.

In order for a compound to surpass the obstacles associated with ADME, it must exhibit certain "drug-like" properties. In 1997, Lipinski et al. [37] devised an algorithm for predicting druglikeness, known as "the rule of 5". Lipinski's rules, as well as some of the more narrow restrictions required by CNS drugs [38, 39], are summarized in the following table:

Table 4: Lipinski's Rule of 5 and the modified rules for CNS drugs

	Lipinski's Rules	CNS Modifications/Additional Rules
1	Molecular weight ≤ 500 g/mol	Molecular weight < 450 g/mol
2	Log P ≤ 5 (P = octanol/water partition coefficient)	Log P between 1.5 and 2.7
3	≤ 5 hydrogen-bond donors	≤ 5 hydrogen-bond donors
4	≤ 10 hydrogen-bond accepters	≤ 10 hydrogen-bond accepters
5	—	N atoms + O atoms ≤ 5
6	—	PSA ≤ 90 Å (PSA = polar surface area)
7	—	≤ 5 rotatable bonds

It should be noted that human metabolism can be exploited through the use of prodrugs—biologically inactive compounds that are converted to active drugs by metabolic pathways in the body. The prodrug approach can be very beneficial, as it may serve to optimize the bioavailability of a drug by altering its metabolic stability or increasing its membrane transport capabilities. The use of a prodrug can also reduce the

presence of various side effects or even improve the taste and smell of a drug, the latter being important for the development of children's medications. An example of a prodrug is fosphenytoin, a phosphate ester that is converted to phenytoin after being cleaved in vivo by alkaline phosphatases. Fosphenytoin is more aqueous soluble than phenytoin and thus easier to administer by intravenous injection [40].
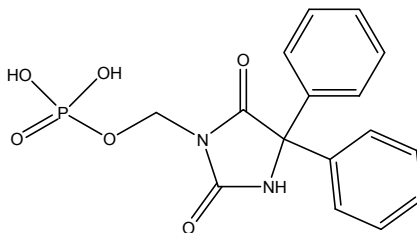
Figure 7: Fosphenytoin

1.2.2.3 Toxicity Testing

An optimized compound must successfully pass preclinical toxicity testing in multiple different species of non-human mammals before it can be evaluated in humans. A variety of toxicity tests exist, including those that evaluate a compound's acute, subacute and chronic toxicities, mutagenic potential, carcinogenic potential, and effect on reproductive performance [29].

1.2.2.4 Clinical Trials

Human clinical drug trials are divided into phases I-IV. During phase I, the general safety of the drug candidate is assessed in a group of 25-45 healthy volunteers who do not have the targeted disorder. Phase II trials evaluate both the efficacy and safety of the drug candidate in a group of 20-150 participants who have the targeted disorder. Phase III is normally a multi-center, double-blind, placebo-controlled, randomized clinical trial conducted in hundreds or thousands of patients with the disorder. Upon successful completion of phase III, a drug may be approved for the market. The long-

term surveillance of a drug after it has been approved (phase IV clinical trials) may result in its removal from the market if adverse unforeseen effects are detected [29]. The overall process of clinical testing is rigorous; 90% of all drug candidates that make it to human trials do not receive approval [28].

1.2.2.5   Additional Drug Criteria and Other Considerations

The molecular drug requirements mentioned so far have only been directed at safety and efficacy. However, the marketing of a drug must also be feasible from an economic standpoint. In order for a drug to be profitable and worth marketing, it should have minimal side effects and few or no alternatives (little competition). Its synthesis must be rapid, inexpensive, efficient (few steps; high yield), and scalable for mass production. Ideally, the use and synthesis of the drug should be patentable, and the targeted disease should be common or chronic/recurrent [29].

1.3   The Need for New Antiepileptic Drugs

Epilepsy is one of the most commonly encountered neurological conditions. The disorder is estimated to affect 0.5-1% of the global population, which translates to approximately 50 million people worldwide [41]. Only 50-60% of these individuals are able to control their seizures with available medications [13], and in doing so they are often plagued with adverse side effects, many of which are listed in table 5 [42, 43, 44, 45, 46]. Evidence also suggests that almost all existing AEDs increase the risk of birth defects if taken during pregnancy [47]. This is not surprising, as drugs that are capable of crossing the BBB are likely to permeate through the placental barrier, as well.

Table 5: Known side effects of various anticonvulsant drugs

Anticonvulsant	Side Effects
Carbamazepine	Nausea, drowsiness, ataxia, slurred speech, vertigo, blurred vision, diplopia, aplastic anemia, dermatological reactions, bone marrow depression
Benzodiazepines (i.e., clonazepam)	Sedation, confusion, poor concentration, difficulty with speech, ataxia, motor incoordination, diplopia, vertigo, muscle weakness, amnesia, irritability, aggression, hostility, impulsivity, depression, insomnia, dependence
Phenytoin	Nausea and vomiting, dermatitis, gum overgrowth, increased body hair, ataxia, dizziness, confusion, blurred vision, diplopia, tremors, loss of taste, insomnia, irritability, restlessness, weight loss, headache, hallucinations, delusions, paranoia, psychosis, depression, anemia, acne, osteopenia
Sodium Valproate	Nausea and vomiting, hair loss, weight gain, tremors, gastrointestinal distress, paresthesia, thrombocytopenia, liver dysfunction, pancreatitis, menstrual irregularities
Ethosuximide	Nausea and vomiting, sedation, dizziness abdominal pain, anorexia, headache, skin rash, hiccups
Primidone & Phenobarbital	Nausea, skin rash, sedation, lethargy, alteration of sleep cycle, agitation, behavioural changes, hyperactivity, ataxia, hepatotoxicity, agranulocytosis, serum sickness, diminished libido, dependence
Gabapentin	Gastrointestinal upset, drowsiness, fatigue, dizziness, shortness of breath, diplopia, slurred speech
Lamotrigine	Nausea and vomiting, drowsiness, insomnia, ataxia, blurred vision, dizziness, headache, life-threatening rashes, facial swelling, lymphadenopathy, fever, hair loss
Felbamate	Nausea and vomiting, drowsiness, headache, insomnia, anorexia, aplastic anemia, hepatotoxicity
Topiramate	Nausea, drowsiness, fatigue, dizziness, ataxia, confusion, paresthesia, diplopia, difficulty with speech, impaired concentration, anorexia, kidney stones
Oxcarbazepine	Nausea and vomiting, drowsiness, dizziness, headache, ataxia, diplopia, hyponatremia, skin rash, toxic epidermal necrolysis
Vigabatrin	Drowsiness, dizziness, fatigue, confusion, weight gain, peripheral visual field defects, tremor, athetosis, dystonia, mood disturbances, depression, psychosis
Levetiracetam	Drowsiness, dizziness, headache, anorexia, nervousness and anxiety, agitation, aggression, depression
Tiagabine	Drowsiness, dizziness, muscle weakness, ataxia, nervousness, tremor, impaired concentration, depression, amnesia, insomnia
Pregabalin	Drowsiness, dizziness, weakness, headache, ataxia, weight gain, peripheral edema
Zonisamide	Drowsiness, fatigue, dizziness, ataxia, confusion, anorexia, impaired concentration, oligohidrosis and hyperthermia, kidney stones
Rufinamide	Nausea and vomiting, drowsiness, fatigue, diplopia, ataxia, fever, skin rash, anorexia, headache, decreased coordination, vertigo, tremor, nystagmus, abdominal pain, dyspepsia, diarrhea, constipation

Furthermore, no current antiepileptic therapies prevent or slow the progression of the disorder; all available antiepileptic medications are merely symptomatic and do not in any way target the underlying causes of epilepsy. The lack of preventative treatment for epilepsy is unacceptable, as the disorder can be debilitating and even life threatening: the unpredictability of and associated stigma of epilepsy often lead to negative psychosocial and socioeconomic implications [48]; epileptic patients are usually at a high risk of injury due to falls or the violent nature of various seizure types, and between 0.35-9.3 out of every 1000 individuals with the disorder succumb to sudden unexpected death in epilepsy (SUDEP) each year [49].

It is true that alternative treatments for epilepsy exist, including the use of specific diets or surgery, but certain drawbacks render their use quite limited. Food regimens, such as the ketogenic diet, are again merely symptomatic therapies and have associated risks, including high serum cholesterol in adults [50] and growth retardation in children [51]. Additionally, therapeutic diets for epilepsy are only moderately successful, rarely allowing patients to become seizure-free. Surgical removal of epileptic foci is effective and often curative, but can only be used for the relatively few cases in which the seizure focus is detectable, localized to one small area, and in a location where its removal will not cause unacceptable neurological or cognitive deficits [20, 52].

It is clear that epilepsy research remains a necessity so that we may achieve the development of antiepileptogenic agents, as well as improved anticonvulsants, such as those with less harmful side effects, reduced teratogenic effects, and the ability to treat drug-resistant epilepsy.

1.4 The Goal of this Thesis

A critical review of the treatment of epilepsy certainly demonstrates the inadequacy of current antiepileptic therapies. Clearly, there is a significant need for the development of improved anticonvulsants and the discovery of curative or preventative epilepsy medications. Therefore, the primary goal of this thesis is to contribute to the advancement of antiepileptic drug research through the strategic application of medicinal chemistry and rational drug design. In particular, this thesis will focus on seeking out new anticonvulsant platforms and exploring a series of low-toxicity uracil derivatives that may be both anti-ictogenic and antiepileptogenic in nature.

Chapter 2: Project Descriptions

2.1   Project 1: In Silico Search for Exogenous Anticonvulsants

Project 1 is focused on the discovery of new lead compounds based on novel antiepileptic drug design. In particular, its goal is the identification of novel anticonvulsant scaffolds capable of sodium channel blockade.

2.1.1   The Sodium Channel Pharmacophore

The pharmacophore can be defined as the bioactive face of a drug molecule; it is the subset of atoms within a molecule that forms intermolecular bonds with the targeted receptor and enables the desired biological response. All drug molecules that bind a specific receptor must share a common pharmacophore made up of similarly oriented constituents, arranged such that they exhibit complementarity to the active site [29].

Based on molecular dynamic simulations of several sodium channel blockers, Unverferth [53] and other researchers [54] have suggested that the sodium channel pharmacophore consists of an electron donor group (D), an aromatic group or other hydrophobic moiety (R), and a hydrogen bond acceptor-donor group (HAD) geometrically arranged as shown in figure 8a. The electron donor group is often a carbonyl oxygen, and the HAD unit typically consists of an NH group. This is exemplified by the pharmacophoric regions of the sodium channel blockers carbamazepine and phenytoin, which are highlighted in red in figure 8b.
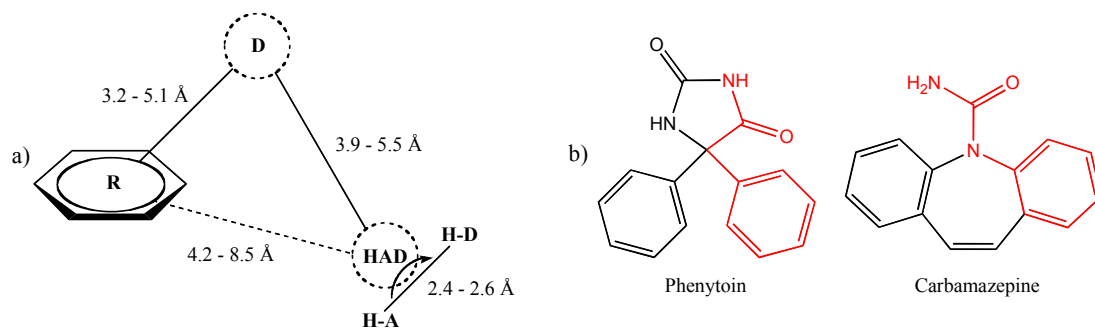
Figure 8: a) The sodium channel pharmacophore and b) the sodium channel pharmacophores of phenytoin and carbamazepine (shown in red)

2.1.2   Project 1 Outline:

The Molecular Operating Environment (MOE) [55] was used to perform an in silico substructure search on a database of over eight million exogenous compounds (compounds not endogenous to the human body) in order to identify those with the potential to block the action propagated via neuronal sodium channels. Thus, the substructure used for the search was the sodium channel pharmacophore—more specifically, the pharmacophore of phenytoin: an amide group separated from a phenyl ring by one carbon unit (see figure 8b). After the results were filtered for druglikeness, over 20 thousand hits were identified, of which 74 had a molecular weight between 100-200 g/mol, 8,788 had a molecular weight between 200-300 g/mol, and 11,773 had a molecular weight between 300-400 g/mol. Since the mean molecular weight of marketed CNS drugs is approximately 310 g/mol [39], it was decided to manually narrow down the list of hits ranging from 200-300 g/mol to a total of 19 that were commercially available. Each of the selected compounds were then purchased from Sigma Aldrich and sent to the National Institutes of Health (NIH) for biological evaluation and toxicity testing. The structures of these compounds are shown in figure 9.
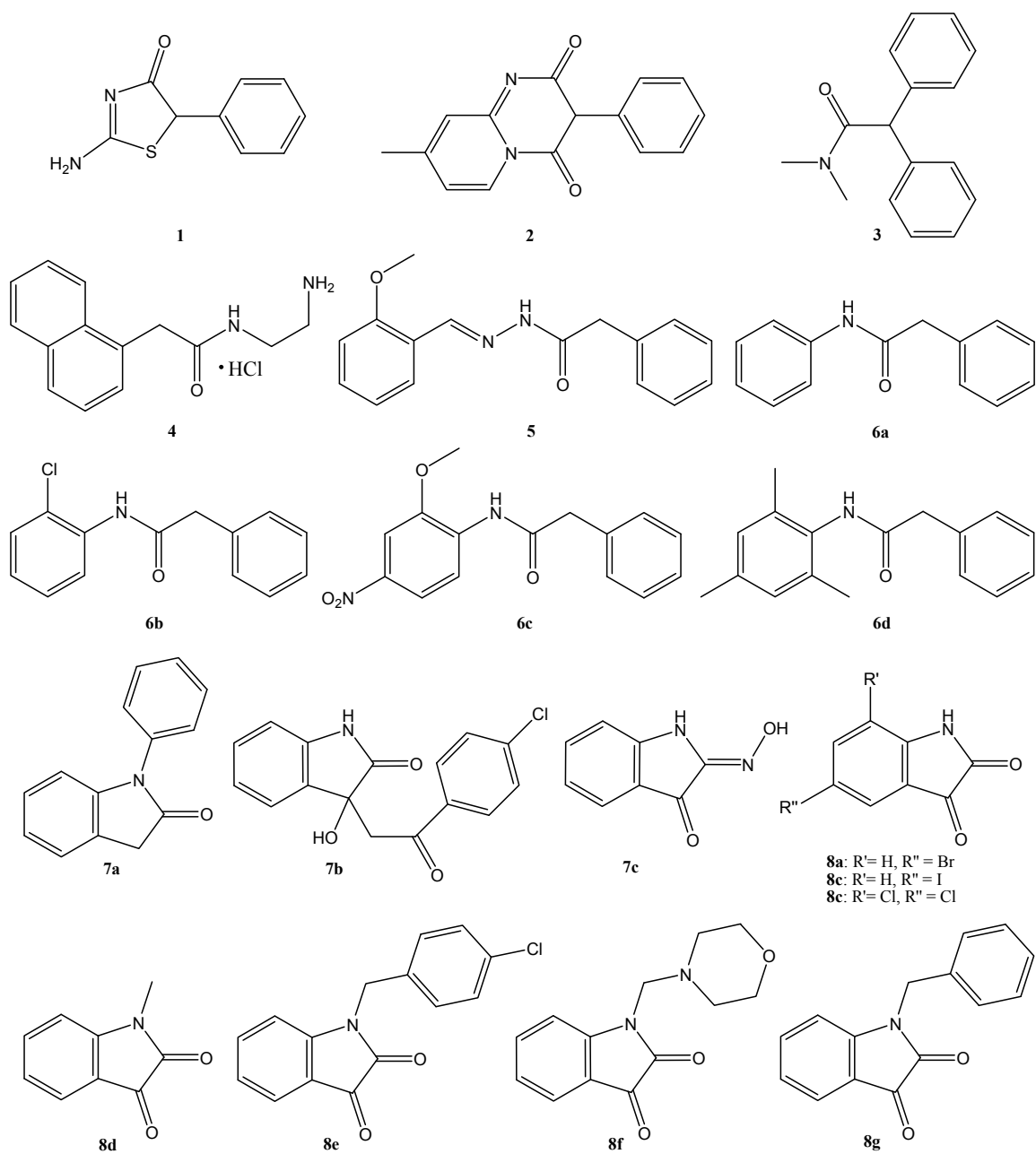
Figure 9: Exogenous compounds sent to NIH for biological evaluation

2.2   Project 2: The Development of Uracils as Endogenous AEDs

The focus of project 2 is directed toward the optimization of an endogenous

antiepileptic lead compound (i.e. a compound normally found in the human brain). The

ultimate goal is to design a drug that overcomes the major downfalls of current epilepsy

medications; a drug that exhibits not only reduced toxicity and improved anticonvulsant

activity, but also preventative or curative properties. The uracil platform was chosen as

the molecular starting point for this project after an extensive literature search and a

review of the preliminary experimentation conducted by previous members of the

Weaver research group.

2.2.1   Uracil as a Lead Compound: Active Prodrug Rationale

Uracil is a naturally occurring pyrimidine base that is essential to cellular life and

ubiquitous within the human body. Uracil and 5-methyluracil (thymine) are two of the

five major nucleobases found in RNA, DNA, and other nucleic acids [56].
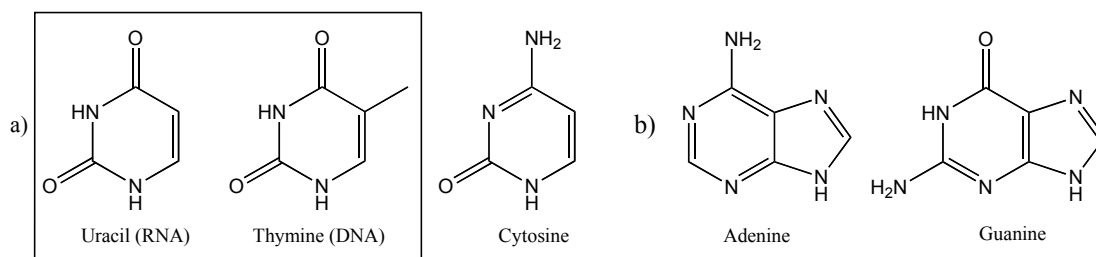
Figure 10: The five major nucleobases

As can be seen in the figure above, uracil contains a cyclic ureide-like ring.

Therefore, it is not unreasonable to suggest that uracil and its analogues (collectively

referred to as "uracils") are capable of anticonvulsant activity. Preliminary investigations

conducted by the Weaver group have demonstrated that many uracils are, in fact,

protective against both electrically and chemically induced seizures in rat and mouse

models [57]. Uracils are most structurally similar to the hydantoins (see table 1), and as such it is presumed that they exert their anti-seizure effects via sodium channel blockade.

Multiple anticonvulsant sodium channel blockers are available to the public already, but like all other epilepsy medications, they have associated adverse side effects. The toxicity of current AEDs is not altogether surprising, as they were developed from exogenous scaffolds. The uracil platform, however, is endogenous to the human body and could, in theory, allow for the development of low-toxicity analogues. Indeed, previously tested uracils exhibited few immediate adverse effects in toxicity studies conducted at NIH [57].

Furthermore, uracils are desirable for use as antiepileptic drugs because they are metabolized within the body to β-amino acids according to the pathway [57] shown in scheme 2:
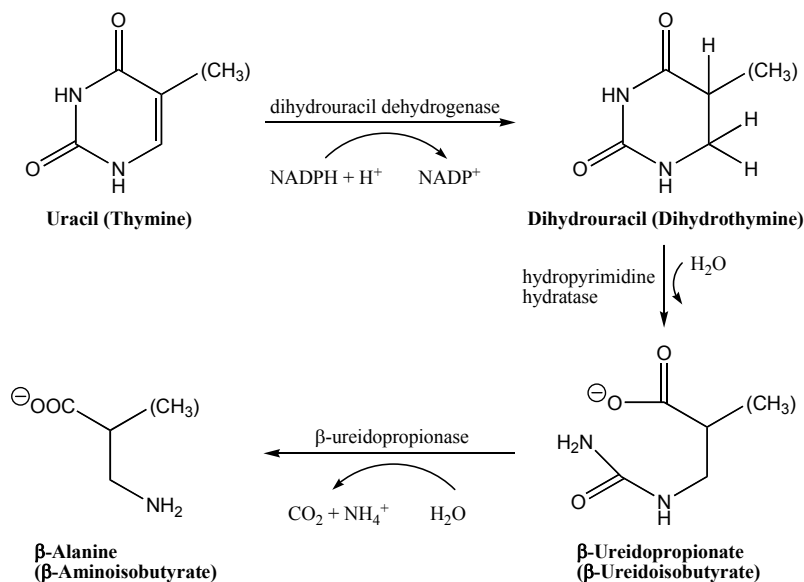
Scheme 2: The metabolic breakdown of uracil and thymine into β -amino acids

Like uracils, β-amino acid metabolites are also believed to be viable for the treatment of epilepsy. This hypothesis is based primarily on the growing evidence for the therapeutic potential of β-alanine.

β-Alanine is a structural intermediate between the inhibitory neurotransmitters glycine (an α-amino acid) and GABA (a γ-amino acid). Unsurprisingly, research suggests that β-alanine may also act as an inhibitory neurotransmitter: a) β-alanine is endogenous to the CNS and present in concentrations comparable to other key neurotransmitters, such as acetylcholine, norepinephrine, and dopamine b) β-alanine is released from neurons in a Ca^{2+} dependent manner c) β-alanine is capable of binding to a number of receptor sites within the CNS, including the glycine co-agonist site on the NMDA receptor complex, the glycine receptor site, $GABA_A$ and $GABA_C$ receptor sites, as well as receptor sites involved with the GAT-mediated glial uptake of GABA and d) β-alanine can inhibit neuronal excitability [58].

Additionally, β-alanine exhibits low toxicity in humans, even at high concentrations: β-alanine is an essential building block for carnosine—an important dipeptide found in skeletal muscle—and is taken in large doses on a regular basis by many body builders, who experience very few side effects [59].

It is therefore believed that β-alanine—a non-toxic small-molecule neurotransmitter that induces both GABAergic and glutamatergic inhibition—is another ideal molecular starting point for anticonvulsant drug design. In fact, β-alanine has displayed promising activity in a broad range of NIH seizure models. Furthermore, studies conducted by the Weaver group using the spontaneous recurrent seizure (SRS) model (a pilocarpine-induced seizure model of epileptogenesis [60]) has revealed that β-

alanine is able prevent the development of recurring seizures in rats with a success rate of over 50%, meaning that it is also neuroprotective and capable of impeding epileptogenesis.

This synopsis of the antiepileptic nature of uracils and their β-amino acid metabolites clearly demonstrates the potential of uracil analogues as low-toxicity, multiple-action, active prodrugs that target both ictogenesis and epileptogenesis.

2.2.2 Project 2 Outline

An array of uracil analogues were designed, synthesized, and sent to NIH for biological evaluation and toxicity testing. As can be seen from the figure below, uracil analogues can be generated by varying the substituents at platform positions N^1, N^3, C^5, and C^6.
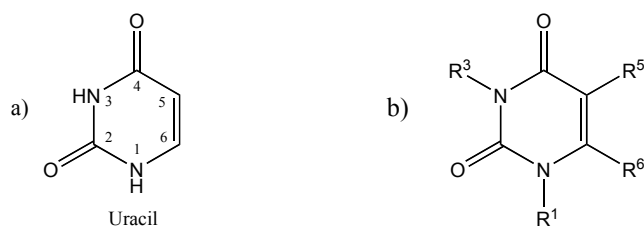
Figure 11: a) Conventional numbering pattern and b) possible substitution sites of the uracil platform

To determine which analogues were to be synthesized, an SAR was conducted using the biological data collected from the Weaver group's previously tested uracils. The majority of the previously synthesized uracils that displayed in vivo anticonvulsant activity, as well as a few derivatives that displayed weak or no activity, are shown in figure 12. The most promising of these analogues, compound **vi**, had comparable activity to and lower toxicity than current anticonvulsant drugs.
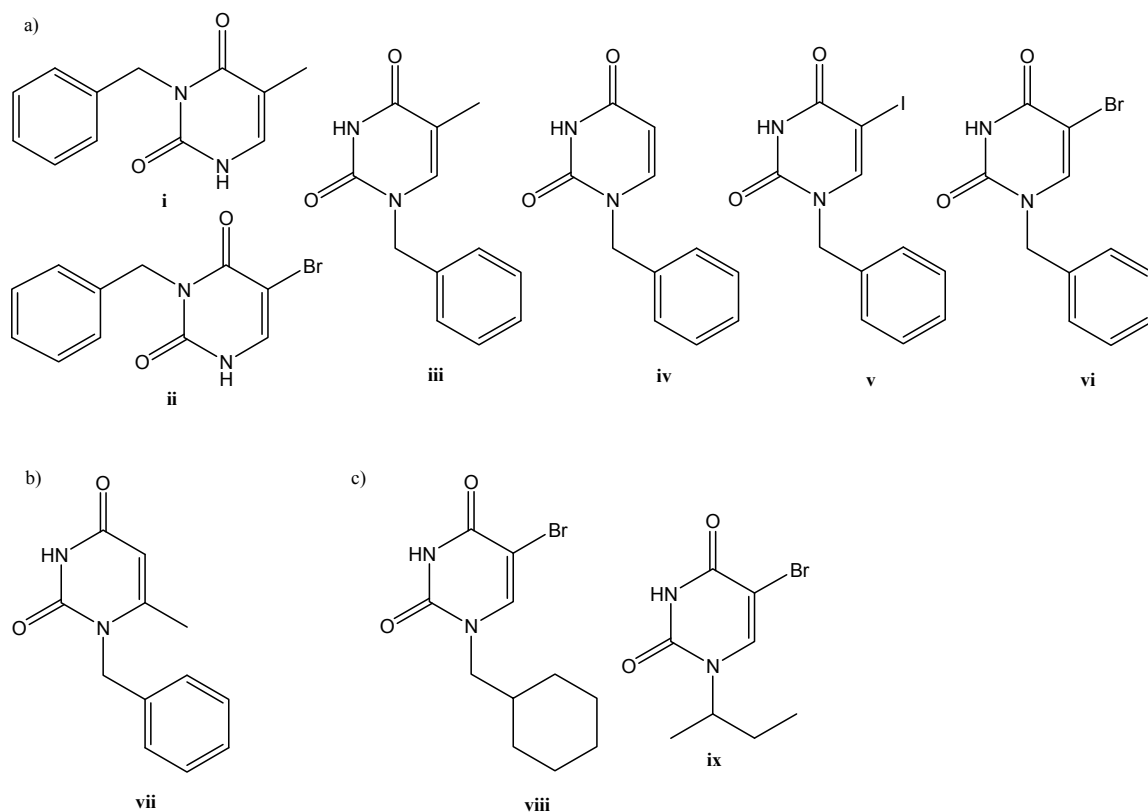
Figure 12: Various previously synthesized uracils with a) the highest anticonvulsant activity, b) weak anticonvulsant activity, and c) no anticonvulsant activity

Several trends were revealed when the uracils with higher activity were compared to those with weak or no activity:

1) For substitutions at N^1 and N^3:

    a. Substitution at *either* N^1 or N^3 increases anticonvulsant activity, but N^3-substituted analogues typically display higher toxicity

    b. Concurrent substitution at *both* N^1 and N^3 results in the complete loss of anticonvulsant activity

    c. Of all the N-substitutents tested, the benzyl group displays the most promising biological profile

2) For substitutions at C^5 and C^6:

    a. Substitution at C^6 is unfavourable: any substituent other than H typically increases toxicity and reduces biological activity

    b. Substitution at C^5 with moderately small substituents (such as CH_3, I, and especially Br) rather than larger groups (such as alkyl chains and rings) or smaller groups (such as H) improves biological activity

Using these observations as a guideline for analogue design, a series of N^1- and C^5-substituted uracils were synthesized, where R^1 substitutents consisted of various substituted benzyl groups and other aromatic moieties, and R^5 substituents were relatively small groups (Br, H, CH_3, I, CF_3, NO_2, Cl, and F). A few uracil derivatives containing both N^1 and N^3 substituents were also synthesized simply to verify observation 1b. As new uracil derivatives were synthesized, the correlation between their structure and activity was analyzed in an SAR to guide further analogue synthesis. A QSAR was also performed after the biological results for a sufficient number of analogues (preferably $\geq$ 30) became available (vide infra). Finally, several uracil analogues that displayed in vivo anticonvulsant activity in NIH models were also submitted to Chantest for in vitro sodium channel binding studies to investigate their validity as sodium channel blockers.

In total, 39 different uracils were synthesized. The structures of these compounds are shown in figure 13.

9a: R^5 = Br
9b: R^5 = CH$_3$
9c: R^5 = H
9d: R^5 = NO$_2$
9e: R^5 = I
9f: R^5 = CF$_3$

10a: R^5 = Br
10b: R^5 = NO$_2$
10c: R^5 = CF$_3$
10d: R^5 = I

11a: R^5 = I
11b: R^5 = CH$_3$
11c: R^5 = H

12a: R^5 = Br
12b: R^5 = H
12c: R^5 = CH$_3$
12d: R^5 = I
12e: R^5 = Cl

13a: R^5 = Br
13b: R^5 = H
13c: R^5 = CH$_3$

14a: R^5 = Br
14b: R^5 = H
14c: R^5 = CH$_3$

15a: R^5 = Br
15b: R^5 = H
15c: R^5 = CH$_3$
15d: R^5 = Cl

16

17

18

19

20

21a: R^5 = Br
21b: R^5 = Cl

22a: R^5 = Cl
22b: R^5 = F

23

24
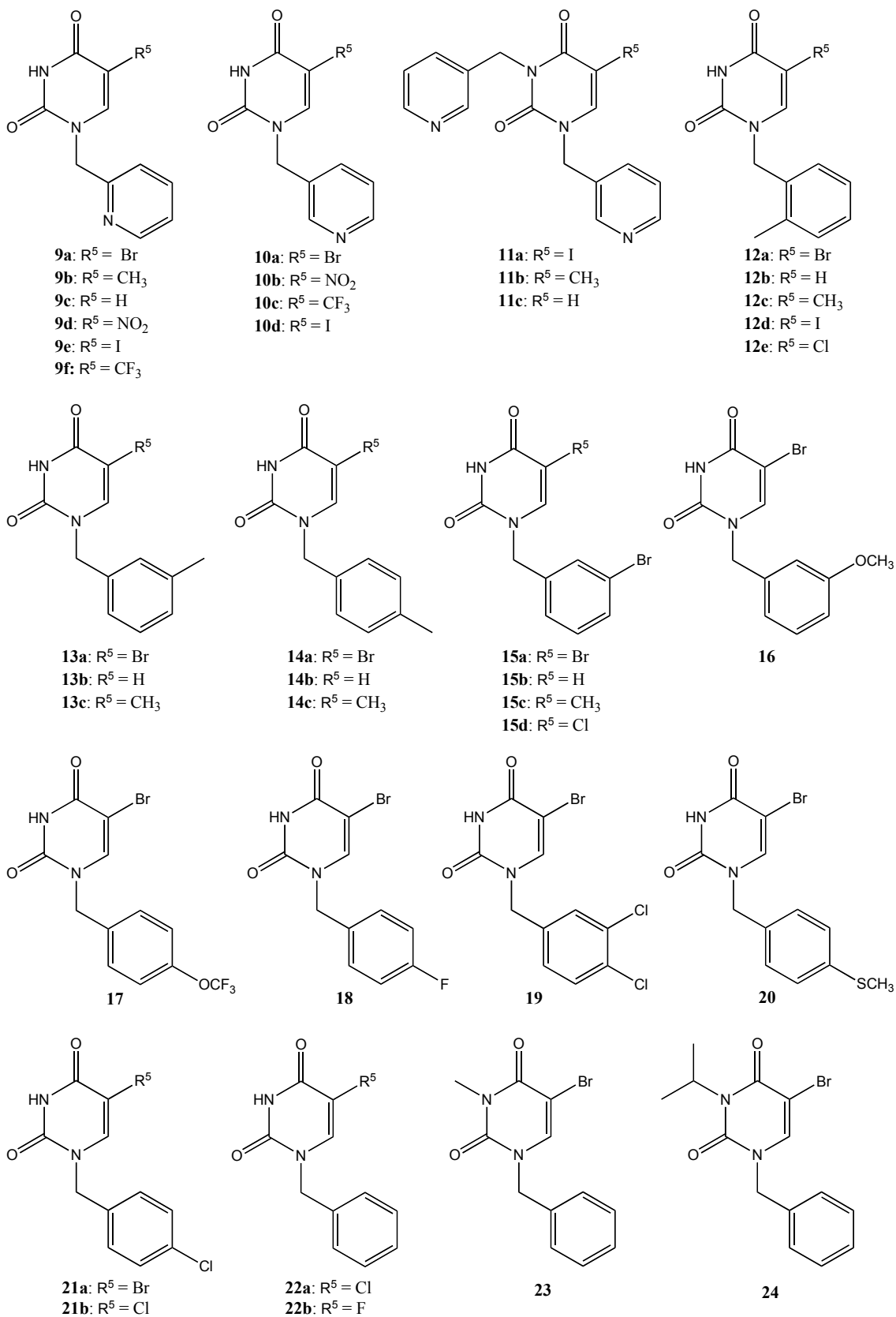
Figure 13: Synthesized uracil derivatives sent to NIH for biological testing

38

Chapter 3: Synthesis of Uracils

3.1   Background Information

There are six possible tautomeric forms of uracil [61]. The structures of these tautomers are shown in figure 14:
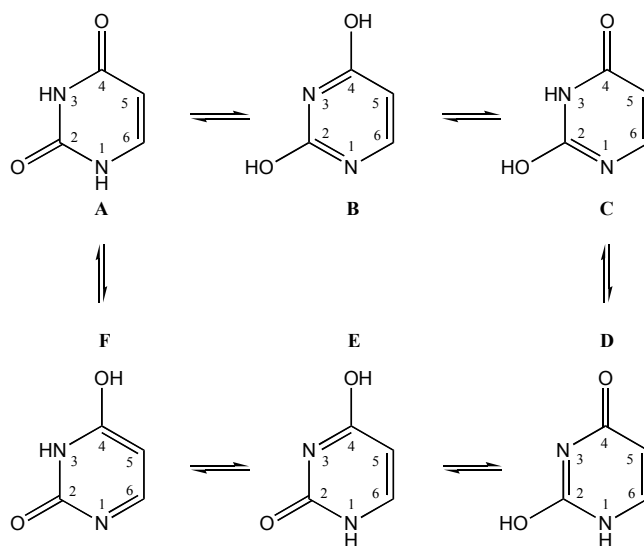
Figure 14: The tautomeric forms of uracil

When considering only the most stable rotomer of each tautomer, density functional theory (DFT) calculations suggest that the order of stability is as follows: A > C > E > B > D > F, with the diketo form of uracil (A) being most stable [62, 63]. The fact that tautomer C has higher stability than tautomers D and E indicates that N^1 is more acidic than N^3. DFT computations have supported this claim, as the deprotonization energies for N^1 and N^3 in the diketo form of uracil have been calculated to be 1392.6 kJ/mol and 1448.1 kJ/mol, respectively [63]. Furthermore, Jonas et al. [64] have estimated the pK_a of N^1-H to be 9.43 and the pKa of N^3-H to be 13.2 in water at 25˚C. This information should be kept in mind when approaching the synthesis of uracil analogues.

3.2   **Synthetic Approaches for Uracils**

3.2.1   **Synthetic Methods for Uracil Ring Formation**

      Uracil ring formation is most commonly achieved by the condensation of urea or thiourea with various β-keto esters. Reactions of this type, as well as a number of related synthetic methods for uracils, will be briefly described in this section.

<u>Fischer and Roeder's Synthesis:</u>

      The first successful laboratory synthesis of uracil was achieved by Fischer and Roeder in 1901 [65, 66]. Their synthesis involved the condensation of urea and ethyl acrylate into dihydrouracil, followed by bromination and debromination with alkali:

Urea   Ethyl acrylate   Dihydrouracil   Uracil
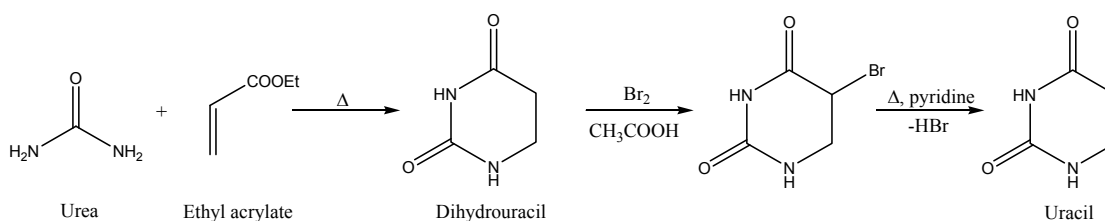
Scheme 3: Fischer and Roeder's synthesis of uracil

Unfortunately, Fischer and Roeder's synthesis of uracils generally results in low yields.

<u>Wheeler and Liddle's Synthesis:</u>

      In Wheeler and Liddle's synthesis [65, 66], urea or thiourea is reacted with a β-keto ester. When thiourea is used, the resulting sulfur-containing product must be subsequently heated in aqueous acid to afford the desired uracil.

(66%)
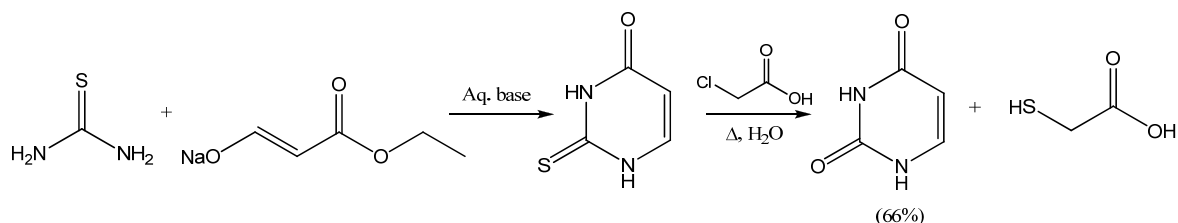
Scheme 4: Wheeler and Liddle's synthesis of uracil

Wheeler and Liddle's synthesis is moderately yielding and quite versatile, making it one of the more commonly used techniques for the synthesis of uracils.

Davidson-Baudisch Synthesis:

The Davidson-Baudisch synthesis [65] of uracil is a simple one-pot method involving the treatment of urea and malic acid with fuming sulfuric acid:
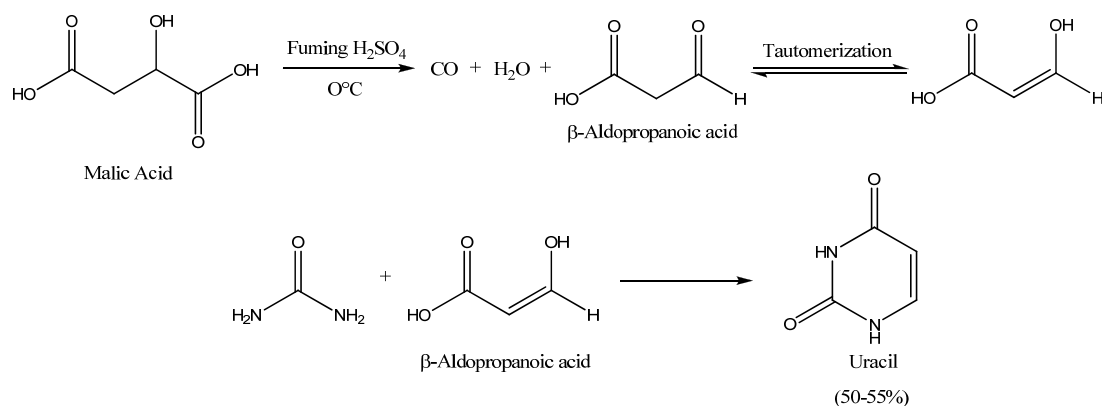
Scheme 5: Davidson and Baudisch's synthesis of uracil

The Davidson-Baudisch synthesis is facile and can afford various uracils in moderate yields.

Bergmann Synthesis:

In the Bergmann synthesis [67], a substituted cyanacetic acid is condensed with urea in the presence of acetic anhydride and subsequently reduced by catalytic hydrogenation.
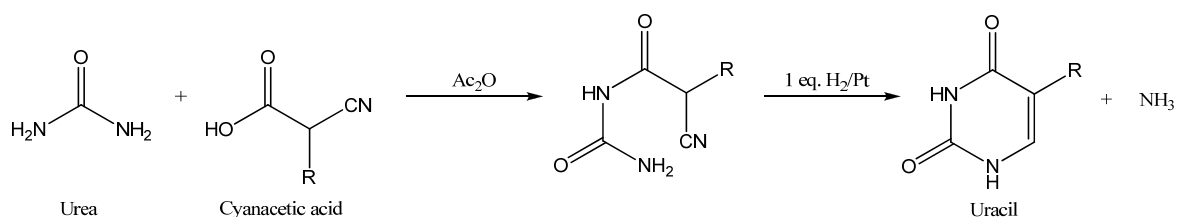
Scheme 6: Bergmann's synthesis of uracil derivatives

Reactions of this type generally proceed in moderate yield and, unlike many of the aforementioned syntheses, do not require harsh conditions or the removal of sulfur.

Hofmann Degradation:

Uracil ring formation can also be achieved through the Hofmann-like rearrangement of an α,β-unsaturated diamide using oxidative reagents such as NaOCl or PhI(OAc)$_2$ [68]. This reaction proceeds through an isocyanate intermediate as shown below:
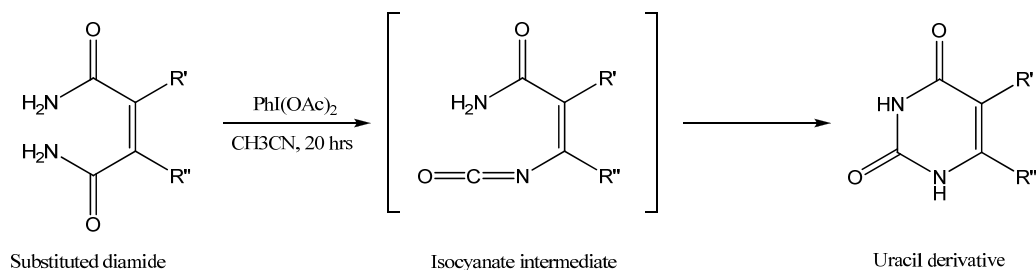
Scheme 7: Uracil formation via a Hofmann-like rearrangement

Reactions of this type are fairly versatile and often afford excellent yields.

3.2.2 Synthetic Methods for the Preparation of Substituted Uracils

The analogue synthesis in this thesis is concentrated on uracil substitution sites N^1, N^3, and C^5; thus, C^6 uracil substitutions will not be discussed. In addition, C-C bond formation at both C^5 and C^6 are also not a primary focus of this thesis and will not be covered.

3.2.2.1 The Synthesis of C^5-Substituted Uracils

C^5 uracil substitutents of particular interest for the synthesis of uracil analogues in this thesis are CH$_3$, F, Br, Cl, I, NO$_2$, and CF$_3$. Some synthetic methods for the preparation of these derivatives have been previously discussed in section 4.2.1; C^5-

substituted uracils can be synthesized by many of the aforementioned methods for uracil ring formation if appropriately substituted starting materials are used. For example, 5-methyluracil (thymine) can be prepared from i) ethyl methacrylate using Fischer and Roeder's synthesis ii) sodium formylpropanoic ester using Wheeler and Liddle's synthesis, or iii) 2-cyanopropanoic acid using the Bergmann synthesis.

5-Halouracils can be obtained in a similar fashion. However, they can also be prepared from the direct halogenation of uracil using elemental halogens or N-halosuccinimides [69, 70]:
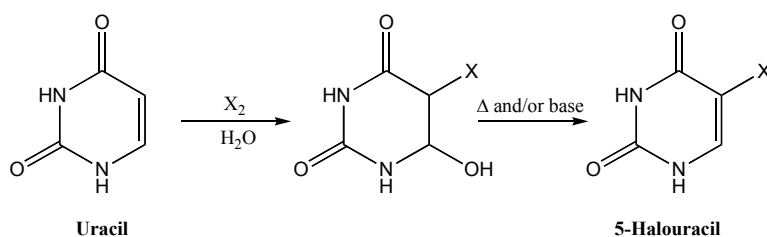
Scheme 8: The synthesis of 5-halouracils via elemental halogenation

Much research has gone into the C^5-fluorination of uracil due to the clinical use of 5-fluorouracil—an anticancer agent that causes cell death by its misincorporation into nucleic acids and its inhibition of essential biosynthetic pathways [71]. C^5-fluorination can be achieved by a number of reagents, including fluoromethyl hypofluorite (FCH_2OF) [72], cesium fluoroxysulfate ($CsSO_4F$) [72], fluoroxytrifluoromethane (CF_3OF) [73], and acetyl hypofluorite (CH_3COOF) [74].

5-Nitrouracil is most often synthesized by the direct C^5-nitration of uracil. This can be accomplished using reagents such as nitric acid and sulfuric acid [75], palladium(II) acetate and sodium nitrite [76], copper(II) nitrate and acetic anhydride [77], and nitronium tetrafluoroborate (NO_2BF_4) [77].

Lastly, 5-(trifluoromethyl)uracil can be prepared by several methods, including the

direct C^5-trifluoromethylation of uracil with aqueous bis(trifluoromethyl) mercury in the presence of azoisobutyronitrile (AIBN). Unfortunately, this synthesis suffers from multiple disadvantages such as low yields and the use of highly toxic reagents. The superior synthesis of 5-(trifluoromethyl)uracil involves the chlorination of thymine, first with phosphorus oxychloride in the presence of a tertiary amine and then with elemental chlorine, followed by fluorination with hydrogen fluoride and subsequent hydrolysis using aqueous potassium or sodium fluoride [78]. This method is quite high yielding and used prominently in industry:
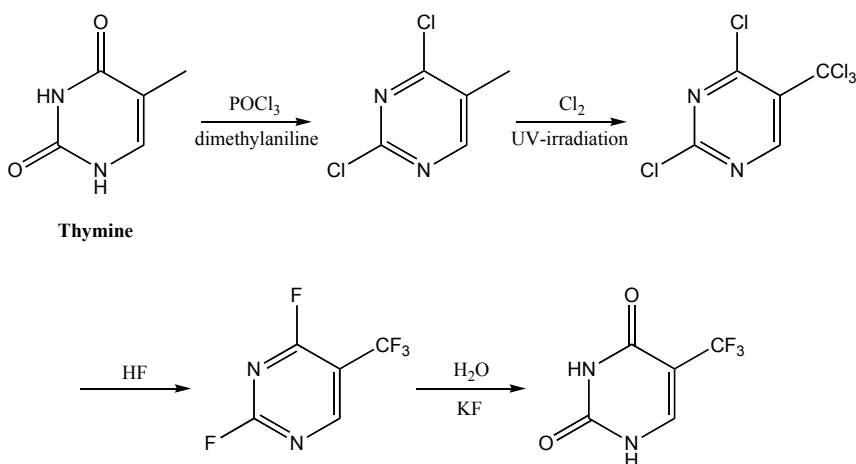
Scheme 9: The industrial synthesis of 5-(trifluoromethyl)uracil

3.2.2.2   The Synthesis of N-Substituted Uracils

The synthesis of N-substituted uracil analogues can also be carried out through various methods of uracil ring formation if appropriate starting materials, such as N-substituted ureas or thioureas, are used. However, it is difficult to achieve regioselectivity in this fashion.

A more practical approach to N-substituted uracil analogue synthesis is the direct N^1 and/or N^3-alkylation of uracils. As mentioned earlier, it is believed that N^1-H of uracil is more acidic than N^3-H, indicating that substitutions involving the use of base and

various alkyl halides should proceed more readily at N^1. While this is true in some cases, a mixture of N^1 and N^3 mono- and disubstituted uracil products is often obtained. The ratio between these three products is highly dependent on the reaction conditions, the equivalents of substituting reagents used, and the substituents already present on the starting uracil [79, 80, 81].

N^1- or N^3-specific substitutions can be made more favourable by employing uracil protecting groups (UPGs). An ideal UPG would be one that directs alkylation completely to either N^1 or N^3, is stable enough to withstand the substitution reaction conditions, and is labile enough to be removed without difficulty after reaction completion. Many existing UPGs are limited due to poor N-selectivity or harsh deprotection steps [82], but an acceptable level of success has been achieved through the methods reviewed below.

N^1-Directed Uracil Substitution:

The substitution of uracils at N^1 can be facilitated by the direct protection of N^3, although UPGs that exclusively react with N^3 are uncommon. However, the N^3-protection of some uracils can be ahchieved indirectly. For example, when uracil or thymine is reacted with excess benzoyl chloride, the N^1,N^3-dibenzoylated products initially obtained can be quickly decomposed to their monosubstituted 3-benzoyl derivatives via mildly basic conditions [83] or chromatography on alumina [84]:
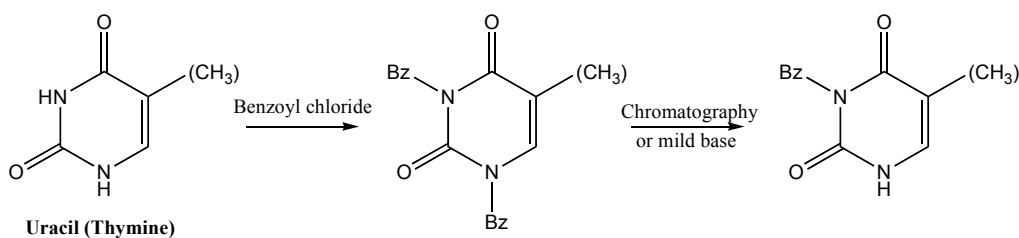
Scheme 10: The indirect N^3-benzoylation of uracil or thymine

Alternatively, N^1-substitution can be made more favourable through the steric hindrance of N^3-substitution. This can be accomplished by protecting the uracil oxygens with bulky functionalities, such as the trimethylsilyl group (figure 15). Bis(trimethyl-silyl)acetamide (BSA) [85] or hexamethyldisilazane (HMDS) and trimethylsilyl chloride (TMSCl) [86] can be used for the trimethylsilylation of uracils.
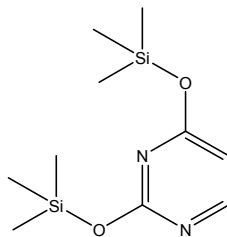
Figure 15: Trimethylsilylated uracil

N^3-Directed Uracil Substitution:

N^3-substitution is primarily facilitated through the direct protection of N^1 (scheme 11). A number of UPGs have been successfully used for the N^1-protection of uracils, including the benzhydryl, 2-(trimethylsilyl)ethoxymethyl (SEM), benzyl, benzyloxymethyl (BOM), methylthiomethyl (MTM), and p-methoxybenzyl (PMB) groups [82, 87, 88].
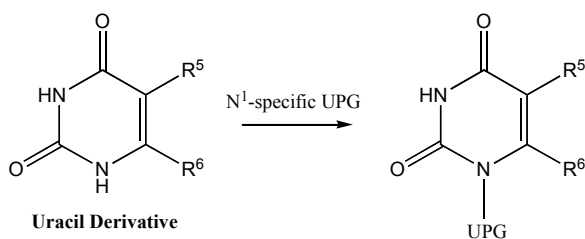
Scheme 11: The N^1-protection of uracils

3.3   Discussion of Uracil Analogue Synthesis

N^1 and N^3 uracil substitutions were the primary synthetic foci for this project, as all necessary 5-substituted uracil starting materials (figure 16) were commercially available.
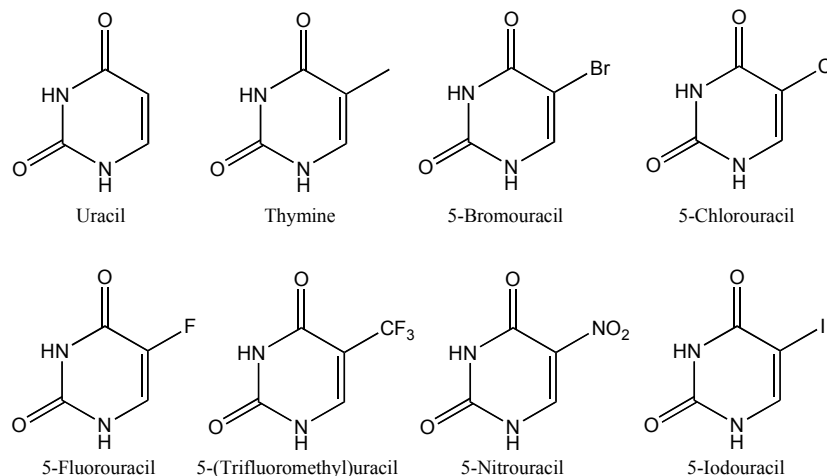
Figure 16: 5-Substituted uracil starting materials

In total, 39 compounds were synthesized and submitted for biological testing. A literature search reveals that 22 of these compounds (**9b**, **9d-f 10a**, **10c-d**, **11a-c**, **12a**, **12d-e**, **13a**, **13c**, **14c**, **15c-d**, **17**, **20**, **21b**, and **24**) are novel. At least 300 mg of each compound were required for biological testing at NIH. In the interest of time, none of the syntheses used for the preparation of these compounds were optimized.

3.3.1 N^1-Pyridinylmethyl Substituted Uracils

Although the SAR conducted on previous compounds revealed that an N^1 benzyl substituent enhances uracil antiseizure activity, the effect of other aromatic functionalities has not yet been investigated. Research [36] suggests that various heterocyclic aromatic ring systems, such as pyridine, furan, thiophene, and pyrrole, can serve as phenyl bioisosteres. Thus, a pyridinylmethyl-substituted group of uracil analogues is an appropriate series to pursue.

The (bromomethyl)pyridine starting materials necessary for the synthesis of N^1-(pyridinylmethyl)uracils are only commercially available as hydrobromide salts. Since these starting materials require neutralization regardless of the method used, simple one-pot base-driven substitutions were viewed to be the most convenient route of synthesis and were used in the production of all pyridinylmethyl-substituted uracil derivatives. Since this type of synthesis does not employ the use of UPGs, Nuclear Overhauser Enhancement Spectroscopy (NOESY) was used to verify that all isolated monoalkylation products were in fact substituted at N^1 rather than N^3. In the NOESY spectrum of each monosubstituted product, strong correlations were exhibited between H^6 of the uracil platform and at least one of the aromatic protons, as well as both methylene protons, of the pyridinylmethyl group.

3.3.1.1 The Synthesis of the 2-Pyridinylmethyl Uracil Derivatives

The methods used for the preparation of the 2-pyridinylmethyl uracil series are shown in schemes 12 and 13:
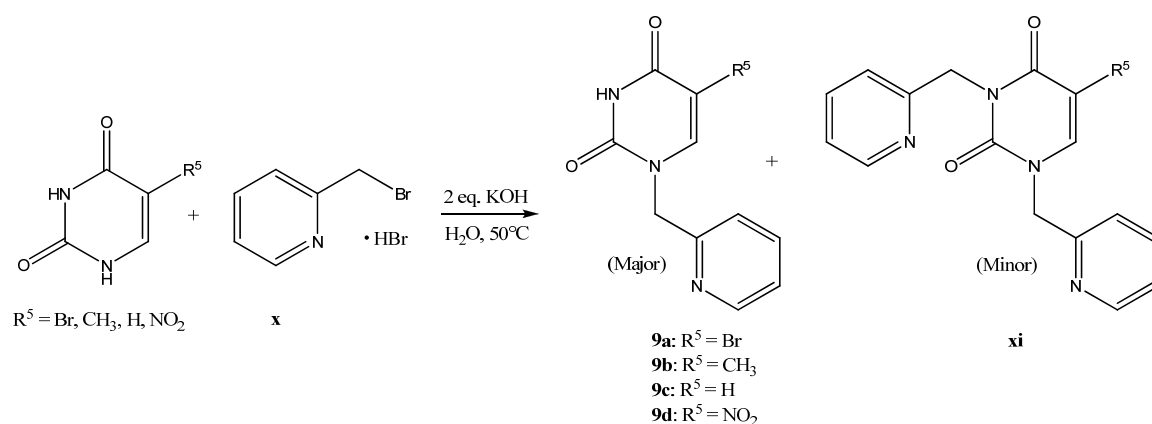
Scheme 12: The synthesis of various N^1-(2-pyridinylmethyl)uracils in water
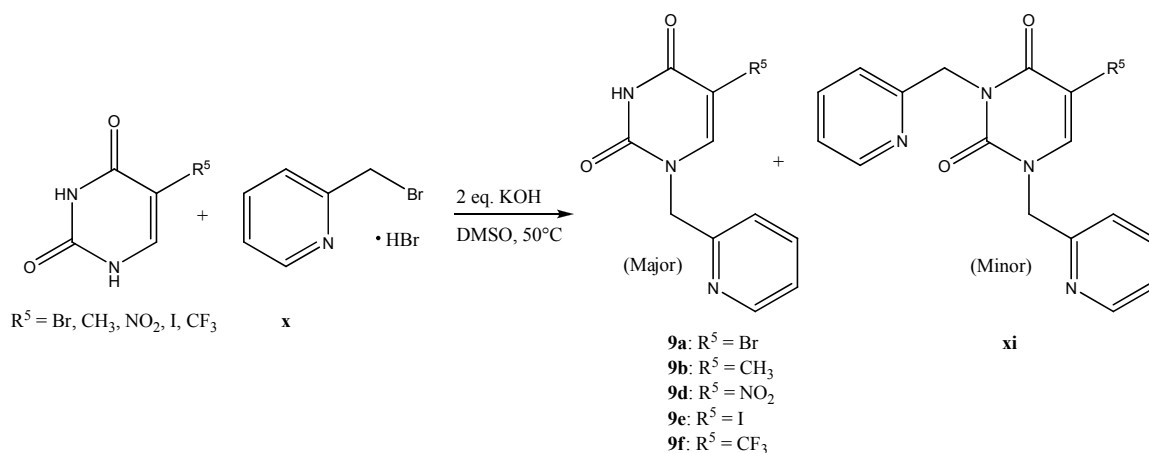
Scheme 13: The synthesis of various N^1-(2-pyridinylmethyl)uracils in DMSO

Due to the low solubility of uracils in many organic solvents, literature procedures

for alkaline uracil N-substitutions typically involve the use of dimethylformamide (DMF)

or dimethylsulfoxide (DMSO). However, these high-boiling polar aprotic solvents are

inconvenient to use, as they are difficult to remove. Furthermore, it has been shown by

previous synthetic work conducted in the Weaver group that under similar conditions to

those in scheme 13, DMSO tends to cause the C^5-bromination of uracils when R^5 = H

(see scheme 14) [89]. Therefore, DMSO cannot be used for the above conversion of

uracil into **9c**.
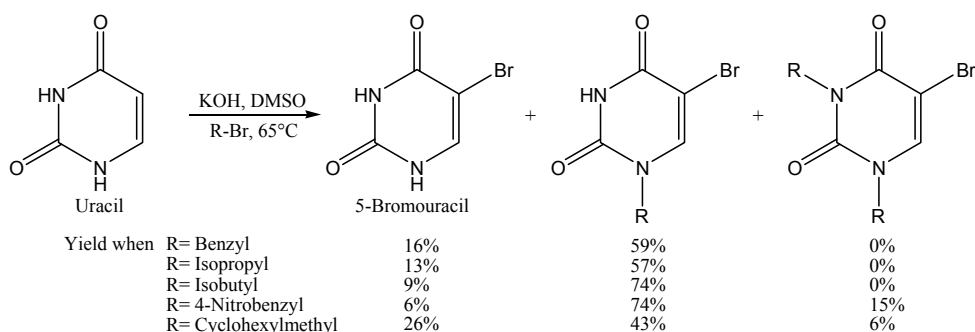
Scheme 14: The C^5-bromination of uracil in DMSO

Although water has been reported as the solvent in some cases [90], aqueous

reactions do not appear to be a widely explored avenue for N-substituted uracil synthesis.

With the intention of further investigating this concept, water was chosen as the solvent

for the first attempt at synthesizing compounds **9a-d**. Potassium hydroxide (KOH) was

used as the base, and the reaction was carried out at 50°C to aid in the dissolution of

starting materials. Thin layer chromatography (TLC) indicated that two products formed

during the reaction. The complete removal of these products from the reaction mixture

required numerous extractions (at least 5 x 30 mL) in a polar solvent combination of 2:1

chloroform-butanol. Analysis of the extracted residue by TLC revealed contamination

with varying amounts of starting material. Purification by silica gel column

chromatography proved to be difficult due to the low solubility of the crude material in

the elution solvent mixture and the small difference in R_f values between the products

($\Delta R_f = 0.04$-0.08). However, pure recrystallized portions of each major product (N^1-

monosubstituted derivatives **9a-d**) were isolated in yields of 16-41% (see table 6).

Accurate yields of the minor N^1,N^3-disubstituted products (**xi** derivatives) were not able

to be obtained, but the formation of these compounds was verified by ^{1}H Nuclear

Magnetic Resonance (NMR) spectroscopy.

Upon switching the solvent of this synthesis from water to DMSO, comparable

yields were obtained. Additionally, the use of DMSO permitted a more facile and much

less time-consuming isolation and purification process. The desired monosubstituted

products were triturated out of the cooled reaction mixture using distilled water and

collected via filtration. Each crude product was essentially free of uracil starting material,

enabling purification to be achieved through recrystallization. The N^1-monosubstituted

derivatives **9a-b** and **9d-f** were again formed as major products, this time in yields of 26-

46% (see table 6). TLC evidence suggests that the disubstituted **xi** derivatives were still formed in minor proportions, but no attempts were made to isolate these products.

Table 6: Reaction times and yields for the preparation of N^1-(2-pyridinylmethyl)uracils

Compound:	Solvent: H$_2$O		Solvent: DMSO	
	Reaction Time:	Yield:	Reaction Time:	Yield:
9a	19 hrs	41%	21 hrs	29%
9b	17 hrs	26%	17 hrs	26%
9c	17 hrs	27%	-	-
9d	18 hrs	16%	19 hrs	44%
9e	-	-	19 hrs	46%
9f	-	-	20 hrs	35%

Uracil N-substitutions in both DMSO and water saw moderate N^1-selectivity, but neither solvent afforded the desired products in very high yield. While DMSO allowed for facile isolation and purification, the work-up for the aqueous reactions was quite tedious. However, water as a solvent did permit an environmentally friendly synthesis of **9c** without the occurrence of bromination, therefore aqueous reactions of this type are worthy of further investigation.

3.3.1.2   The Synthesis of the 3-Pyridinylmethyl Uracil Derivatives

When the synthesis of the 3-pyridinylmethyl uracil series was attempted via scheme 13, a simple method of triturating the desired products out of DMSO was not found. Therefore, in an attempt to avoid the time-consuming work-ups necessitated by both schemes 12 and 13, and also achieve higher yields and N^1-selectivity, an alternative preparation was devised.

Literature suggests that the strong non-nucleophilic base 1,8-diazabicyclo[5.4.0]-undec-7-ene (DBU) can be advantageous as a deprotonating agent for the N-substitution of uracils. Firstly, DBU-uracil complexes are soluble in a wider range of solvents than the

alkali metal salts of uracils, enabling the substitution reactions to be carried out in lower-boiling solvents, such as acetonitrile (CH_3CN). Furthermore, DBU has been reported to permit N^1-regioselectivity during uracil substitution reactions. However, increased equivalents of base and alkyl bromide, as well as high temperatures and longer reaction times, have been shown to produce disubstituted and products [91, 92].

The preparation of various N^1-(3-pyridinylmethyl) uracil derivaties was therefore attempted using DBU in acetonitrile, as depicted in schemes 15-17:
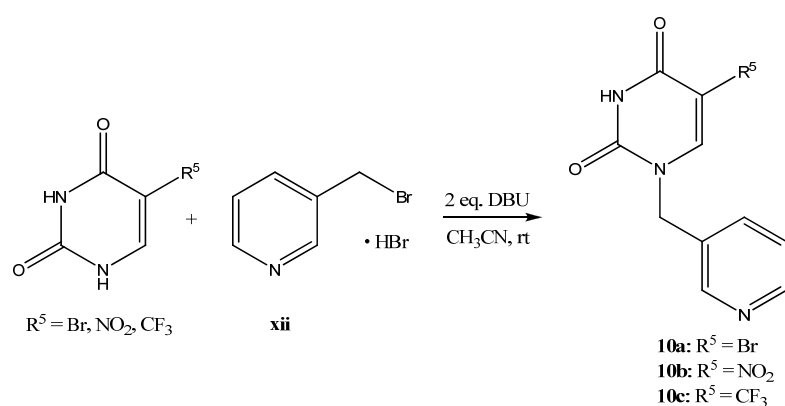
Scheme 15: The preparation of N1-(3-pyridinylmethyl)uracil derivatives **10a-c**
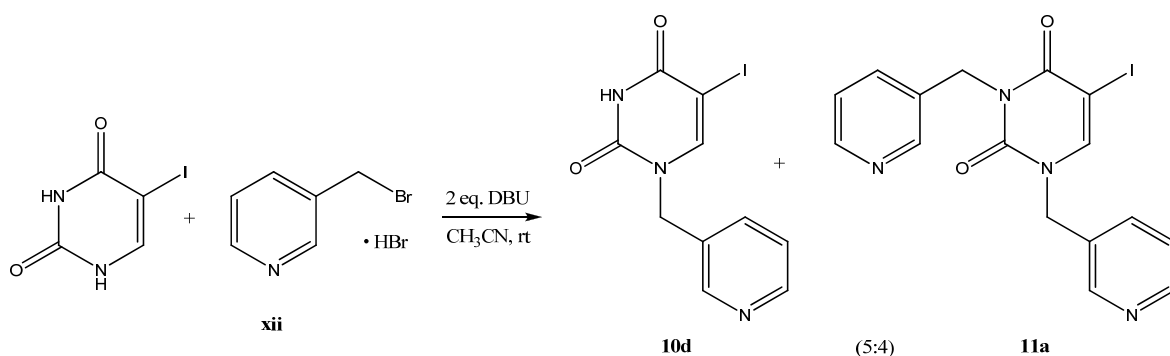
Scheme 16: The preparation of (3-pyridinylmethyl)uracil derivatives **10d** and **11a**

52
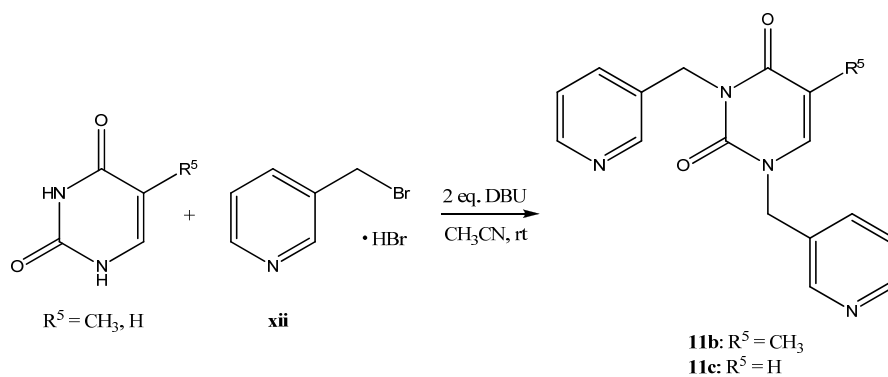
Scheme 17: The preparation of N^1,N^3-disubstituted (3-pyridinylmethyl)uracil derivatives **11b-c**

The desired N^1-monosubstituted derivatives **10a-c** were the sole products formed in reactions of 3-(bromomethyl)pyridine (**xii**) with 5-nitrouracil, 5-(trifluoromethyl)-uracil, and 5-bromouracil, although TLC evidence suggests that very minute traces of the disubstituted product may have formed in the latter case (scheme 15). However, the reaction between **xii** and 5-iodouracil resulted in a 5:4 mixture of monosubstituted (**10d**) and disubstituted (**11a**) products (scheme 16), and only disubstitution occurred in the cases of thymine and uracil (scheme 17).

Upon examination of these findings, a trend emerges: it appears that at room temperature the substitution pattern is greatly influenced by the electron-withdrawing capacity of the C^5 uracil substituent. As can be seen in figure 17, the more strongly electron-withdrawing the substituent is, the more N^1-selective the reaction becomes:
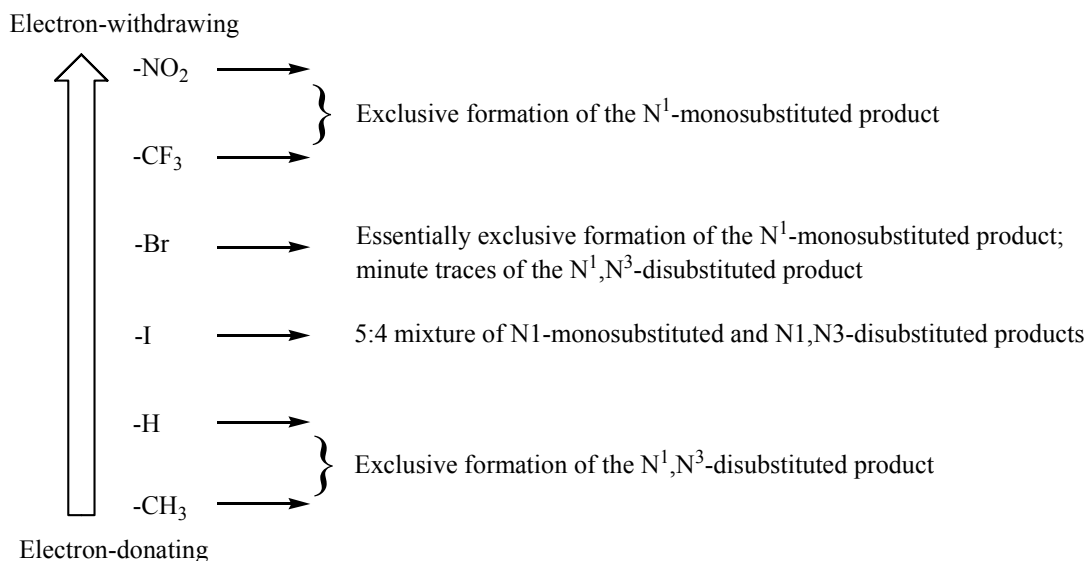
Figure 17: Electronic trend found in schemes 15-17

It is suspected that an electron-withdrawing group (EWG) at C^5 causes inductive

stabilization (and resonance stabilization in the case of 5-nitrouracil) of the N^1-

deprotonated uracil anion, as shown in figure 18. This stabilization likely increases the

acidity of the N^1-H proton, making N^1-substitution more favourable. Indeed, literature

supports this theory; using UV-vis spectroscopy, Privat et al. [93] determined the aqueous

pKa values for C^5-substituted uracils, where $R^5 = NO_2$, F, Cl, Br, I, H, and CH_3, to be

5.30, 7.93, 7.92, 7.91, 8.13, 9.42, and 9.75, respectively.
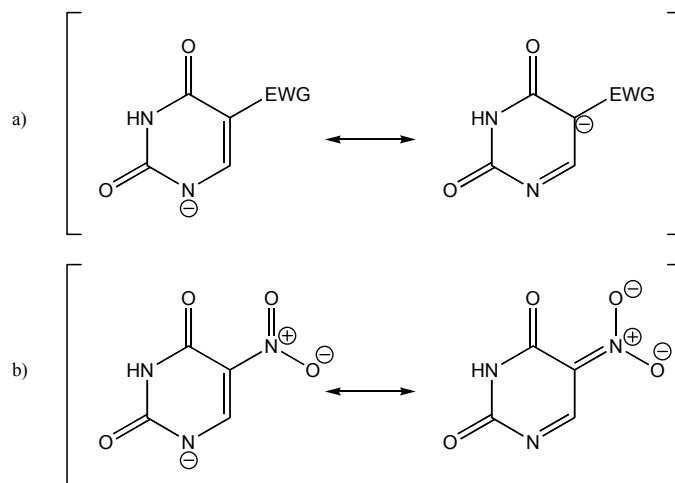
Figure 18: a) Inductive or b) resonance stabalization of the N^1-deprotonated uracil anion when C^5 = EWG

The yields for all synthesized 3-pyridinylmethyl compounds are shown in table 7. Specifically for the monosubstituted derivatives, the yields (19-40%) were comparable to those seen in the 2-pyridinylmethyl series. A facile work-up and purification process could again be employed; the desired products precipitated during the course of the reaction, allowing collection via filtration and purification via recrystallization. As was the case for **10c**, column chromatography performed on the reaction filtrate could provide additional product and improve yields, although solubility issues again complicated this procedure.

Table 7: Reaction times and yields for the preparation of the (3-pyridinylmethyl)uracils **10a-d** and **11a-c**

Compound	Reaction Temperature and Time	Yield
10a	Room temp (24 hrs)	31%
10b	Room temp (24 hrs)	19%
10c	Room temp (17 hrs), reflux (7 hrs)	40%
10d	Room temp (8hrs)	25%
11a	Room temp (8hrs)	20%
11b	Room temp (22 hrs)	34%
11c	Room temp (20 hrs)	29%

It is true that the yields and purification processes involved in the syntheses of the 3-pyridinylmethyl monosubstituted uracils were not an improvement over the methods described in section 4.3.1.1 of this thesis, but the use of DBU as the base and acetonitrile as the solvent did permit a much higher degree of N^1 selectivity in certain cases. Furthermore, it is believed that reduced temperatures and shorter reaction times could improve the N^1-selectivity in the less selective cases, although no attempts have yet been made to do so.

3.3.2   The Benzylated Uracil Derivatives

3.3.2.1   The Synthesis of the N^1-Monobenzylated Uracil Derivatives

N^1-benzylations were carried out using various substituted benzyl bromides (R-Br), a comprehensive list of which is shown in the first column of table 8. All uracil starting materials were protected via trimethylsilylation to promote N^1-substitution. The protection of these 5-substituted uracils with trimethylsilyl (TMS) groups was achieved using methods similar to those of Romeo [85] or Jayakanthan [86].

Romeo et al. accomplished the trimethylsilylation of thymine using N,O-(bis)trimethylsilylacetamide (BSA) in acetonitrile at room temperature. This procedure, followed by the addition of the various substituted benzyl bromides as shown in scheme 18, was used for the preparation of benzylated thymine derivatives **12c**, **13c**, **14c**, and **15c**. Pure portions of these products were afforded in moderate to high yields (59-88%; see table 8). The trimethylsilylation process was relatively rapid (<10 minutes) and did not require the use of heat. Isolation and purification of the desired products could be easily achieved: quenching the cooled reaction mixture with ethanol (EtOH) caused the precipitation of the products, which were then collected via filtration and recrystallized.
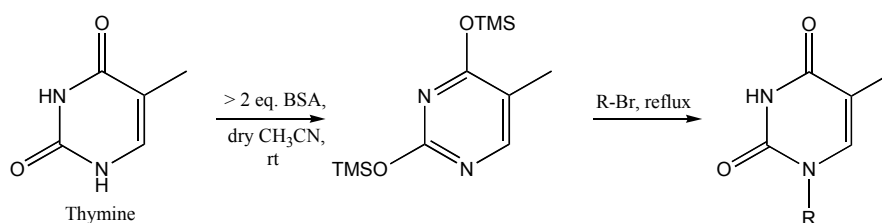
Scheme 18: The trimethylsilylation and benzylation of thymine

The complete dissolution and trimethylsilylation of the remaining uracil starting materials could not be achieved through the procedure outlined above. Thus, Jayaknthan's method (or a variation thereof) was used instead. Jayaknthan et al.

accomplished the trimethylsilylation of uracil by refluxing in 1,1,1,3,3,3-hexamethyl-

disilizane (HMDS) and a catalytic amount of trimethylsilyl chloride (TMSCl). This

procedure, followed by the addition of the various substituted benzyl bromides as shown

in scheme 19, was used for the preparation of the benzylated uracil derivatives **12b**, **13b**,

14b, and **15b**. Pure portions of these products were also afforded in moderate to high

yields (64-98%; see table 8). The trimethylsilylation process was slower than that of

Romeo et al. (~1 hour), and required higher temperatures (135°C).
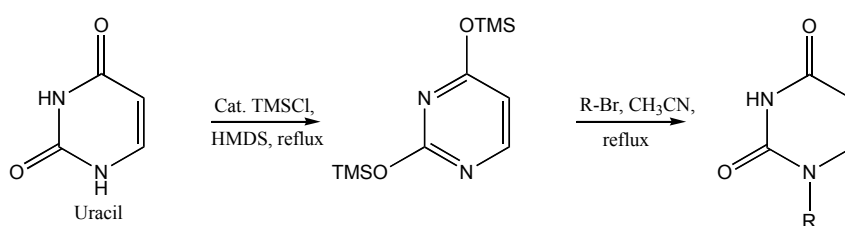
Scheme 19: The trimethylsilylation and benzylation of uracil

Catalytic amounts of TMSCl were insufficient for the complete dissolution and

trimethylsilylation of the 5-halouracil starting materials; it was found that 2 full

equivalents of TMSCl were required. Therefore the 5-bromouracil derivatives (**12a**, **13a**,

14a, **15a**, **16-20**, **18a**, and **iv**), the 5-chlorouracil derivatives (**12e**, **15d**, **21b**, and **22a**), the

5-iodo derivative (**12d**), and the 5-fluoro derivative (**22b**) were all synthesized according

to scheme 20 in yields ranging from 32-96% (see table 8). The trimethylsilylation process

still required approximately 1 hour and temperatures of 135°C.
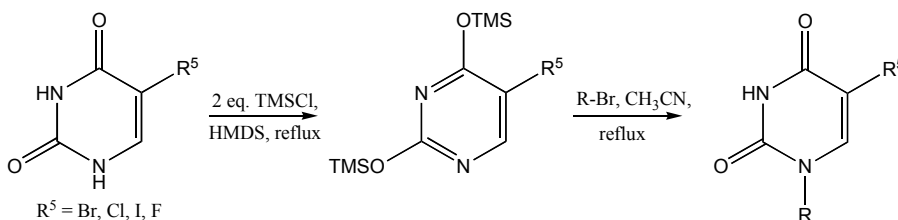
Scheme 20: The trimethylsilylation and benzylation of the 5-halouracils

Table 8: The compound formed, reaction time, and yield for the preparations described in schemes 18-20

R-Br, where R =	5-Bromo-uracil	Uracil	Thymine	5-Iodo-uracil	5-Chloro-uracil	5-Fluoro-uracil
o-CH$_3$C$_6$H$_4$CH$_2$-	**12a** 16 hrs 95%	**12b** 3 hrs 88%	**12c** 2.5 hrs 69%	**12d** 4.5 hrs 84%	**12e** 40 hrs 32%	-
m-CH$_3$C$_6$H$_4$CH$_2$-	**13a** 17 hrs 81%	**13b** 7 hrs 98%	**13c** 2.5 hrs 88%	-	-	-
p-CH$_3$C$_6$H$_4$CH$_2$-	**14a** 21 hrs 87%	**14b** 15 hrs 77%	**14c** 4 hrs 59%	-	-	-
m-BrC$_6$H$_4$CH$_2$-	**15a** 18 hrs 96%	**15b** 15hrs 64%	**15c** 8 hrs 59%	-	**15d** 35 hrs 48%	-
m-OCH$_3$C$_6$H$_4$CH$_2$-	**16** 40 hrs 78%	-	-	-	-	-
p-OCF$_3$C$_6$H$_4$CH$_2$-	**17** 30 hrs 68%	-	-	-	-	-
p-FC$_6$H$_4$CH$_2$-	**18** 22 hrs 74%	-	-	-	-	-
3,4-Cl$_2$C$_6$H$_3$CH$_2$-	**19** 33 hrs 76%	-	-	-	-	-
p-SCH$_3$C$_6$H$_4$CH$_2$-	**20** 40 hrs 63%	-	-	-	-	-
p-ClC$_6$H$_4$CH$_2$-	**21a** 27 hrs 64%	-	-	-	**21b** 48 hrs 79%	-
C$_6$H$_5$CH$_2$-	**vi** 40 hrs 96%	-	-	-	**22a** 30 hrs 67%	**22b** 24 hrs 53%

Overall, the use of TMS-protected uracils did permit substitution to occur with extremely high N[1]-selectivity, as the formation of N[3]-monosubstituted or N[1],N[3]-disubstituted products was not observed in any case. For the most part, yields were moderate or high. Substitution reaction times ranged widely, and appeared to be dependent on both the substituted benzyl bromide and the uracil starting material used.

An obvious trend once more emerged in relation to the electron withdrawing capability of

the C^5-uracil substituent: with the exception of the unsubstituted benzyl series (**vi** and

22a-b), the reaction time increased with the electron-withdrawing strength of R^5. Again,

it is believed the inductive and resonance stabilization of the N^1-anion brought on by a

C^5-EWG plays a role in this pattern, reducing the rate of attack on the R-Br.

3.3.2.2.1   The X-Ray Crystal Structures for Derivatives vi and 22a

Some combination of ^{1}H, ^{13}C, and NOESY NMR spectroscopy and mass

spectrometry (MS) was used to verify the structures of all synthesized uracil derivatives.

However, these methods do not provide detailed information about molecular

conformation—information that is invaluable to the medicinal chemist, as it can be used

to help deduce the mode of action of a drug or the shape of a target receptor.

X-ray crystallography, however, does provide insight into the 3D conformation of

a molecule, and the x-ray crystal structures were obtained for the synthesized uracil

derivatives **vi** and **22a**. The crystal structure and full cell for both of these compounds

were quite similar, so only those for **vi** are shown (figures 19-20). The results are

consistent with the published x-ray crystallographic data for 1-benzyl-5-fluorouracil

(**22b**) [94].
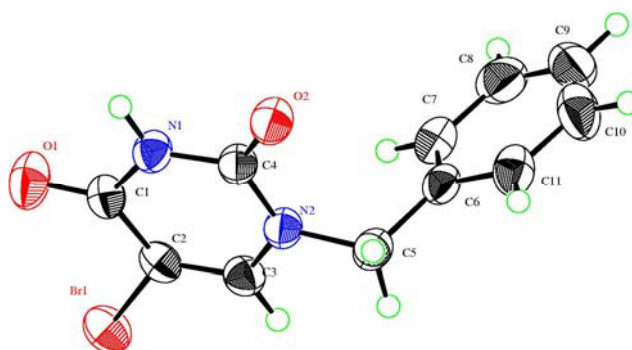
Figure 19: The crystal structure of **vi**

The four C-N bond lengths in the pyrimidine rings of both **vi** and **22a** range from 1.368-1.393 Å. These distances are shorter than typical C-N single bonds (1.443 Å) and longer than typical C=N double bonds (1.269 Å) [94], suggesting the delocalization of electrons between these bonds and the uracil C=O bonds. The C-N bonds (1.471-1.474 Å) and C-C bonds (both 1.510 Å) between the uracil and phenyl rings in each structure indicate that there is no conjugation between the two rings in either case.
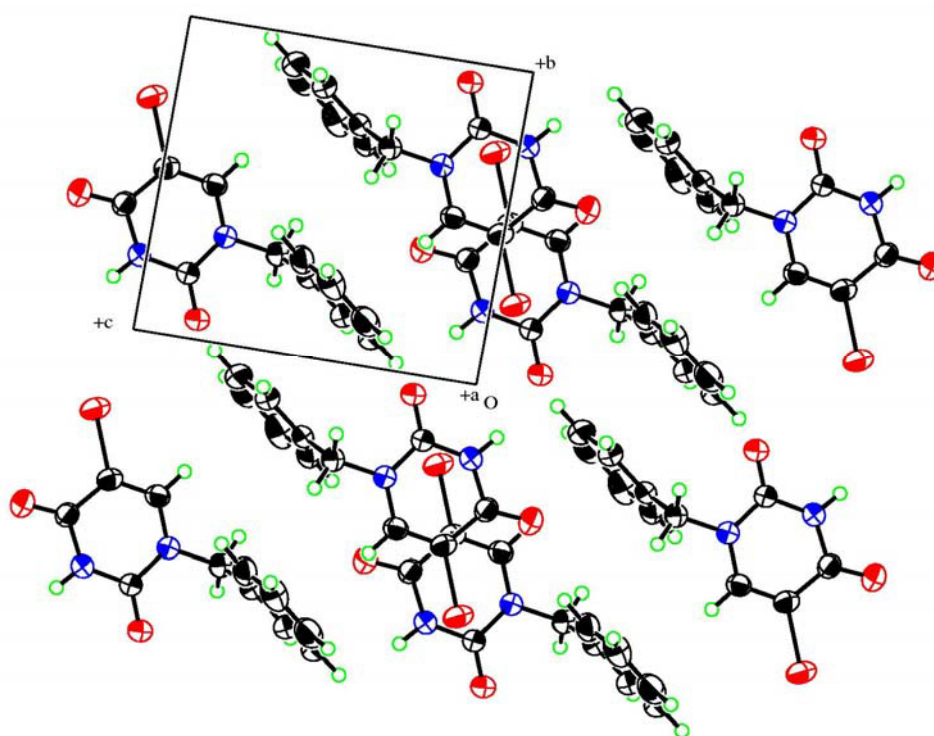
Figure 20: The full cell of **vi**

An interesting series of intermolecular interactions appear in the full cell of these two compounds. As can be seen from the full cell of **vi** (figure 20), there is evidence of weak C^2=O---H-Ph interactions and of π-π stacking between aromatic ring systems. A dimer-like structure also appears to form via N^3-H---O=C^2 hydrogen bonding between adjacent pyrimidine ring systems. Finally, a charge transfer interaction seems to exist

between the C-Br (or C-Cl) bond of one pyrimidine ring and the centrosymmetrically related pyrimidine ring system.

3.3.2.2 The Synthesis of the N^1-Benzylated, N^3-Alkylated Uracil Derivatives

The syntheses of compounds **23** and **24** were successfully completed using derivative **iv** as the uracil starting material (see schemes 21 and 22). The N^3-deprotonation of **iv** was accomplished with DBU, and subsequent N^3-substitution was achieved through the addition of an excess of the appropriate alkyl iodide. Column chromatography was used for isolation without complication, as each product was completely soluble in the elution solvent mixture. Recrystallization afforded pure **23** and **24** in yields of 98% and 75%, respectively.
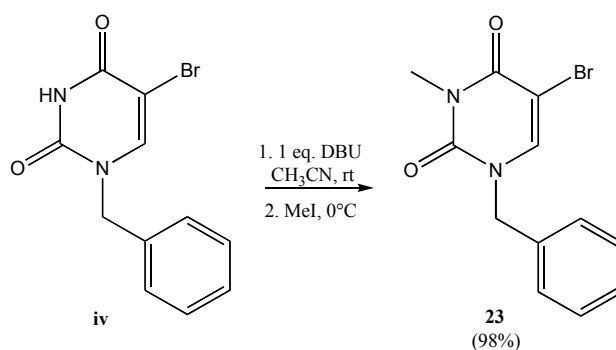
Scheme 21: The preparation of **23** from **vi**
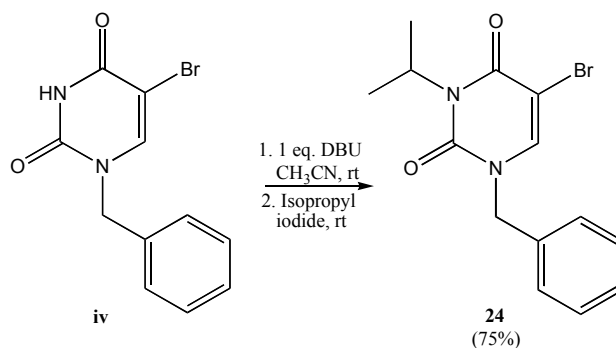
Scheme 22: The preparation of **24** from **vi**

Chapter 4: Experimental Procedures for the Synthesis of Uracils

4.1   **General Methods**

All starting materials were obtained from commercial sources (Sigma-Aldrich, TCI America, or Oakwood Products) and were used as received. Dry acetonitrile was purchased from EMD Chemicals. Every reaction was carried out under an inert atmosphere (argon). All ^{1}H, ^{13}C, and NOESY NMR spectra were recorded with a Bruker AV 500 MHz NMR spectrometer using DMSO- d_6 from Sigma-Aldrich as the solvent, and signals are reported as delta (δ) values in parts per million relative to tetramethyl-silane (TMS). Mass spectrometry data was obtained by Dr. Xaio Feng using a Bruker microTOF Focus orthogonal ESI-TOF mass spectrometer, and all masses were detected as sodium adducts $(M+Na)^+$ or protonated molecular ions $(M+H)^+$. X-ray crystallographic data was obtained by Dr. Stanley Cameron using a high-speed Rigaku ACF5R four-circle diffractometer (see appendicies A and B for further experimental details). Melting points were taken with a Mel-Temp II Laboratory Device, and all reported values are uncorrected. All thin layer chromatography (TLC) was performed using glass supported TLC plates from Sigma-Aldrich with a particle size of 17 μm, and all compounds were visualized on the plates using ultraviolet (UV) light.

4.2   **Experimental Procedures**

4.2.1   **Synthesis of 5-bromo-1-(2-pyridinylmethyl)uracil (9a)**

Method 1:

A solution of KOH (0.1500 g, 2.67 mmol), 5-bromouracil (0.2501 g, 1.31 mmol), and 2-(bromomethyl)pyridine (0.3403 g, 1.34 mmol) was stirred in distilled water (7 mL, 388.7 mmol) at 50°C. The reaction was left to proceed for 19 hours, while being

monitored by TLC for completion. After cooling the reaction to room temperature, the product was extracted into 2:1 chloroform-butanol (6 x 30 mL) and dried over magnesium sulfate. The solvent was then removed by rotary evaporation and the product was isolated from the resulting residue by column chromatography using 6% methanol (MeOH) in dichloromethane (DCM). Multiple recrystallizations in isopropanol afforded pure **9a** as a flakey white solid (0.1499 g, 0.53 mmol, 41% yield).

Method 2:

A solution of potassium hydroxide (KOH; 0.3506 g, 6.25 mmol), 5-bromouracil (0.6001 g, 3.14 mmol), and 2-(bromomethyl)pyridine (0.8011 g, 3.17 mmol) was stirred in dimethyl sulfoxide (DMSO) (15 mL, 211.3 mmol) at 50°C. The reaction was left to proceed for 21 hours, while being monitored by thin layer chromatography (TLC) for completion. After cooling the reaction to room temperature, the product was triturated out by adding 20 mL of distilled water and allowing the mixture to stir in an ice bath for 20 minutes. The precipitate was collected by suction filtration, washed with cold water, and recrystallized multiple times in isopropanol to afford pure **9a** as a flakey white solid (0.2569 g, 0.911 mmol, 29% yield); mp: 141-142°C (decomposed); ^{1}H NMR (DMSO-d_6): δ 11.84 (s, 1H), 8.53 (dd, J = 1.0 Hz, J = 5.0 Hz, 1H), 8.35 (s, 1H), 7.82-7.79 (m, 1H), 7.37-7.31 (m, 2H), 5.02 (s, 2H); ^{13}C NMR (DMSO-d_6): δ 159.8, 155.3, 150.4, 149.2, 146.4, 137.0, 122.8, 121.6, 94.5, 52.0; HRMS calculated for $C_{10}H_8BrN_3O_2Na^+$: 303.9692, found: 303.9671.

4.2.2   Synthesis of 5-methyl-1-(2-pyridinylmethyl)uracil (9b)

Method 1:

A solution of KOH (0.2307 g, 4.11 mmol), thymine (0.2501 g, 1.98 mmol), and 2-(bromomethyl)pyridine (0.5005 g, 1.98 mmol) was stirred in distilled water (7 mL, 388.7 mmol) at 50°C. The reaction was left to proceed for 17 hours, while being monitored by TLC for completion. After cooling the reaction to room temperature, the product was extracted into 2:1 chloroform-butanol (6 x 30 mL) and dried over magnesium sulfate. The solvent was then removed by rotary evaporation and the product was isolated from the resulting residue by column chromatography using 6% MeOH in DCM. Multiple recrystallizations in isopropanol afforded pure **9a** as a fine white needle-like solid (0.1108 g, 0.51 mmol, 26% yield).

Method 2:

A solution of KOH (0.4501 g, 8.02 mmol), 5-methyluracil (0.5002 g, 3.97 mmol), and 2-(bromomethyl)pyridine (1.0102 g, 3.99 mmol) was stirred in DMSO (15 mL, 211.3 mmol) at 50°C. The reaction was left to proceed for 17 hours, while being monitored by TLC for completion. After cooling the reaction to room temperature, the product was triturated out by adding 20 mL of distilled water and allowing the mixture to stir in an ice bath for 20 minutes. The precipitate was collected by suction filtration, washed with cold water, and recrystallized multiple times in isopropanol to afford pure **9b** as a fine white needle-like solid (0.2233 g, 1.03 mmol, 26% yield); mp: 207-210°C; ^{1}H NMR (DMSO-d_6): δ 11.32 (s, 1H), 8.53 (ddd, J = 0.8 Hz, J = 1.5 Hz, J = 2.5 Hz, 1H), 7.81-7.78 (m, 1H), 7.62 (d, J = 2.5 Hz, 1H), 7.32-7.29 (m, 2H), 4.95 (s, 2H), 1.78 (d, J = 1.0 Hz, 3H); ^{13}C NMR (DMSO- d_6): δ 164.4, 155.9, 151.0, 149.2, 142.2, 136.9, 122.6, 121.5, 108.4, 53.0, 11. 9; HRMS calculated for $C_{11}H_{11}N_3O_2Na^+$: 240.0743, found: 240.0738.

4.2.3   **Synthesis of 1-(2-pyridinylmethyl)uracil (9c)**

A solution of KOH (0.5003 g, 8.92 mmol), uracil (0.5001 g, 4.46 mmol), and 2-(bromomethyl)pyridine (1.1403 g, 4.45 mmol) was stirred in distilled water (7 mL, 388.7 mmol) at 50°C. The reaction was left to proceed for 17 hours, while being monitored by TLC for completion. After cooling the reaction to room temperature, the product was extracted into 2:1 chloroform-butanol (6x 30 mL) and dried over magnesium sulfate. The solvent was then removed by rotary evaporation and the product was isolated from the resulting residue by column chromatography using 6% MeOH in DCM. Multiple recrystallizations in distilled water afforded pure **9c** as a white crystalline solid (0.2409 g, 1.19 mmol, 27% yield); mp: 185-186°C (lit. 186°C [95]); ^{1}H NMR (DMSO- d_6): δ 11.33 (s, 1H), 8.56-8.55 (m, 1H), 7.88-7.85 (m, 1H), 7.75 (d, J = 8.0 Hz, 1H), 5.63 (dd, J = 2.0 Hz, J = 7.5 Hz, 1H), 5.01 (s, 1H); ^{13}C NMR (DMSO- d_6): δ 163.9, 155.7, 151.0, 149.4, 149.2, 146.6, 136.9, 122.6, 121.5, 100.8, 51.8; HRMS calculated for $C_{10}H_9N_3O_2H^+$: 204.0768, found: 204.0769.

4.2.4   **Synthesis of 5-nitro-1-(2-pyridinylmethyl)uracil (9d)**

Method 1:

A solution of KOH (0.1802 g, 3.21 mmol), 5-nitrouracil (0.2503 g, 1.59 mmol), and 2-(bromomethyl)pyridine (0.4110 g, 1.62 mmol) was stirred in distilled water (7 mL, 388.7 mmol) at 50°C. The reaction was left to proceed for 18 hours, while being monitored by TLC for completion. After cooling the reaction to room temperature, the product was extracted into 2:1 chloroform-butanol (7 x 30 mL) and dried over magnesium sulfate. The solvent was then removed by rotary evaporation and the product was isolated from the resulting residue by column chromatography using 6% MeOH in

DCM. Multiple recrystallizations in 50% acetonitrile in EtOH afforded pure **9d** as an off white powery white solid (0.0616 g, 0.25 mmol, 16% yield).

Method 2:

A solution of KOH (0.3604 g, 6.42 mmol), 5-nitrouracil (0.4992 g, 3.18 mmol), and 2-(bromomethyl)pyridine (0.8210 g, 3.25 mmol) was stirred in DMSO (15 mL, 211.3 mmol) at 50°C. The reaction was left to proceed for 19 hours, while being monitored by TLC for completion. After cooling the reaction to room temperature, the product was triturated out by adding 20 mL of distilled water and allowing the mixture to stir in an ice bath for 20 minutes. The precipitate was then collected by suction filtration, washed with cold water, and recrystallized multiple times in 50% acetonitrile in EtOH to afford pure **9e** as an off-white powdery solid (0.3443 g, 1.39 mmol, 44% yield); mp: 257-260°C (decomposed); ^{1}H NMR (DMSO- d$_6$): δ 12.13 (s, 1H), 9.48 (s, 1H), 8.53 (ddd, $J = 0.5$ Hz, $J = 1.5$ Hz, $J = 2.0$ Hz, 1H), 7.84-7.81 (m, 1H), 7.46 (d, $J = 8.0$ Hz, 1H), 7.35-7.33 (m, 1H), 5.23 (s, 2H); ^{13}C NMR (DMSO- d$_6$): δ 155.1, 154.4, 151.7, 149.3, 149.2, 137.1, 124.8, 122.9, 121.8, 52.8; HRMS calculated for C$_{10}$H$_8$N$_4$O$_4$Na$^+$: 271.0438, found: 271.0431.

4.2.5   Synthesis of 5-iodo-1-(2-pyridinylmethyl)uracil (9e)

A solution of KOH (0.3601 g, 6.42 mmol), 5-iodouracil (0.7509 g, 3.16 mmol), and 2-(bromomethyl)pyridine (0.8010 g, 3.17 mmol) was stirred in DMSO (15 mL, 211.3 mmol) at 50°C. The reaction was left to proceed for 19 hours, while being monitored by TLC for completion. After cooling the reaction to room temperature, the product was triturated out by adding 20 mL of distilled water and allowing the mixture to stir in an ice

bath for 20 minutes. The precipitate was collected by suction filtration, washed with cold water, and recrystallized multiple times in isopropanol to afford pure **9c** as a clear crystalline solid (0.4768 g, 1.44 mmol, 46% yield); mp: 216-218°C (decomposed); ^{1}H NMR (DMSO- d_6): δ 11.70 (s, 1H), 8.53-8.52 (m, 1H), 8.33 (s, 1H), 7.81-7.78 (m, 1H), 7.34 (d, J = 7.8 Hz, 1H), 7.33-7.30 (m, 1H), 5.01 (s, 2H); ^{13}C NMR (DMSO- d_6): δ 161.2, 155.5, 150.9, 150.7, 149.2, 137.0, 122.7, 121.6, 68.0, 51.9; HRMS calculated for $C_{10}H_8IN_3O_2$: , found: 351.9541.

4.2.6   Synthesis of 5-trifluoromethyl-1-(2-pyridinylmethyl)uracil (9f)

A solution of KOH (0.1607 g, 2.86 mmol), 5-trifluoromethyluracil (0.0.2503 g, 1.39 mmol), and 2-(bromomethyl)pyridine (0.3602 g, 1.42 mmol) was stirred in DMSO (10 mL, 140.8 mmol) at 50°C. The reaction was left to proceed for 20 hours, while being monitored by TLC for completion. After cooling the reaction to room temperature, the product was triturated out by adding 20 mL of distilled water and allowing the mixture to stir in an ice bath for 20 minutes. The precipitate was collected by suction filtration, washed with cold water, and recrystallized multiple times in 33% MeOH in EtOH to afford pure **9d** as small thin clear crystals (0.1311 g, 0.483 mmol, 35% yield); mp: 224-226°C; ^{1}H NMR (DMSO- d_6): δ 11.91 (s, 1H), 8.57 (s, 1H), 8.53 (d, J = 4.4 Hz, 1H), 7.83-7.79 (m, 1H), 7.40 (d, J = 7.8 Hz, 1H), 7.34-7.31 (m, 1H), 5.11 (s, 2H); ^{13}C NMR (DMSO- d_6): δ 159.58, 155.01, 150.17, 149.22, 148.5-148.5 (m, 1C), 137.0, 122.8 (q, J = 268.9 Hz, 1C), 122.8, 121.7, 101.9 (q, J = 32.1 Hz, 1C), 52.34; HRMS calculated for $C_{11}H_8F_3N_3O_2Na^+$: 294.0461, found: 294.0468.

4.2.7　　　　Synthesis of 5-bromo-1-(3-pyridinylmethyl)uracil (10a)

A suspension of 5-bromouracil (1.5007 g, 7.86 mmol) was stirred in acetonitrile

(35 mL, 662.5 mmol) and DBU (1.25 mL, 8.36 mmol) at room temperature until it

completely dissolved (10 minutes). 3-(Bromomethyl)pyridine (2.3801 g, 9.41 mmol) was

then added, followed by additional DBU (1.25 mL, 8.36 mmol). The resulting solution

was left to stir for 24 hours at room temperature, while being monitored by TLC for

completion. The precipitate formed during the reaction was removed by suction filtration,

washed with cold acetonitrile, and recrystallized multiple times in mixture of 15%

acetonitrile, 20% MeOH, and 65% water to afford pure **10a** as transparent yellow needle-

like crystals (0.6852 g, 2.43 mmol, 31% yield); mp: 230-231°C; ^{1}H NMR (DMSO- d_6): δ

11.88 (s, 1H), 8.60 (d, J = 1.8 Hz, 1H), 8.52 (dd, J = 1.5 Hz, J = 4.8 Hz, 1H), 8.45 (s,

1H), 7.77 (d, J = 7.9 Hz, 1H), 7.40 (dd, J = 0.6 Hz, J = 4.8 Hz, 1H), 4.91 (s, 2H); ^{13}C

NMR (DMSO- d_6): δ 159.6, 150.4, 149.1, 149.0, 145.1, 135.5, 132.1, 123.7, 95.4, 48.7;

HRMS calculated for $C_{10}H_8BrN_3O_2H^+$: 281.9873, found: 281.9876.

4.2.8　　　　Synthesis of 5-nitro-1-(3-pyridinylmethyl)uracil (10b)

A suspension of 5-nitrouracil (0.5013 g, 3.19 mmol) was stirred in acetonitrile (15

mL, 283.9 mmol) and DBU (0.50 mL, 3.34 mmol) at room temperature until it

completely dissolved (10 minutes). 3-(Bromomethyl)pyridine (1.0402 g, 4.11 mmol) was

then added, followed by additional DBU (0.50 mL, 3.34 mmol). The resulting solution

was left to stir for 24 hours at room temperature, while being monitored by TLC for

completion. The precipitate formed during the reaction was removed by suction filtration,

washed with cold acetonitrile, and recrystallized multiple times in 20% MeOH in

acetonitrile to afford pure **10b** as an off-white powder (0.1536 g, 0.619 mmol, 19%

yield); mp: 285-287°C (decomposed); ^{1}H NMR (DMSO- d_6): δ 12.10 (s, 1H), 9.54 (s, 1H), 8.65 (s, 1H), 8.53 (d, $J = 3.9$ Hz, 1H), 7.84 (d, $J = 7.9$ Hz, 1H), 7.40 (dd, $J = 4.8$ Hz, $J = 7.8$ Hz, 1H), 5.10 (s, 2H); ^{13}C NMR (DMSO- d_6): δ 155.1, 150.7, 149.4, 149.3, 149.1, 135.7, 131.3, 125.5, 123.6, 50.0; HRMS calculated for $C_{10}H_8N_4O_4H^+$: 249.0618, found: 249.0618.

4.2.9 Synthesis of 5-trifluoromethyl-1-(3-pyridinylmethyl)uracil (10c)

A suspension of 5-trifluoromethyluracil (1.1005 g, 6.11 mmol) was stirred in acetonitrile (15 mL, 283.9 mmol) and DBU (0.90 mL, 6.02 mmol) at room temperature until it completely dissolved (10 minutes). 3-(Bromomethyl)pyridine (2.0002 g, 7.91 mmol) was then added, followed by additional DBU (0.95 mL, 9.35 mmol). The resulting solution was left to stir for 17 hours at room temperature and then refluxed for 7 hours, while being monitored by TLC for completion. After cooling the reaction to room temperature, the precipitate formed was removed by suction filtration and washed with cold acetonitrile. The solvent was removed from the filtrate by rotary evaporation, and additional product was isolated from the residue by column chromatography using a solvent system of 5% MeOH, 15% hexanes, 50% DCM, and 30% EtOAc. All portions of the recovered product were combined and recrystallized multiple times in 15% acetonitrile in MeOH to afford pure **10c** as a powdery white solid (0.6699 g, 2.47 mmol, 40% yield); mp: 225-226°C; ^{1}H NMR (DMSO- d_6): δ 11.93 (s, 1H), 8.65 (s, 1H), 8.61 (d, $J = 1.6$ Hz, 1H), 8.52 (dd, $J = 1.3$ Hz, $J = 4.7$ Hz, 1H), 7.79 (d, $J = 7.9$ Hz, 1H), 7.40 (dd, $J = 4.8$ Hz, $J = 7.8$ Hz, 1H), 5.00 (s, 2H); ^{13}C NMR (DMSO- d_6): δ 159.4, 150.2, 149.1, 149.0, 147.4-147.3 (m, 1C), 135.5, 131.8, 123.6, 122.7 (q, $J = 269.1$ Hz, 1C), 102.7 (q, $J = 32.0$ Hz, 1C), 49.3; HRMS calculated for $C_{11}H_8F_3N_3O_2H^+$: 272.0641, found: 272.0636.

4.2.10   Synthesis of 5-iodo-1-(3-pyridinylmethyl)uracil (10d) and 5-iodo-1,3-di(3-pyridinylmethyl)uracil (11a)

A suspension of 5-iodouracil (1.2003 g, 5.04 mmol) was stirred in acetonitrile (25 mL, 473.2 mmol) and DBU (0.80 mL, 5.35 mmol) at room temperature until it completely dissolved (20 minutes). 3-(Bromomethyl)pyridine (1.5307 g, 6.05 mmol) was then added, followed by additional DBU (0.80 mL, 5.35 mmol). The resulting solution was left to stir for 8 hours at room temperature, while being monitored by TLC. The solvent was then removed by rotary evaporation and a mixture of products **10b** and **11c** was isolated from the residue by column chromatography using a solvent system of 8.5% MeOH in DCM. To separate the products, a suspension of the collected solid was stirred in 20 mL of 1M NaOH for 10 minutes. The undissolved material was then collected by suction filtration and washed with iced cold water, while the filtrate was set aside for later use. The filtered solid was recrystallized multiple times in 25% acetonitrile in distilled water to afford pure **11a** as a fluffy white solid (0.2571 g, 0.612 mmol, 20% yield); mp: 209-211°C; ^{1}H NMR (DMSO- d_6): δ 8.60 (d, J = 1.8 Hz, 1H), 8.54 (s, 1H), 8.53-8.52 (m, 2H), 8.47 (dd, J = 1.4 Hz, J = 4.7 Hz, 1H), 7.78 (d, J = 7.9 Hz, 1H), 7.67 (d, J = 7.9 Hz, 1H), 7.39 (dd, J = 4.8 Hz, J = 7.7 Hz, 1H), 7.34 (dd, J = 4.8 Hz, J = 7.7 Hz, 1H), 5.04 (s, 2H), 4.98 (s, 2H); ^{13}C NMR (DMSO- d_6): δ 160.0, 151.0, 149.2, 149.1, 149.0, 148.6, 148.5, 135.6, 135.5, 132.4, 132.0, 123.7, 123.5, 67.9, 49.9, 43.0; HRMS calculated for $C_{16}H_{13}IN_4O_2H^+$: 421.0156, found: 421.0155.

The filtrate that had been set aside was then neutralized using 1M HCl. The resulting precipitate was removed by suction filtration, washed with ice cold water, and recrystallized multiple times in a mixture of 20% acetonitrile, 10% MeOH, and 70%

distilled water to afford pure **10d** as a fluffy white solid (0.4099 g, 1.25 mmol, 25%

yield); mp: 241-242°C (decomposed); ^{1}H NMR (DMSO- d$_6$): δ 11.72 (s, 1H), 8.59 (d, $J =$

1.7 Hz, 1H), 8.52 (dd, $J = 1.4$ Hz, $J = 4.7$ Hz, 1H), 8.43 (s, 1H), 7.76-7.74 (m, 1H), 7.39

(dd, $J = 4.8$ Hz, $J = 7.6$ Hz, 1H), 4.91 (s, 2H); ^{13}C NMR (DMSO- d$_6$): δ 161.0, 150.8,

149.6, 149.1, 149.0, 135.5, 132.3, 123.7, 69.0, 48.5; HRMS calculated for

$C_{10}H_8IN_3O_2H^+$: 329.9734, found: 329.9728.

4.2.11   Synthesis of 5-methyl-1,3-di(3-pyridinylmethyl)uracil (11b)

A suspension of 5-methyluracil (0.2509 g, 1.99 mmol) was stirred in acetonitrile

(15 mL, 284.0 mmol) and DBU (0.35 mL, 2.34 mmol) at room temperature until it

completely dissolved (10 minutes). 3-(Bromomethyl)pyridine (0.6511 g, 2.57 mmol) was

then added, followed by additional DBU (0.25 mL, 1.67 mmol). The resulting solution

was left to stir for 22 hours while being monitored by TLC for completion. The solvent

was then removed from the reaction mixture by rotary evaporation. After the product was

isolated from the resulting residue by column chromatography using a solvent system of

9% MeOH in DCM, it was recrystallized multiple times in distilled water to afford pure

11b as a powdery white solid (0.1352 g, 0.438 mmol, 34% yield); mp: 98-100°C; ^{1}H

NMR (DMSO- d$_6$): δ 8.59 (d, $J = 1.8$ Hz, 1H), 8.52-8.51 (m, 2H), 8.46 (dd, $J = 1.6$ Hz, J

$= 4.8$ Hz, 1H), 7.84 (d, $J = 1.2$ Hz, 1H), 7.76-7.73 (m, 1H), 7.68-7.66 (m, 1H), 7.39 (ddd,

$J = 0.6$ Hz, $J = 4.8$ Hz, $J = 7.8$ Hz, 1H), 7.33 (ddd, $J = 0.6$ Hz, $J = 4.8$ Hz, $J = 7.8$ Hz,

1H), 5.02 (s, 2H), 4.95 (s, 2H), 1.84 (d, $J = 1.1$ Hz, 3H); ^{13}C NMR (DMSO- d$_6$): δ 163.0,

151.1, 149.2, 149.0, 149.0, 148.5, 140.3, 135.5, 135.4, 132.8, 132.3, 123.7, 123.5, 108.5,

49.3, 41.6, 12.6; HRMS calculated for $C_{17}H_{16}N_4O_2H^+$: 309.1346, found: 309.1332.

4.2.12   Synthesis of 1,3-di(3-pyridinylmethyl)uracil (11c)

A suspension of uracil (0.6002 g, 5.35 mmol) was stirred in acetonitrile (15 mL, 283.9 mmol) and DBU (0.80 mL, 5.35 mmol) at room temperature until it completely dissolved (10 minutes). 3-(Bromomethyl)pyridine (1.76 g, 6.96 mmol) was then added, followed by additional DBU (0.80 mL, 5.35 mmol). The resulting solution was left to stir for 20 hours while being monitored by TLC for completion. The solvent was then removed from the reaction mixture by rotary evaporation. After the product was isolated from the resulting residue by column chromatography using a solvent system of 10% MeOH in dichloromethane (DCM), it was recrystallized multiple times in 5% hexanes in ethyl acetate (EtOAc) to afford pure **11c** as a fluffy white solid (0.3010 g, 1.02 mmol, 29% yield); mp: 228-231°C; ^{1}H NMR (DMSO- d_6): δ 8.59 (d, J = 1.8 Hz, 1H), 8.53-8.51 (m, 2H), 8.46 (dd, J = 1.6 Hz, J = 4.8 Hz, 1H), 7.96 (d, J = 7.9 Hz, 1H), 7.75 (m, 1H), 7.66 (m, 1H), 7.39 (ddd, J = 7.8 Hz, J = 4.8 Hz, J = 0.66 Hz, 1H), 7.34 (ddd, J = 7.8 Hz, J = 4.8 Hz, J = 0.7 Hz, 1H), 5.84 (d, J = 7.9 Hz, 1H), 5.00 (s, 2H), 4.98 (s, 2H); ^{13}C NMR (DMSO- d_6): δ 162.3, 151.2, 149.1, 149.0, 148.5, 144.5, 135.5, 135.4, 132.7, 132.2, 123.7, 123.5, 100.8, 49.6, 41.3; HRMS calculated for $C_{16}H_{14}N_4O_2H^+$: 295.1190, found: 295.1174.

4.2.13   Synthesis of 5-bromo-1-(2-methylbenzyl)uracil (12a)

A suspension of 5-bromouracil (0.5009 g, 2.62 mmol) in HMDS (4 mL, 19.2 mmol) and TMSCl (0.70 mL, 5.53 mmol) was refluxed at 135°C until all components dissolved (~1 hour). The reaction mixture was then cooled to 60°C, whereupon dry acetonitrile (5 mL, 94.6 mmol) and 2-methylbenzyl bromide (0.45 mL, 3.37 mmol) were

added. This mixture was refluxed at 90°C for 16 hours, while being monitored by TLC for completion. The reaction was then cooled to 60°C and quenched with 10 mL of EtOH (added drop-wise). The resulting precipitate was collected by suction filtration, washed with cold EtOH, and recrystallized multiple times in 25% acetonitrile in EtOH to afford pure **12a** as a clear crystalline solid (0.7329 g, 2.48 mmol, 95% yield); mp: 223-225°C (decomposed); ^{1}H NMR (DMSO- d$_6$): δ 11.76 (s, 1H), 8.19 (s, 1H), 7.23-7.18 (m, 3H), 7.02 (d, J = 6.3 Hz, 1H), 4.89 (s, 2H), 2.30 (s, 3H); ^{13}C NMR (DMSO- d$_6$): δ 159.7, 150.4, 145.2, 135.4, 134.4, 130.2, 127.4, 126.2, 95.2, 48.6, 18.7; HRMS calculated for $C_{12}H_{11}BrN_2O_2Na^+$: 316.9896, found: 316.9906.

4.2.14   Synthesis of 1-(2-methylbenzyl)uracil (12b)

A suspension of uracil (0.5002 g, 4.46 mmol) in HMDS (5 mL, 23.9 mmol) and TMSCl (0.10 mL, 0.79 mmol) was refluxed at 135°C until all components dissolved (~1 hour). The reaction mixture was then cooled to 60°C, whereupon dry acetonitrile (5 mL, 94.6 mmol) and 2-methylbenzyl bromide (0.65 mL, 4.87 mmol) were added. This mixture was refluxed at 90°C for 3 hours, while being monitored by TLC for completion. The reaction was then cooled to 60°C and quenched with 10 mL of EtOH (added drop-wise). The resulting precipitate (crude **12b**) was collected by suction filtration and washed with cold EtOH. The solvent was removed from the filtrate by rotary evaporation, and additional product was isolated from the residue by column chromatography using a solvent system of 7% MeOH in DCM. All portions of the recovered product were combined and recrystallized multiple times in 25% acetonitrile in EtOH to afford pure **12b** as powdery white crystals (0.8495 g, 3.93 mmol, 88% yield); mp: 226-228°C; ^{1}H NMR (DMSO- d$_6$): δ 11.33 (s, 1H), 7.60 (d, J = 7.8 Hz, 1H), 7.23-

7.20 (m, 3H), 6.98 (d, J = 6.4 Hz, 1H), 5.63 (d, J = 7.8 Hz, 1H), 4.89 (s, 2H), 2.29 (s, 3H); ^{13}C NMR (DMSO- d$_6$): δ 163.7, 151.1, 145.5, 135.5, 134.7, 130.3, 127.4, 126.3, 126.1, 101.4, 48.1, 18.7; HRMS calculated for C$_{12}$H$_{12}$N$_2$O$_2$Na$^+$: 239.0791, found: 239.0784.

4.2.15　　　Synthesis of 5-methyl-1-(2-methylbenzyl)uracil (12c)

A suspension of 5-methyluracil (0.5005 g, 3.97 mmol) in dry acetonitrile (7 mL, 132.5 mmol) and BSA (2.20 mL, 9.00 mmol) was stirred at room temperature until all components dissolved (~10 minutes). Subsequently, 2-methylbenzyl bromide (0.60 mL, 4.49 mmol) was added. This mixture was then refluxed at 90°C for 2.5 hours, while being monitored by TLC for completion. After cooling the reaction to 60°C and quenching with 15 mL of EtOH (added drop-wise), the solvent was removed by rotary evaporation. The resulting residue was then recrystallized multiple times in 30% acetonitrile in EtOH to afford pure **12c** as small white crystals (0.6299 g, 2.74 mmol, 69% yield); mp: 221-223°C; ^{1}H NMR (DMSO- d$_6$): δ 11.38 (s, 1H), 7.48 (d, J = 1.1 Hz, 1H), 7.22-7.18 (m, 3H), 6.97 (d, J = 6.0 Hz, 1H), 4.85 (s, 2H), 2.30 (s, 3H), 1.77 (d, J = 0.9 Hz, 3H); ^{13}C NMR (DMSO- d$_6$): δ 164.3, 151.1, 141.2, 135.5, 134.8, 130.2, 127.3, 126.2, 126.1, 109.1, 47.8, 18.7, 12.0; HRMS calculated for C$_{13}$H$_{14}$N$_2$O$_2$Na$^+$: 253.0947, found: 253.0939.

4.2.16　　　Synthesis of 5-iodo-1-(2-methylbenzyl)uracil (12d)

A suspension of 5-iodouracil (0.7502 g, 3.15 mmol) in HMDS (5 mL, 23.9 mmol) and TMSCl (0.80 mL, 6.32 mmol) was refluxed at 135°C until all components dissolved (~1 hour). The reaction mixture was then cooled to 60°C, whereupon dry acetonitrile (5 mL, 94.6 mmol) and 2-methylbenzyl bromide (0.45 mL, 3.37 mmol) were added. This mixture was refluxed at 90°C for 4.5 hours, while being monitored by TLC for

completion. The reaction was then cooled to 60°C and quenched with 10 mL of EtOH (added drop-wise). The resulting precipitate was collected by suction filtration, washed with cold EtOH, and recrystallized multiple times in 5% EtOH in acetonitrile to afford pure **12d** as a clear crystalline solid (0.8994 g, 2.63 mmol, 84% yield); mp: 240-242°C; ^{1}H NMR (DMSO- d_6): δ 11.77 (s, 1H), 8.18 (s, 1H), 7.22-7.20 (m, 3H), 6.99-6.97 (m, 1H), 4.89 (s, 2H), 2.29 (s, 3H); ^{13}C NMR (DMSO- d_6): δ 161.1, 150.8, 149.8, 135.4, 134.5, 130.3, 127.4, 126.2, 126.1, 68.8, 48.4, 18.7; HRMS calculated for $C_{12}H_{11}IN_2O_2Na^+$: 364.9757, found: 364.9749.

4.2.17   Synthesis of 5-chloro-1-(2-methylbenzyl)uracil (12e)

A suspension of 5-chlorouracil (1.0001 g, 6.82 mmol) in HMDS (9 mL, 43.2 mmol) and TMSCl (1.75 mL, 13.8 mmol) was refluxed at 135°C until all components dissolved (~1 hour). The reaction mixture was then cooled to 60°C, whereupon dry acetonitrile (8 mL, 151.4 mmol) and 2-methylbenzyl bromide (0.95 mL, 7.11 mmol) were added. This mixture was refluxed at 90°C for 40 hours, while being monitored by TLC for completion. The reaction was then cooled to 60°C and quenched with 15 mL of EtOH (added drop-wise). The resulting precipitate was collected by suction filtration, washed with cold EtOH, and recrystallized multiple times in 30% acetonitrile in EtOH to afford pure **12e** as a clear crystalline solid (0.5395 g, 2.15 mmol, 32% yield); mp: 227-229°C; ^{1}H NMR (DMSO- d_6): δ 11.93 (s, 1H), 8.12 (s, 1H), 7.23-7.17 (m, 3H), 7.03 (d, J = 6.46 Hz, 1H), 4.89 (s, 2H), 2.30 (s, 3H); ^{13}C NMR (DMSO- d_6): δ 159.5, 150.2, 142.8, 135.5, 134.3, 130.3, 127.5, 126.2, 126.2, 106.7, 48.6, 18.7; HRMS calculated for $C_{12}H_{11}ClN_2O_2Na^+$: 273.0401, found: 273.0400.

4.2.18   Synthesis of 5-bromo-1-(3-methylbenzyl)uracil (13a)

A suspension of 5-bromouracil (0.5012 g, 2.62 mmol) in HMDS (5 mL, 23.9 mmol) and TMSCl (0.70 mL, 5.53 mmol) was refluxed at 135°C until all components dissolved (~1 hour). The reaction mixture was then cooled to 60°C, whereupon dry acetonitrile (5 mL, 94.6 mmol) and 3-methylbenzyl bromide (0.45 mL, 3.33 mmol) were added. This mixture was refluxed at 90°C for 17 hours, while being monitored by TLC for completion. The reaction was then cooled to 60°C and quenched with 10 mL of EtOH (added drop-wise). The resulting precipitate was collected by suction filtration, washed with cold EtOH, and recrystallized multiple times in 25% acetonitrile in EtOH to afford pure **13a** as a clear crystalline solid (0.6231 g, 2.11 mmol, 81% yield); mp: 197-199°C; ^{1}H NMR (DMSO- d_6): δ 11.82 (s, 1H), 8.35 (s, 1H), 7.27-7.24 (m, 1H), 7.14-7.11 (m, 3H), 4.85 (s, 2H), 2.30 (s, 3H); ^{13}C NMR (DMSO- d_6): δ 159.6, 150.4, 145.2, 137.9, 136.4, 128.6, 128.4, 128.1, 124.6, 95.1, 50.6, 21.0; HRMS calculated for $C_{12}H_{11}BrN_2O_2Na+$: 316.9896, found: 316.9897.

4.2.19   Synthesis of 1-(3-methylbenzyl)uracil (13b)

A suspension of uracil (0.5004 g, 4.46 mmol) in HMDS (5 mL, 23.9 mmol) and TMSCl (0.10 mL, 0.79 mmol) was refluxed at 135°C until all components dissolved (~1 hour). The reaction mixture was then cooled to 60°C, whereupon dry acetonitrile (5 mL, 94.6 mmol) and 3-methylbenzyl bromide (0.65 mL, 4.81 mmol) were added. This mixture was refluxed at 90°C for 7 hours, while being monitored by TLC for completion. The reaction was then cooled to 60°C and quenched with 10 mL of EtOH (added drop-wise). The resulting precipitate (crude **13b**) was collected by suction filtration and washed with cold EtOH. The solvent was removed from the filtrate by rotary

evaporation, and additional product was isolated from the residue by column chromatography using a solvent system of 6% MeOH in DCM. All portions of the recovered product were combined and recrystallized multiple times in 25% acetonitrile in EtOH to afford pure **10b** as a clear crystalline solid (0.9480 g, 4.38 mmol, 98% yield); mp: 147-148°C (lit. 149-150°C [96]); ^{1}H NMR (DMSO- d_6): δ 11.33 (s, 1H), 7.75 (d, $J =$ 7.8 Hz, 1H), 7.27-7.24 (m, 1H), 7.13-7.08 (m, 3H), 5.60 (d, $J =$ 7.8 Hz, 1H), 4.84 (s, 2H), 2.30 (s, 3H); ^{13}C NMR (DMSO- d_6): δ 163.7, 151.0, 145.66, 137.9, 136.8, 128.6, 128.3, 128.0, 124.5, 101.3, 50.2, 21.0; HRMS calculated for $C_{12}H_{12}N_2O_2Na^+$: 239.0791, found: 239.0784.

4.2.20 Synthesis of 5-methyl-1-(3-methylbenzyl)uracil (13c)

A suspension of 5-methyluracil (0.5007 g, 3.97 mmol) in dry acetonitrile (7 mL, 132.5 mmol) and BSA (2.20 mL, 9.00 mmol) was stirred at room temperature until all components dissolved (~10 minutes). Subsequently, 3-methylbenzyl bromide (0.60 mL, 4.44 mmol) was added. This mixture was then refluxed at 90°C for 2.5 hours, while being monitored by TLC for completion. After cooling the reaction to 60°C and quenching with 15 mL of EtOH (added drop-wise), the solvent was removed by rotary evaporation. The resulting residue was then recrystallized multiple times in isopropanol to afford pure **13c** as a clear crystalline solid (0.8011 g, 3.48 mmol, 88% yield); mp: 166-169°C; ^{1}H NMR (DMSO- d_6): δ 11.33 (s, 1H), 7.62 (d, $J =$ 1.1 Hz, 1H), 7.27-7.23 (m, 1H), 7.12-7.08 (m, 3H), 4.80 (s, 2H), 2.30 (s, 3H), 1.76 (d, $J =$ 0.9 Hz, 3H); ^{13}C NMR (DMSO- d_6): δ 164.3, 151.0, 141.3, 137.8, 137.0, 128.6, 128.3, 128.0, 124.5, 109.0, 49.9, 21.0, 12.0; HRMS calculated for $C_{13}H_{14}N_2O_2^+$: 253.0947, found: 253.0939.

4.2.21 Synthesis of 5-bromo-1-(4-methylbenzyl)uracil (14a)

A suspension of 5-bromouracil (0.5002 g, 2.62 mmol) in HMDS (5 mL, 23.9 mmol) and TMSCl (0.70 mL, 5.53 mmol) was refluxed at 135°C until all components dissolved (~1 hour). The reaction mixture was then cooled to 60°C, whereupon dry acetonitrile (5 mL, 94.6 mmol) and 4-methylbenzyl bromide (0.6220 g, 3.36 mmol) were added. This mixture was refluxed at 90°C for 21 hours, while being monitored by TLC for completion. The reaction was then cooled to 60°C and quenched with 10 mL of EtOH (added drop-wise). The resulting precipitate was collected by suction filtration (crude 14a) and washed with cold EtOH. The solvent was removed from the filtrate by rotary evaporation, and additional product was isolated from the residue by column chromatography using a solvent system of 25% EtOAc, 15% hexanes, and 60% DCM. All portions of the recovered product were combined and recrystallized multiple times in 25% acetonitrile in EtOH to afford pure 14a as a clear crystalline solid (0.6753 g, 2.29 mmol, 87% yield); mp: 231-232°C (decomposed) (lit. 201-203°C [97]); ^{1}H NMR (DMSO- d_6): δ 11.83 (s, 1H), 8.34 (s, 1H), 7.23 (d, J = 8.0 Hz, 2H), 7.18 (d, J = 8.0 Hz, 2H), 4.84 (s, 2H), 2.29 (s, 3H); ^{13}C NMR (DMSO- d_6): δ 159.6, 150.3, 145.1, 137.08, 133.5, 129.2, 127.6, 95.0, 50.4, 20.7; HRMS calculated for $C_{12}H_{11}BrN_2O_2Na^+$: 316.9896, found: 316.9882.

4.2.22 Synthesis of 1-(4-methylbenzyl)uracil (14b)

A suspension of uracil (0.5011 g, 4.47 mmol) in HMDS (5 mL, 23.9 mmol) and TMSCl (0.10 mL, 0.79 mmol) was refluxed at 135°C until all components dissolved (~1 hour). The reaction mixture was then cooled to 60°C, whereupon dry acetonitrile (5 mL,

94.6 mmol) and 4-methylbenzyl bromide (0.9080 g, 4.91 mmol) were added. This mixture was refluxed at 90°C for 15 hours, while being monitored by TLC for completion. The reaction was then cooled to 60°C and quenched with 10 mL of EtOH (added drop-wise). The resulting precipitate (crude **14b**) was collected by suction filtration and washed with cold EtOH. The solvent was removed from the filtrate by rotary evaporation, and additional product was isolated from the residue by column chromatography using a solvent system of 30% EtOAc, 15% hexanes, 5% MeOH, and 50% DCM. All portions of the recovered product were combined and recrystallized multiple times in 30% acetonitrile in EtOH to afford pure **14b** as flakey white solid (0.7480 g, 3.46 mmol, 77% yield); mp: 170-172°C; ^{1}H NMR (DMSO- d$_6$): δ 11.31 (s, 1H), 7.74 (d, J = 7.9 Hz, 1H), 7.21-7.16 (m, 4H), 5.59 (d, J = 7.8 Hz, 1H), 4.82 (s, 2H), 2.28 (s, 3H); ^{13}C NMR (DMSO- d$_6$): δ 163.7, 151.0, 145.6, 137.0, 133.9, 129.2, 127.6, 101.3, 50.0, 20.7; HRMS calculated for $C_{12}H_{12}N_2O_2Na^+$: 239.0791, found: 239.0788.

4.2.23   Synthesis of 5-methyl-1-(4-methylbenzyl)uracil (14c)

A suspension of 5-methyluracil (0.5005 g, 3.97 mmol) in dry acetonitrile (7 mL, 132.5 mmol) and BSA (2.20 mL, 9.00 mmol) was stirred at room temperature until all components dissolved (~10 minutes). Subsequently, 4-methylbenzyl bromide (0.8060 g, 4.35 mmol) was added. This mixture was then refluxed at 90°C for 4 hours, while being monitored by TLC for completion. After cooling the reaction to 60°C and quenching with 15 mL of EtOH (added drop-wise), the solvent was removed by rotary evaporation. The resulting residue was then recrystallized multiple times in 25% acetonitrile in EtOH to afford pure **14c** as thin clear crystals (0.5394 g, 2.34 mmol, 59% yield); mp: 222-224°C; ^{1}H NMR (DMSO- d$_6$): δ 11.32 (s, 1H), 7.61 (d, J = 1.1 Hz, 1H), 7.21-7.16 (m, 4H), 4.79

(s, 2H), 2.29 (s, 3H), 1.75 (d, $J = 0.8$ Hz, 3H); ^{13}C NMR (DMSO- d$_6$): δ 164.2, 151.0, 141.2, 136.9, 134.1, 129.2, 127.5, 109.0, 49.7, 20.7, 11.9; HRMS calculated for C$_{13}$H$_{14}$N$_2$O$_2$H$^+$: 231.1128, found: 231.1118.

4.2.24   Synthesis of 5-bromo-1-(3-bromobenzyl)uracil (15a)

A suspension of 5-bromouracil (0.5013 g, 2.62 mmol) in HMDS (5 mL, 23.9 mmol) and TMSCl (0.70 mL, 5.53 mmol) was refluxed at 135°C until all components dissolved (~1 hour). The reaction mixture was then cooled to 60°C, whereupon dry acetonitrile (5 mL, 94.6 mmol) and 3-bromobenzyl bromide (0.8401 g, 3.36 mmol) were added. This mixture was refluxed at 90°C for 18 hours, while being monitored by TLC for completion. The reaction was then cooled to 60°C and quenched with 10 mL of EtOH (added drop-wise). The resulting precipitate was collected by suction filtration (crude **12a**) and washed with cold EtOH. The solvent was removed from the filtrate by rotary evaporation, and additional product was isolated from the residue by column chromatography using a solvent system of 20% EtOAc, 4% MeOH, 56 % hexanes, and 20% DCM. All portions of the recovered product were combined and recrystallized multiple times in 25% acetonitrile in EtOH to afford pure **15a** as a clear crystalline solid (0.9005 g, 2.50 mmol, 96% yield); mp: 188-190°C; ^{1}H NMR (DMSO- d$_6$): δ 11.87 (s, 1H), 8.40 (s, 1H), 7.58 (s, 1H), 7.53-7.51 (m, 1H), 7.35-7.34 (m, 2H), 4.87 (s, 2H); ^{13}C NMR (DMSO- d$_6$): δ 159.7, 150.4, 145.1, 139.2, 130.8, 130.7, 130.4, 126.7, 121.8, 95.4, 50.2; HRMS calculated for C$_{11}$H$_8$Br$_2$N$_2$O$_2$Na$^+$: 380.8845, found: 380.8854.

4.2.25   Synthesis of 1-(3-bromobenzyl)uracil (15b)

A suspension of uracil (0.5001 g, 4.46 mmol) in HMDS (5 mL, 23.9 mmol) and TMSCl (0.10 mL, 0.79 mmol) was refluxed at 135°C until all components dissolved (~1

hour). The reaction mixture was then cooled to 60°C, whereupon dry acetonitrile (5 mL, 94.6 mmol) and 3-bromobenzyl bromide (1.2260 g, 4.91 mmol) were added. This mixture was refluxed at 90°C for 15 hours, while being monitored by TLC for completion. The reaction was then cooled to 60°C and quenched with 10 mL of EtOH (added drop-wise). The resulting precipitate was collected by suction filtration, washed with cold EtOH, and recrystallized multiple times in 35% acetonitrile in EtOH to afford pure **15b** as small transparent yellow crystals (0.8059 g, 2.87 mmol, 64% yield); mp: 168-170°C; ^{1}H NMR (DMSO- d_6): δ 11.37 (s, 1H), 7.80 (d, J = 7.9 Hz, 1H), 7.53-7.51 (m, 2H), 7.36-7.30 (m, 2H), 5.63 (d, J = 7.8 Hz, 1H), 4.87 (s, 2H); ^{13}C NMR (DMSO- d_6): δ 163.7, 151.0, 145.6, 139.6, 130.9, 130.6, 130.3, 126.5, 121.8, 101.5, 49.7; HRMS calculated for $C_{11}H_9BrN_2O_2Na^+$: 302.9740, found: 302.9725.

4.2.26   Synthesis of 1-(3-bromobenzyl)-5-methyluracil (15c)

A suspension of 5-methyluracil (0.5010 g, 3.97 mmol) in dry acetonitrile (7 mL, 132.5 mmol) and BSA (2.20 mL, 9.00 mmol) was stirred at room temperature until all components dissolved (~10 minutes). Subsequently, 3-bromobenzyl bromide (1.0901 g, 4.36 mmol) was added. This mixture was then refluxed at 90°C for 8 hours, while being monitored by TLC for completion. The reaction was then cooled to 60°C and quenched with 15 mL of EtOH (added drop-wise). The resulting precipitate was collected by suction filtration, washed with cold EtOH, and recrystallized multiple times in 35% acetonitrile in EtOH to afford pure **15c** as a powdery white solid (0.6892 g, 2.34 mmol, 59% yield); mp: 171-172°C; ^{1}H NMR (DMSO- d_6): δ 11.37 (s, 1H), 7.67 (d, J = 0.9 Hz, 1H), 7.53-7.51 (m, 2H), 7.35-7.30 (m, 2H), 4.83 (s, 2H), 1.76 (d, J = 0.4 Hz, 3H); [13]C

NMR (DMSO- d_6): δ 164.2, 151.0, 141.2, 139.8, 130.9, 130.5, 130.3, 126.5, 121.8, 109.2, 49.5, 12.0; HRMS calculated for $C_{12}H_{11}BrN_2O_2Na^+$: 316.9896, found: 316.9905.

4.2.27 Synthesis of 1-(3-bromobenzyl)-5-chlorouracil (15d)

A suspension of 5-chlorouracil (1.0006 g, 6.82 mmol) in HMDS (9 mL, 43.2 mmol) and TMSCl (1.75 mL, 13.8 mmol) was refluxed at 135°C until all components dissolved (~1.5 hour). The reaction mixture was then cooled to 60°C, whereupon dry acetonitrile (7 mL, 132.5 mmol) and 3-bromobenzyl bromide (1.7910, 7.17 mmol) were added. This mixture was refluxed at 90°C for 35 hours, while being monitored by TLC for completion. After cooling the reaction to 60°C and quenching with 10 mL of EtOH (added drop-wise), the solvent was removed by rotary evaporation. The product was isolated from the resulting residue by column chromatography using a solvent system of 20% EtOAc, 55% hexanes, 5% MeOH, and 20% DCM. The product was then recrystallized multiple times in 30% acetonitrile in EtOH to afford pure **15d** as a transparent yellow crystalline solid (1.0307 g, 3.27 mmol, 48% yield); mp: 180-182°C; ^{1}H NMR (DMSO- d_6): δ 11.90 (s, 1H), 8.33 (s, 1H), 7.59 (s, 1H), 7.56-7.51 (m, 1H), 7.35-7.34 (m, 2H), 4.87 (s, 2H); ^{13}C NMR (DMSO- d_6): δ 159.5, 150.2, 142.8, 139.1, 130.8, 130.7, 130.4, 126.7, 121.8, 106.8, 50.3; HRMS calculated for $C_{11}H_8BrClN_2O_2Na^+$: 336.9350, found: 336.9337.

4.2.28 Synthesis of 5-bromo-1-(3-methoxybenzyl)uracil (16)

A suspension of 5-bromouracil (1.0011 g, 5.24 mmol) in HMDS (10 mL, 47.8 mmol) and TMSCl (1.35 mL, 10.7 mmol) was refluxed at 135°C until all components dissolved (~1 hour). The reaction mixture was then cooled to 60°C, whereupon dry acetonitrile (10 mL, 189.2 mmol) and 3-methoxybenzyl bromide (0.80 mL, 5.71 mmol)

were added. This mixture was refluxed at 90°C for 40 hours, while being monitored by

TLC for completion. The reaction was then cooled to 60°C and quenched with 20 mL of

EtOH (added drop-wise). The resulting precipitate was collected by suction filtration,

washed with cold EtOH, and recrystallized multiple times in 30% acetonitrile in EtOH to

afford pure **16** as thin clear crystals (1.2740 g, 4.09 mmol, 78% yield); mp: 177-179°C;

^{1}H NMR (DMSO- d_6): δ 11.84 (s, 1H), 8.36 (s, 1H), 7.29 (m, 1H), 6.91-6.88 (m, 3H),

4.85 (s, 2H), 3.75 (s, 3H); ^{13}C NMR (DMSO- d_6): δ 159.6, 159.4, 150.4, 145.1, 138.0,

129.9, 119.6, 113.5, 113.0, 95.1, 55.1, 50.6; HRMS calculated for $C_{12}H_{11}BrN_2O_3Na^+$:

332.9845, found: 332.9835.

4.2.29   Synthesis of 5-bromo-1-(4-trifluoromethoxybenzyl)uracil (17)

A suspension of 5-bromouracil (0.6775 g, 3.55 mmol) in HMDS (5 mL, 38.4

mmol) and TMSCl (0.90 mL, 7.10 mmol) was refluxed at 135°C until all components

dissolved (~1 hour). The reaction mixture was then cooled to 60°C, whereupon dry

acetonitrile (5 mL, 94.6 mmol) and 4-trifluoromethoxybenzyl bromide (0.60 mL, 3.73

mmol) were added. This mixture was refluxed at 90°C for 30 hours, while being

monitored by TLC for completion. After the reaction was cooled to 60°C and quenched

with 10 mL of EtOH (added drop-wise), the solvent was removed by rotary evaporation.

The product was isolated from the resulting residue by column chromatography using a

solvent system of 30% EtOAc, 15% hexanes, and 55% DCM. The product was then

recrystallized multiple times in 25% acetonitrile in EtOH to afford pure **17** as a clear

crystalline solid (0.8808 g, 2.41 mmol, 68% yield); mp: 220-222°C; ^{1}H NMR (DMSO-

d_6): δ 11.88 (s, 1H), 8.42 (s, 1H), 7.47 (d, $J = 8.7$ Hz, 2H), 7.37 (d, $J = 8.1$ Hz, 2H), 4.91

(s, 2H); ^{13}C NMR (DMSO- d_6): δ 159.7, 150.4, 147.8, 145.2, 136.0, 129.6, 121.2, 120.1

(q, $J = 256.3$ Hz, 1C); HRMS calculated for $C_{12}H_8BrF_3N_2O_3Na^+$: 386.9563, found: 386.9554.

4.2.30 Synthesis of 5-bromo-1-(4-fluorobenzyl)uracil (18)

A suspension of 5-bromouracil (0.5009 g, 2.62 mmol) in HMDS (5 mL, 23.9 mmol) and TMSCl (0.70 mL, 5.53 mmol) was refluxed at 135°C until all components dissolved (~1 hour). The reaction mixture was then cooled to 60°C, whereupon dry acetonitrile (5 mL, 94.6 mmol) and 4-fluorobenzyl bromide (0.42 mL, 3.37 mmol) were added. This mixture was refluxed at 90°C for 22 hours, while being monitored by TLC for completion. After cooling the reaction to 60°C and quenching with 10 mL of EtOH (added drop-wise), the solvent was removed by rotary evaporation. The product was isolated from the resulting residue by column chromatography using a solvent system of 30% EtOAc, 30% hexanes, and 40% DCM. The product was then recrystallized multiple times in 30% acetonitrile in EtOH to afford pure **18** as a clear crystalline solid (0.5793 g, 1.94 mmol, 74% yield); mp: 225-227°C; ^{1}H NMR (DMSO- d_6): δ 11.85 (s, 1H), 8.39 (s, 1H), 7.41 (dd, $J = 5.5$ Hz, $J = 8.8$ Hz, 2H) 7.20 (m, 2H), 4.86 (s, 2H); ^{13}C NMR (DMSO- d_6): δ 161.7 (d, $J = 243.7$ Hz, 1C), 159.6, 150.4, 145.0, 132.7 (d, $J = 2.6$ Hz, 1C), 129.9 (d, $J = 8.3$ Hz, 2C), 115.4 (d, $J = 21.4$ Hz, 2C), 95.2, 50.1; HRMS calculated for $C_{11}H_8BrFN_2O_2Na^+$: 320.9645, found: 320.9648.

4.2.31 Synthesis of 5-bromo-1-(3,4-dichlorobenzyl)uracil (19)

A suspension of 5-bromouracil (0.5009 g, 2.62 mmol) in HMDS (5 mL, 23.9 mmol) and TMSCl (0.70 mL, 5.53 mmol) was refluxed at 135°C until all components dissolved (~1 hour). The reaction mixture was then cooled to 60°C, whereupon dry acetonitrile (5 mL, 94.6 mmol) and 3,4-dichlorobenzyl bromide (0.50 mL, 3.49 mmol)

were added. This mixture was refluxed at 90°C for 33 hours, while being monitored by TLC for completion. The reaction was then cooled to 60°C and quenched with 10 mL of EtOH (added drop-wise). The resulting precipitate was collected by suction filtration (crude **19**) and washed with cold EtOH. The solvent was removed from the filtrate by rotary evaporation, and additional product was isolated from the residue by column chromatography using a solvent system of 15% hexanes, 5% MeOH, and 80% DCM. All portions of the recovered product were combined and recrystallized multiple times in 25% acetonitrile in EtOH to afford pure **19** as a white crystalline solid (0.6956 g, 1.99 mmol, 76% yield); mp: 143-145°C; ^{1}H NMR (DMSO- d_6): δ 11.86 (s, 1H), 8.39 (s, 1H), 7.66 (d, J = 2.0 Hz, 1H), 7.63 (d, J = 8.3 Hz, 1H), 7.34 (dd, J = 2.1 Hz, J = 8.3 Hz, 1H), 4.87 (s, 2H); ^{13}C NMR (DMSO- d_6): δ 159.6, 150.4, 145.0, 137.5, 131.1, 130.8, 130.4, 129.8, 128.0, 95.4, 49.8; HRMS calculated for $C_{11}H_7BrCl_2N_2O_2Na^+$: 370.8960, found: 370.8957.

4.2.32   Synthesis of 5-bromo-1-(4-methythiobenzyl)uracil (20)

A suspension of 5-bromouracil (0.8006 g, 4.19 mmol) in HMDS (8 mL, 38.4 mmol) and TMSCl (1.10 mL, 8.70 mmol) was refluxed at 135°C until all components dissolved (~1 hour). The reaction mixture was then cooled to 60°C, whereupon dry acetonitrile (8 mL, 151.4 mmol) and 4-methylthiobenzyl bromide (0.9550 g, 4.40 mmol) were added. This mixture was refluxed at 90°C for 40 hours, while being monitored by TLC for completion. The reaction was then cooled to 60°C and quenched with 15 mL of EtOH (added drop-wise). The resulting precipitate was collected by suction filtration, washed with cold EtOH, and recrystallized multiple times in 30% acetonitrile in EtOH to afford pure **20** as a clear crystalline solid (0.8620 g, 2.63 mmol, 63% yield); mp: 223-

225°C; ^{1}H NMR (DMSO- d$_6$): δ 11.85 (s, 1H), 8.37 (s, 1H), 7.30 (dd, J = 2.0 Hz, J = 6.5 Hz, 2H), 7.26 (dd, J = 2.0 Hz, J = 6.5 Hz, 2H), 4.83 (s, 2H), 2.47 (s, 3H); ^{13}C NMR (DMSO- d$_6$): δ 159.6, 150.4, 145.1, 137.9, 133.0, 128.4, 126.1, 95.1, 50.3, 14.6; HRMS calculated for C$_{12}$H$_{11}$BrN$_2$O$_2$SNa$^+$: 348.9617, found: 348.9607.

4.2.33 Synthesis of 5-bromo-1-(4-chlorobenzyl)uracil (21a)

A suspension of 5-bromouracil (0.5008 g, 2.62 mmol) in HMDS (5 mL, 23.9 mmol) and TMSCl (0.70 mL, 5.53 mmol) was refluxed at 135°C until all components dissolved (~1 hour). The reaction mixture was then cooled to 60°C, whereupon dry acetonitrile (5 mL, 94.6 mmol) and 4-chlorobenzyl bromide (0.7001 g, 3.41 mmol) were added. This mixture was refluxed at 90°C for 27 hours, while being monitored by TLC for completion. The reaction was then cooled to 60°C and quenched with 10 mL of EtOH (added drop-wise). The resulting precipitate was collected by suction filtration (crude **21a**) and washed with cold EtOH. The solvent was removed from the filtrate by rotary evaporation, and additional product was isolated from the residue by column chromatography using a solvent system of 30% EtOAc, 15% hexanes, and 55% DCM. All portions of the recovered product were combined and recrystallized multiple times in 30% acetonitrile in EtOH to afford pure **21a** as powdery white crystals (0.5270 g, 1.67 mmol, 64% yield); mp: 239-240°C; ^{1}H NMR (DMSO- d$_6$): δ 11.86 (s, 1H), 8.39 (s, 1H), 7.44-7.42 (m, 2H), 7.38-7.36 (m, 2H), 4.87 (s, 2H); ^{13}C NMR (DMSO- d$_6$): δ 159.63, 150.4, 145.1, 135.5, 132.4, 129.5, 128.6, 95.2, 50.1; HRMS calculated for C$_{11}$H$_8$BrClN$_2$O$_2$Na$^+$: 336.9350, found: 336.9345.

4.2.34   Synthesis of 5-chloro-1-(4-chlorobenzyl)-uracil (21b)

A suspension of 5-chlorouracil (0.8007 g, 5.46 mmol) in HMDS (8 mL, 38.4 mmol) and TMSCl (1.40 mL, 11.1 mmol) was refluxed at 135°C until all components dissolved (~1 hour). The reaction mixture was then cooled to 60°C, whereupon dry acetonitrile (8 mL, 151.4 mmol) and 4-chlorobenzyl bromide (1.4512 g, 7.06 mmol) were added. This mixture was refluxed at 90°C for 48 hours, while being monitored by TLC for completion. The reaction was then cooled to 60°C and quenched with 10 mL of EtOH (added drop-wise). The resulting precipitate was collected by suction filtration, washed with cold EtOH, and recrystallized multiple times in 30% acetonitrile in EtOH to afford pure **21b** as a clear crystalline solid (1.1676 g, 4.31 mmol, 79% yield); mp: 247-249°C; ^{1}H NMR (DMSO- d_6): δ 11.90 (s, 1H), 8.32 (s, 1H), 7.45-7.36 (m, 4H), 4.87 (s, 2H); ^{13}C NMR (DMSO- d_6): δ 159.5, 150.2, 142.8, 135.4, 132.4, 129.5, 128.6, 106.7, 50.2; HRMS calculated for $C_{11}H_8Cl_2N_2O_2Na^+$: 292.9855, found: 292.9841.

4.2.35   Synthesis of 1-benzyl-5-chlorouracil (22a)

A suspension of 5-chlorouracil (0.5002 g, 3.41 mmol) in HMDS (5 mL, 23.9 mmol) and TMSCl (0.90 mL, 7.12 mmol) was refluxed at 135°C until all components dissolved (~1 hour). The reaction mixture was then cooled to 60°C, whereupon dry acetonitrile (5 mL, 94.6 mmol) and benzyl bromide (0.45 mL, 3.79 mmol) were added. This mixture was refluxed at 90°C for 30 hours, while being monitored by TLC. The reaction was then cooled to 60°C and quenched with 10 mL of EtOH (added drop-wise). The resulting precipitate was collected by suction filtration, washed with cold EtOH, and recrystallized multiple times in 30% acetonitrile in EtOH to afford pure **22a** as a clear crystalline solid (0.5368 g, 2.27 mmol, 67% yield); mp: 206-208°C; ^{1}H NMR (DMSO-

d_6): δ 11.90 (s, 1H), 8.32 (s, 1H), 7.38-7.36 (m, 2H), 7.34-7.30 (m, 3H), 4.89 (s, 2H); ^{13}C NMR (DMSO- d_6): δ 159.5, 150.2, 142.9, 136.5, 128.7, 127.8, 127.5, 106.6, 50.8; HRMS calculated for $C_{11}H_9ClN_2O_2Na^+$: 259.0245, found: 259.0238; x-ray crystallographic evidence is presented in appendix A.

4.2.36 Synthesis of 1-benzyl-5-fluorouracil (22b)

A suspension of 5-fluorouracil (0.5002 g, 3.85 mmol) in HMDS (5 mL, 23.9 mmol) and TMSCl (1.00 mL, 7.91 mmol) was refluxed at 135°C until all components dissolved (~1 hour). The reaction mixture was then cooled to 60°C, whereupon dry acetonitrile (5 mL, 94.6 mmol) and benzyl bromide (0.50 mL, 4.21 mmol) were added. This mixture was refluxed at 90°C for 24 hours, while being monitored by TLC. The reaction was then cooled to 60°C and quenched with 10 mL of EtOH (added drop-wise). The resulting precipitate was collected by suction filtration, washed with cold EtOH, and recrystallized multiple times in 30% acetonitrile in EtOH to afford pure **22b** as a clear crystalline solid (0.4499 g, 2.04 mmol, 53% yield); mp: 167-168°C (lit. 166-168°C [98]); ^{1}H NMR (DMSO- d_6): δ 11.86 (s, 1H), 8.23 (d, *J* = 6.7 Hz, 1H), 7.39-7.36 (m, 2H), 7.34-7.30 (m, 3H), 4.84 (s, 2H); ^{13}C NMR (DMSO- d_6): δ 157.4 (d, *J* = 25.8 Hz, 1C), 149.7, 139.8 (d, *J* = 229.8 Hz, 1C), 136.5, 130.0 (d, *J* = 33.4 Hz, 1C), 128.6, 127.7, 127.5, 50.6; HRMS calculated for $C_{11}H_9FN_2O_2Na^+$: 243.0540, found: 243.0544.

4.2.37 Synthesis of 1-benzyl-5-bromouracil (vi)

A suspension of 5-bromouracil (5.0018 g, 26.2 mmol) in HMDS (30 mL, 143.4 mmol) and TMSCl (6.60 mL, 52.2 mmol) was refluxed at 135°C until all components dissolved (~1 hour). The reaction mixture was then cooled to 60°C, whereupon dry acetonitrile (20 mL, 378.4 mmol) and benzyl bromide (3.30 mL, 27.8 mmol) were added.

This mixture was refluxed at 90°C for 40 hours, while being monitored by TLC for completion. The reaction was then cooled to 60°C and quenched with 10 mL of EtOH (added drop-wise). The resulting precipitate was collected by suction filtration, washed with cold EtOH, and recrystallized multiple times in 25% acetonitrile in EtOH to afford pure **vi** as a clear crystalline solid (7.0979 g, 25.2 mmol, 96% yield); mp: 203-204°C (lit. 202-204°C [57]); ^{1}H NMR and ^{13}C NMR (DMSO- d_6) spectra were consistent with literature; x-ray crystallographic evidence is presented in appendix B.

4.2.38   Synthesis of 1-benzyl-5-bromo-3-methyluracil (23)

A suspension of 1-benzyl-5-bromouracil (**vi**; 1.1635 g, 4.14 mmol), DBU (0.65 mL, 4.35 mmol), and acetonitrile (5 mL, 94.6 mmol) was stirred at room temperature until all components dissolved (~10 min). After the addition of methyl iodide (MeI; 2.60 mL, 41.7 mmol), the reaction mixture was stirred in an ice bath for 3 hours while being monitored by TLC for completion. The solvent and excess MeI were removed by rotary evaporation. The product was isolated from the resulting residue by column chromatography using 30% EtOAc in hexanes. Recrystallization in 10% acetonitrile, 20% isopropanol, and 70% EtOH afforded **23** as a clear crystalline solid (1.2026 g, 4.07 mmol, 98% yield; mp: 114-117°C; ^{1}H NMR (DMSO- d_6): δ 8.46 (s, 1H), 7.38-7.30 (m, 5H), 4.96 (s, 2H), 3.23 (s, 3H); ^{13}C NMR (DMSO- d_6): δ 159.0, 150.6, 143.5, 136.3, 128.6, 127.8, 127.6, 94.4, 51.9, 28.8; HRMS calculated for $C_{12}H_{11}BrN_2O_2Na^+$: 316.9896, found: 316.9893.

4.2.39   Synthesis of 1-benzyl-5-bromo-3-isopropyluracil (24)

A suspension of 1-benzyl-5-bromouracil (**vi**; 1.1661 g, 4.15 mmol), DBU (0.70 mL, 4.68 mmol), and acetonitrile (5 mL, 94.6 mmol) was stirred at room temperature

until all components dissolved (~10 min). After the addition of isopropyl iodide (1.45

mL, 14.5 mmol), the reaction mixture was stirred at room temperature for 30 hours while

being monitored by TLC for completion. The solvent and excess isopropyl iodide were

removed by rotary evaporation. The product was isolated from the resulting residue by

column chromatography using 15% EtOAc in hexanes. Recrystallization in 15%

acetonitrile in isopropanol afforded **23** as a white flakey solid (1.0108 g, 3.13 mmol, 75%

yield; mp: 86-87°C; ^{1}H NMR (DMSO- d_6): δ 8.42 (s, 1H), 7.39-7.30 (m, 5H), 5.07 (h, $J =$

6.9 Hz, 1H), 4.93 (s, 2H), 1.37 (d, $J = 6.9$ Hz, 6H); ^{13}C NMR (DMSO- d_6): δ 159.0,

150.2, 143.8, 136.4, 128.7, 127.8, 127.5, 94.9, 51.7, 18.9; HRMS calculated for

$C_{14}H_{15}BrN_2O_2Na^{+}$: 345.0209, found: 345.0212.

Chapter 5: Biological Testing

5.1 General Protocols

In vivo biological testing was conducted by the Epilepsy Branch of NIH in Bethesda, Maryland as part of the Anticonvulsant Screening Project (ASP). All in vivo studies were carried out in male Carworth Farms No. 1 mice that ranged from 18.0-27.0 g in weight. Test compounds were delivered via intraperitoneal (i.p.) injection at doses ranging from 30-300 mg/kg. The anticonvulsant activity of submitted compounds was primarily evaluated using two tests: the maximal electroshock (MES) seizure test and the subcutaneous metrazol (ScMET) seizure test. A select few compounds were also evaluated in the six-hertz psychomotor (6 Hz) test. Preliminary neurotoxicity screening was performed using a standardized rotorod ataxia test. Other general toxicities observed in the mice, such as loss of the righting reflex, sedation, or death, were also monitored throughout all in vivo experiments.

In vitro sodium channel binding assays were carried out by Chantest, a commercial ion-channel screening company located in Cleveland, Ohio. 8 uracil derivatives that displayed in vivo anticonvulsant activity in NIH models (**vi**, **9a**, **12b**, **12e**, **15a-c**, and **21a**,) were chosen for evaluation.

5.1.1 The Maximal Electroshock Seizure Test

The MES test [99], also known as the maximal seizure pattern test, is a very reliable method for the identification of chemical agents that prevent the dissemination of a seizure. In the MES mouse model, an electrical stimulus of 50 mA is applied for 0.2 s at 60 Hz through corneal electrodes primed with a drop of electrolyte solution that contains an anesthetic. In control mice, this electrical sequence initiates a convulsive episode that

is behaviourally and electrographically similar to generalized tonic-clonic seizures in humans. In test subjects, the electrical current is delivered 0.25, 0.5, 1, 2, 4, or 6 hrs after the experimental compound has been administered (i.p.) in doses of 30, 100, or 300 mg/kg. The anticonvulsant activity of the compound is judged based on its ability to impede the hind-limb tonic extensor component of the MES-induced seizure.

5.1.2 The Subcutaneous Metrazol Seizure Test

The ScMET test [99] identifies chemical agents capable of raising the seizure threshold. In the ScMET mouse model, a GABA antagonist known as metrazol or pentylenetetraole (PTZ) is administered via subcutaneous (s.c.) injection at a dose of 85 mg/kg.
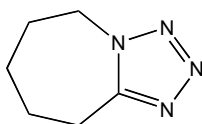
Figure 21: Metrazol

In control mice, this chemoconvulsant produces seizures representative of those found in human absence epilepsy, although they manifest behaviourally as clonic spasms persisting for at least 5 s in duration. In test subjects, PTZ convulsions are induced 0.5 and 4 hrs after the experimental compound has been administered (i.p.) in doses of 30, 100, or 300 mg/kg. Animals are then monitored for 0.5 hrs. The anti-ictogenic activity of the compound is assessed based on its ability to prevent PTZ-induced seizures.

5.1.3 The Six-Hertz Psychomotor Test

Most commercially available seizure medications are active in either the MES test or the ScMET test, which is why these two models are key components of the initial anticonvulsant screening process. However, basing the decision to pursue further

investigation on these two tests alone is likely to result in only the discovery of "me-too" drugs, meaning that other potential AEDs with novel modes of action could be overlooked. Furthermore, MES and ScMET are models of generalized seizures and are not geared toward the discovery of treatments for resistant partial epilepsies. The 6 Hz test is often employed to help address these problems. Take for example the case of Levetiracetam, a currently marketed drug frequently used as an adjunctive therapy for partial seizures. Levetiracetam was found to be inactive in both the MES and ScMET tests, but active in 6 Hz test [100].

In the 6 Hz mouse model, a low frequency (6 Hz), long duration (3s) electrical stimulus of 32 mA is applied to the eyes through corneal electrodes. In control mice, this current initiates transient clonic seizures of low severity followed by a period of behavioural automatisms, such as whisker twitching or jaw chomping. In test subjects, the stimulus is delivered 0.25, 1, 2, and 4 hours after the experimental compound has been administered (i.p.) at a dose of 100 mg/kg. Prevention of the electrically induced seizures is indicative of anticonvulsant activity. 6 Hz seizures are believed to model those of drug-resistant epilepsy because they are insensitive to phenytoin and other AEDs.

5.1.4 The Rotorod Ataxia Test

The neurotoxicity of an experimental compound can be evaluated in mice using the standardized rotorod ataxia test [99]. In this method, test subjects are place on a rotorod that is rotating at 6 rpm. While healthy control mice can successfully maintain equilibrium on the rotorod for extended periods of time, mice with neurological deficits will be unable to do so. Thus, neurotoxicity is determined based on the inability of a test mouse to balance on the rotorod for one minute. At least two successive trials are

performed at 0.25, 0.5, 1, 2, 4, or 6 hrs after the experimental compound has been administered (i.p.) in doses of 30, 100, or 300 mg/kg.

5.1.5   Sodium Channel Binding Assays

Experimental compounds were run against all available sodium channels (Nav1.2 through Nav1.7) at concentrations of 10μM and 100μM using a 384 well plate-based automated patch clamp instrument.

5.2   Biological Results

The sections that follow contain tabulated data collected from the in vivo studies performed. Data pertaining to compounds that displayed activity or toxicity are bolded in their respective tables. In each table, "N/F" is the number of mice that were active or toxic over the number tested, and"P" indicates that the results are still pending. The sodium channel binding studies are currently underway; hence, no results from these in vitro assays have been reported.

Table 9: MES and ScMET test results for exogenous compounds from project 1

	N/F for MES Testing										N/F for SCMET Testing					
Dose (mg/kg)	30		100						300		30		100		300	
Time (hrs)	0.5	4.0	0.25	0.5	1.0	2.0	4.0	6.0	0.5	4.0	0.5	4.0	0.5	4.0	0.5	4.0
Cpd: **1**	0/1	**1/1**	-	0/3	-	-	**2/3**	-	0/1	**1/1**	0/1	0/1	0/1	0/1	0/1	0/1
2	0/1	0/1	-	0/3	-	-	0/3	-	0/1	0/1	0/1	0/1	0/1	0/1	0/1	0/1
3	0/1	0/1	-	0/3	-	-	0/3	-	0/1	0/1	0/1	0/1	0/1	0/1	0/1	0/1
4	0/1	0/1	0/3	0/3	0/3	-	0/3	-	**1/1**	-	0/1	0/1	0/1	0/1	0/1	-
5	0/1	0/1	-	0/3	-	-	0/3	-	0/1	0/1	0/1	0/1	0/1	0/1	0/1	0/1
6a	0/1	0/1	0/3	0/3	0/3	-	0/3	-	**1/1**	0/1	0/1	0/1	0/1	0/1	0/1	0/1
6b	0/1	0/1	-	0/3	-	-	0/3	-	0/1	0/1	0/1	0/1	0/1	0/1	0/1	0/1
6c	0/1	0/1	-	0/3	-	-	0/3	-	0/1	0/1	0/1	0/1	0/1	0/1	0/1	0/1
6d	0/1	0/1	-	**2/3**	-	-	0/3	-	**1/1**	0/1	0/1	0/1	0/1	0/1	**3/5**	0/1
7a	0/1	0/1	**3/3**	0/3	0/3	0/3	0/3	0/3	**1/1**	**1/1**	0/1	0/1	0/1	0/1	0/1	0/1
7b	0/1	0/1	-	0/3	-	-	0/3	-	0/1	0/1	0/1	0/1	0/1	0/1	0/1	0/1
7c	0/1	0/1	-	**1/3**	-	-	0/3	-	**1/1**	0/1	0/1	0/1	0/1	0/1	**1/1**	0/1
8a	0/1	0/1	-	**3/3**	-	-	0/3	-	**1/1**	**1/1**	0/1	0/1	0/1	0/1	0/1	0/1
8b	0/1	0/1	-	**1/3**	-	-	0/3	-	**1/1**	0/1	0/1	0/1	0/1	0/1	0/1	0/1
8c	0/1	0/1	-	**1/3**	-	-	0/3	-	**1/1**	0/1	0/1	0/1	0/1	0/1	0/1	0/1
8d	0/1	0/1	-	**1/3**	-	-	0/3	-	**1/1**	0/1	0/1	0/1	0/1	0/1	**1/1**	0/1
8e	0/1	0/1	-	0/3	-	-	0/3	-	0/1	0/1	0/1	0/1	0/1	0/1	0/1	0/1
8f	0/1	0/1	-	0/3	-	-	**1/3**	-	0/1	**1/1**	0/1	0/1	0/1	0/1	0/1	0/1
8g	P	P	P	P	P	P	P	P	P	P	P	P	P	P	P	P

Table 10: 6 Hz test results for exogenous compounds from project 1

	N/F for 6 Hz Testing				
Dose (mg/kg)	100				
Time (hrs)	0.25	0.5	1.0	2.0	4.0
Cpd: **7a**	**4/4**	**3/4**	**1/4**	0/4	0/4
8a	0/4	0/4	**1/4**	0/4	0/4
8b	0/4	0/4	0/4	0/4	0/4
8c	**2/4**	**2/4**	0/4	0/4	0/4
8f	**1/4**	**3/4**	0/4	0/4	**1/4**

Table 11: Rotorod ataxia test results for exogenous compounds from project 1

Dose (mg/kg)	30		100						300		Other Toxic Effects Observed
Time (hrs)	0.5	4.0	0.25	0.5	1.0	2.0	4.0	6.0	0.5	4.0	
1	0/4	0/2	-	0/8	-	-	0/4	-	0/4	0/2	-
2	0/4	0/2	-	0/8	-	-	0/4	-	0/4	0/2	-
3	0/4	0/2	-	0/8	-	-	0/4	-	0/4	0/2	-
4	0/4	0/2	0/3	0/8	0/3	-	0/4	-	**3/4**	**1/1**	Inability to grasp rotorod; diarrhea; death
5	0/4	0/2	-	0/8	-	-	0/4	-	0/4	0/2	-
6a	0/4	0/2	0/3	0/8	0/3	-	0/4	-	0/4	0/2	-
6b	0/4	0/2	-	0/8	-	-	0/4	-	0/4	0/2	-
6c	0/4	0/2	-	0/8	-	-	0/4	-	0/4	0/2	-
6d	0/4	0/2	-	0/8	-	-	0/4	-	0/4	0/2	Myoclonic jerks
7a	0/4	0/2	0/3	0/8	0/3	0/3	0/4	0/3	**4/4**	0/2	-
7b	0/4	0/2	-	0/8	-	-	0/4	-	0/4	0/2	-
7c	0/4	0/2	-	**2/8**	-	-	0/4	-	**4/4**	0/2	Loss of righting reflex; myoclonic jerks
8a	0/4	0/2	-	0/8	-	-	0/4	-	**3/4**	0/2	-
8b	0/4	0/2	0/4	0/8	0/4	0/4	0/4	-	0/4	0/2	-
8c	0/4	0/2	0/4	0/8	0/4	0/4	0/4	-	0/4	0/2	-
8d	0/4	0/2	-	0/8	-	-	0/4	-	**4/4**	0/2	Loss of righting reflex; myoclonic jerks; sedation
8e	0/4	0/2	-	0/8	-	-	0/4	-	0/4	0/2	-
8f	0/4	0/2	0/4	0/8	0/4	0/4	0/4	-	0/4	0/2	-
8g	P	P	P	P	P	P	P	P	P	P	P

5.2.2 Biological Results of Compounds from Project 2

Table 12: MES and ScMET test results for uracil derivatives from project 2 (φPossible outlier)

	N/F for MES Testing										N/F for SCMET Testing					
Dose (mg/kg)	30		100						300		30		100		300	
Time (hrs)	0.5	4.0	0.25	0.5	1.0	2.0	4.0	6.0	0.5	4.0	0.5	4.0	0.5	4.0	0.5	4.0
Cpd: **9a**	0/1	0/1	0/3	0/3	**1/3**	-	0/3	-	**1/1**	0/1	0/1	0/1	0/1	0/1	0/1	0/1
9b	0/1	0/1	0/3	0/3	0/3	-	0/3	-	**1/1**	0/1	0/1	0/1	0/1	0/1	0/1	0/1
9c	P	P	P	P	P	P	P	P	P	P	P	P	P	P	P	P
9d	0/1	0/1	-	0/3	-	-	0/3	-	0/1	0/1	0/1	0/1	0/1	0/1	0/1	0/1
9e	0/1	0/1	0/3	0/3	**1/3**	**2/3**	0/3	0/3	**1/1**	**1/1**	0/1	0/1	0/1	0/1	**4/5**	0/1
9f	0/1	0/1	-	0/3	-	-	0/3	-	0/1	0/1	0/1	0/1	0/1	0/1	0/1	0/1
10a	0/1	0/1	-	0/3	-	-	0/3	-	0/1	0/1	0/1	0/1	0/1	0/1	0/1	0/1
10b	0/1	0/1	-	0/3	-	-	0/3	-	0/1	0/1	0/1	0/1	0/1	0/1	0/1	0/1
10c	0/1	0/1	-	0/3	-	-	φ1/7	-	0/1	0/5	0/1	0/1	0/1	0/1	0/1	0/1
10d	0/1	0/1	-	0/3	-	-	0/3	-	0/1	0/1	0/1	0/1	0/1	0/1	0/1	0/1
11a	0/1	0/1	-	0/3	-	-	0/3	-	0/1	0/1	0/1	0/1	0/1	0/1	0/1	0/1
11b	0/1	0/1	-	0/3	-	0/4	0/3	0/4	0/1	**1/1**	0/1	0/1	0/1	0/1	0/1	0/1
11c	0/1	0/1	-	0/3	-	-	0/3	-	-	-	0/1	0/1	0/1	0/1	-	-
12a	0/1	0/1	-	0/3	-	0/3	0/3	0/3	0/1	**1/1**	0/1	0/1	0/1	0/1	0/1	0/1
12b	0/1	0/1	-	**1/3**	-	-	0/3	-	**1/1**	0/1	0/1	0/1	0/1	0/1	0/1	0/1
12c	0/1	0/1	-	0/3	-	-	0/3	-	0/1	0/1	0/1	0/1	0/1	0/1	0/1	0/1
12d	0/1	0/1	-	0/3	-	-	0/3	-	0/1	0/1	0/1	0/1	0/1	0/1	0/1	0/1
12e	0/1	0/1	-	**1/3**	-	-	0/3	-	**1/1**	**1/1**	0/1	0/1	0/1	0/1	0/1	0/1
13a	0/1	0/1	-	0/3	-	-	0/3	-	0/1	0/1	0/1	0/1	0/1	0/1	0/1	0/1
13b	0/1	0/1	-	0/3	-	-	0/3	-	0/1	0/1	0/1	0/1	0/1	0/1	0/1	0/1
13c	0/1	0/1	-	0/3	-	-	0/3	-	0/1	0/1	0/1	0/1	0/1	0/1	0/1	0/1
14a	0/1	0/1	-	0/3	-	-	0/3	-	0/1	0/1	0/1	0/1	0/1	0/1	0/1	0/1
14b	0/1	0/1	-	**1/3**	-	-	0/3	-	**1/1**	0/1	0/1	0/1	0/1	0/1	0/1	0/1
14c	0/1	0/1	0/3	0/3	0/3	-	0/3	-	**1/1**	0/1	0/1	0/1	0/1	0/1	0/1	0/1
15a	0/1	0/1	-	0/3	-	**1/3**	0/3	0/3	0/1	**1/1**	0/1	0/1	0/1	0/1	0/1	0/1
15b	0/1	0/1	0/3	0/3	**1/3**	**1/3**	0/3	0/3	**1/1**	**1/1**	0/1	0/1	0/1	0/1	0/1	0/1
15c	0/1	0/1	-	0/3	-	-	**1/3**	-	**1/1**	**1/1**	0/1	0/1	0/1	0/1	0/1	0/1
15d	0/1	0/1	-	**1/3**	-	-	0/3	-	**1/1**	**1/1**	0/1	0/1	0/1	0/1	**5/5**	0/1
16	0/1	0/1	-	0/3	-	-	0/3	-	0/1	0/1	0/1	0/1	0/1	0/1	0/1	0/1
17	0/1	0/1	-	0/3	-	-	0/3	-	0/1	0/1	0/1	0/1	0/1	0/1	0/1	0/1
18	0/1	0/1	-	0/3	-	0/3	0/3	0/3	0/1	**1/1**	0/1	0/1	0/1	0/1	0/1	0/1
19	0/1	0/1	-	0/3	-	-	0/3	-	0/1	0/1	0/1	0/1	0/1	0/1	0/1	0/1
20	0/1	0/1	-	0/3	-	-	0/3	-	0/1	0/1	0/1	0/1	0/1	0/1	0/1	0/1
21a	0/1	0/1	-	0/3	-	**2/3**	**1/3**	0/3	0/1	**1/1**	0/1	0/1	0/1	0/1	0/1	0/1
21b	P	P	P	P	P	P	P	P	P	P	P	P	P	P	P	P
22a	0/1	0/1	0/3	0/3	**3/3**	-	**1/3**	-	**1/1**	**1/1**	0/1	0/1	0/1	0/1	0/1	0/1
22b	0/1	0/1	-	0/3	-	-	0/3	-	0/1	0/1	0/1	0/1	0/1	0/1	0/1	0/1
23	0/1	0/1	-	0/3	-	-	0/3	-	0/1	0/1	0/1	0/1	0/1	0/1	0/1	0/1
24	P	P	P	P	P	P	P	P	P	P	P	P	P	P	P	P

Table 13: 6 Hz test results for uracil derivatives from project 2

	N/F for 6 Hz Testing				
Dose (mg/kg)	100				
Time (hrs)	0.25	0.5	1.0	2.0	4.0
Cpd: 9a	3/4	2/4	2/4	1/4	1/4
10a	4/4	2/4	2/4	1/4	1/4
12b	4/4	4/4	3/4	0/4	1/4
12e	0/4	3/4	0/4	1/4	0/4
13b	1/4	2/4	1/4	0/4	0/4
13c	0/4	1/4	0/4	2/4	0/4
14b	2/4	2/4	1/4	1/4	0/4
15a	1/4	3/4	1/4	0/4	1/4
15b	4/4	4/4	4/4	4/4	1/4
15c	4/4	4/4	4/4	3/4	1/4
21a	4/4	3/4	4/4	4/4	3/4
22a	1/4	2/4	2/4	1/4	1/4

Table 14: Rotorod ataxia test results for uracil derivatives from project 2

Dose (mg/kg)	30		100						300		Other Toxic Effects Observed
Time (hrs)	0.5	4.0	0.25	0.5	1.0	2.0	4.0	6.0	0.5	4.0	
Cpd: 9a	0/4	0/2	0/4	0/8	0/4	0/4	0/4	-	0/4	0/2	-
9b	0/4	0/2	0/3	**2/8**	0/3	-	0/4	-	**1/4**	0/2	-
9c	P	P	P	P	P	P	P	P	P	P	P
9d	0/4	0/2	-	0/8	-	-	0/4	-	0/4	0/2	-
9e	0/4	0/2	0/3	0/8	0/3	0/3	0/4	0/3	0/4	0/2	-
9f	0/4	0/2	-	0/8	-	-	0/4	-	0/4	0/2	-
10a	0/4	0/2	**3/4**	0/8	0/4	0/4	0/4	-	0/4	0/2	-
10b	0/4	0/2	-	0/8	-	-	0/4	-	0/4	0/2	-
10c	0/4	0/2	-	0/8	-	-	0/4	-	0/4	0/2	-
10d	0/4	0/2	-	0/8	-	-	0/4	-	0/4	0/2	-
11a	0/4	0/2	-	0/8	-	-	0/4	-	0/4	0/2	-
11b	0/4	0/2	-	0/8	-	0/4	0/4	0/4	0/4	0/2	-
11c	0/4	0/2	-	0/8	-	-	0/4	-	**4/4**	-	Death
12a	0/4	0/2	-	0/8	-	0/3	0/4	0/3	**2/4**	0/2	-
12b	0/4	0/2	0/4	0/8	0/4	0/4	0/4	-	0/4	0/2	-
12c	0/4	0/2	-	0/8	-	-	0/4	-	0/4	0/2	-
12d	0/4	0/2	-	0/8	-	-	0/4	-	0/4	0/2	Diarrhea
12e	0/4	0/2	0/4	0/8	0/4	0/4	0/4	-	0/4	0/2	-
13a	0/4	0/2	-	0/8	-	-	0/4	-	0/4	0/2	-
13b	0/4	0/2	0/4	0/8	0/4	0/4	0/4	-	0/4	0/2	-
13c	0/4	0/2	0/4	0/8	0/4	0/4	0/4	-	0/4	0/2	-
14a	0/4	0/2	-	0/8	-	-	0/4	-	0/4	0/2	-
14b	0/4	0/2	0/4	0/8	0/4	0/4	0/4	-	0/4	0/2	-
14c	0/4	0/2	0/3	0/8	0/3	-	0/4	-	0/4	0/2	-
15a	0/4	0/2	0/4	0/8	0/4	0/4	0/4	0/3	0/4	0/2	-
15b	0/4	0/2	0/4	0/8	0/4	0/4	0/4	0/3	0/4	0/2	-
15c	0/4	0/2	0/4	0/8	0/4	0/4	0/4	-	0/4	0/2	-
15d	0/4	0/2	-	0/8	-	-	0/4	-	0/4	0/2	-
16	0/4	0/2	-	0/8	-	-	0/4	-	0/4	0/2	-
17	0/4	0/2	-	0/8	-	-	0/4	-	0/4	0/2	-
18	0/4	0/2	-	0/8	-	0/3	0/4	0/3	0/4	0/2	-
19	0/4	0/2	-	0/8	-	-	0/4	-	0/4	0/2	-
20	0/4	0/2	-	0/8	-	-	0/4	-	0/4	0/2	-
21a	0/4	0/2	0/4	0/8	**1/4**	0/3	0/4	0/3	0/4	0/2	-
21b	P	P	P	P	P	P	P	P	P	P	P
22a	0/4	0/2	0/4	0/8	0/3	0/4	0/4	-	0/4	0/2	-
22b	0/4	0/2	-	0/8	-	-	0/4	-	0/4	0/2	-
23	0/4	0/2	-	0/8	-	-	0/4	-	0/4	0/2	-
24	P	P	P	P	P	P	P	P	P	P	P

5.3   Discussion of the Biological Results

5.3.1   Discussion of Project 1 Biological Results

In total, 19 exogenous compounds containing a sodium channel pharmacophore-like region similar to that of phenytoin were sent to NIH for anticonvulsant screening. Thus far, various biological results for 18 of these compounds have been received. A total of 11 exogenous compounds (**1**, **4**, **6a**, **6d**, **7a**, **7c**, **8a-d**, and **8f**) displayed some level of anti-seizure activity in at least one of the three previously described in vivo models of epilepsy, suggesting that possible classes of anticonvulsant compounds include the phenyl thiazolones (e.g., **1**), naphthalene acetamides (e.g., **4**), the phenyl acetanilides (e.g., **6a**, **6d**), the oxindoles (e.g., **7a**, **7c**), and the isatins (e.g., **8a-d**, **8f**). Indeed, a literature search reveals that the anti-seizure properties of various indoles and isatins have already been reported [101]. The MES test results received from NIH suggest that all five of these molecular classes can, at least to some degree, impede seizure spread. The phenyl acetanilides, oxindoles, and isatins may also be capable of raising the seizure threshold, as **6d**, **7c**, and **8d** all displayed mild ScMET activity. It is interesting to note that, unlike phenytoin, compounds **7a**, **8a**, **8c**, and **8f** were moderately successful in the 6 Hz model, indicating that the oxindoles and isatins may even show therapeutic potential for the treatment of drug-resistant epilepsies.

Unfortunately, compounds **4**, **6d**, **7a**, **7c**, **8a**, and **8d** displayed neurotoxicity in the standardized rotorod test or caused negative side effects, such as the loss of the righting reflex, sedation, and myoclonic jerks. Compound 4 was particularly toxic, as it caused diarrhea, the complete inability of the mice to grasp the rotorod, and death. This demonstrates that, like many current AEDs, most of the previously mentioned classes of

compounds display moderate to high toxicity. However, these potential classes of anticonvulsants should not be disregarded, particularly in cases of phenyl thiazolones, phenyl acetanilides, oxindoles, and isatins. The phenyl thiazolone (**1**) tested displayed no toxicity of any kind, and many evaluated compounds belonging to the remaining three classes were active at a dose of 100 mg/kg, but did not display neurotoxicity until administered at 300 mg/kg. This suggests that the development of active, low-toxicity analogues from all four of these classes may be possible.

Overall, it appears that varying degrees of anti-ictogenic activity are displayed in an array of phenyl thiazolones, naphthalene acetamides, phenyl acetanilides, oxindoles, and isatins. Compounds belonging to all five of these classes are certainly worthy of investigation as novel anticonvulsant scaffolds.

5.3.2　　　Discussion of Project 2 Biological Results

5.3.2.1　　　Overall Observations

A total of 39 uracil derivatives have been sent to NIH for anticonvulsant screening. Thus far, various biological results for 35 of these compounds have been received. In total, 19 uracils (**9a-b**, **9e**, **10a**, **11b**, **12a-b**, **12e**, **13b-c**, **14b-c**, **15a-d**, **18**, **21a**, **22a**) displayed some level of anti-seizure activity in at least one of the three previously described in vivo models of epilepsy. The fact that anticonvulsant activity was detected in 53% of evaluated derivatives clearly demonstrates the great potential of uracils as putative therapeutics for epilepsy.

It is evident from the biological data that uracils exhibit a much higher level of protection against MES seizures than ScMET seizures (**9e** and **15d** were the only derivatives active in the ScMET model). This demonstrates that, like phenytoin, uracils

prevent seizure spread. However, whether or not they are also capable of sodium channel blockade has yet to be determined; further insight into this theory will be provided once the results from the sodium channel binding assays have been received. It appears that many uracil derivatives (**9a**, **10a**, **12b**, **12e**, **13b-c**, **14b**, **15a-c**, **21a**, and **22a**) also display high activity in the 6 Hz model, revealing that they show considerable promise for the treatment of refractory epilepsy.

Although a total of 6 uracil derivatives (**9b**, **10a**, **11c**, **12a**, **12d**, and **21a**) did cause side effects of some kind, the overall toxicity profile of uracil-based compounds appears to be quite favourable. Non-neurotoxic side effects were only observed in 2 cases, one of which involved non-severe effects (**12d**; diarrhea).

The low toxicity of uracil-based compounds becomes particularly apparent when compared to the exogenous compounds tested in Project 1. Only 16% of all active uracil derivatives displayed toxic effects, whereas 56% of the active exogenous compounds displayed toxicity. Furthermore, the extent of neurotoxicity and type of non-neurotoxic side effects were significantly less severe in the uracil derivatives. All of this evidence supports the general use of endogenous drug scaffolds, and suggests that uracil-based compounds may indeed serve as effective, non-toxic anticonvulsants.

5.3.2.2   Further Insight into the Uracil Structure-Activity Relationship

Upon examination of the biological results for project 2, a number of observations can be made with regard to uracil structure. The various uracil properties and structural features from which many of the observations in this section have been drawn are summarized in table 15:

Table 15: Summary of various observations used for uracil SAR (*Log P values calculated in MOE)

Cpd	Active (Y/N)	Toxic (Y/N)	Molecular Weight (g/mol)	*Log P	R^5	R^1	R^3
9a	Y	N	282.0934	0.5010	Br	NC_5H_4-2-CH_2-	H
9b	Y	Y	217.2239	-0.3320	CH_3	NC_5H_4-2-CH_2-	H
9d	N	N	248.1949	-0.3620	NO_2	NC_5H_4-2-CH_2-	H
9e	Y	N	329.0939	0.8930	I	NC_5H_4-2-CH_2-	H
9f	N	N	271.1953	0.3048	CF_3	NC_5H_4-2-CH_2-	H
10a	N	Y	282.0934	0.5390	Br	NC_5H_4-3-CH_2-	H
10b	N	N	248.1949	-0.3240	NO_2	NC_5H_4-3-CH_2-	H
10c	N	N	271.1953	0.3428	CF_3	NC_5H_4-3-CH_2-	H
10d	N	N	329.0939	0.9310	I	NC_5H_4-3-CH_2-	H
11a	N	N	420.2045	1.6830	I	NC_5H_4-3-CH_2-	NC_5H_4-3-CH_2-
11b	Y	N	308.3345	0.4580	CH_3	NC_5H_4-3-CH_2-	NC_5H_4-3-CH_2-
11c	N	Y	294.3080	0.4140	H	NC_5H_4-3-CH_2-	NC_5H_4-3-CH_2-
12a	Y	Y	295.1319	2.0680	Br	o-$CH_3C_6H_4CH_2$-	H
12b	Y	N	216.2359	1.1910	H	o-$CH_3C_6H_4CH_2$-	H
12c	N	N	230.2625	1.2350	CH_3	o-$CH_3C_6H_4CH_2$-	H
12d	N	Y	342.1324	2.4600	I	o-$CH_3C_6H_4CH_2$-	H
12e	Y	N	250.6809	1.8620	Cl	o-$CH_3C_6H_4CH_2$-	H
13a	N	N	295.1319	2.1070	Br	m-$CH_3C_6H_4CH_2$-	H
13b	N	N	216.2359	1.2300	H	m-$CH_3C_6H_4CH_2$-	H
13c	N	N	230.2625	1.2740	CH_3	m-$CH_3C_6H_4CH_2$-	H
14a	N	N	295.1319	2.0700	Br	p-$CH_3C_6H_4CH_2$-	H
14b	Y	N	216.2359	1.1930	H	p-$CH_3C_6H_4CH_2$-	H
14c	Y	N	230.2625	1.2370	CH_3	p-$CH_3C_6H_4CH_2$-	H
15a	Y	N	360.0014	2.6070	Br	m-$BrC_6H_4CH_2$-	H
15b	Y	N	281.1054	1.7300	H	m-$BrC_6H_4CH_2$-	H
15c	Y	N	295.1319	1.7740	CH_3	m-$BrC_6H_4CH_2$-	H
15d	Y	N	315.5504	-	Cl	m-$BrC_6H_4CH_2$-	H
16	N	N	311.1313	1.7650	Br	m-$OCH_3C_6H_4CH_2$-	H
17	N	N	365.1027	-	Br	p-$OCF_3C_6H_4CH_2$-	H
18	Y	N	299.0958	1.9250	Br	p-$FC_6H_4CH_2$-	H
19	N	N	349.9955	2.9910	Br	$3,4$-$Cl_2C_6H_3CH_2$-	H
20	N	N	327.1969	2.3640	Br	p-$SCH_3C_6H_4CH_2$-	H
21a	Y	Y	315.5504	2.3640	Br	p-$ClC_6H_4CH_2$-	H
22a	Y	N	236.6544	1.5660	Cl	$C_6H_5CH_2$-	H
22b	N	N	220.1998	1.1270	F	$C_6H_5CH_2$-	H
iii	Y	Y	216.2359	0.9390	CH_3	$C_6H_5CH_2$-	H
iv	Y	Y	202.2093	0.8950	H	$C_6H_5CH_2$-	H
v	Y	Y	328.1058	2.1640	I	$C_6H_5CH_2$-	H
vi	Y	Y	281.1054	1.7720	Br	$C_6H_5CH_2$-	H
Average for active:			273.8019	1.4109	-	-	-
Average for inactive:			291.9612	1.2306	-	-	-
Average for cpds **9-11**:				0.4207	-	-	-
Average for cpds **12-22** and iii-vi				1.7564	-	-	-

103

The biological results indicate that, unlike the benzyl group, the 2-pyridinylmethyl and 3-pyridinylmethyl groups are not appropriate N^1-uracil substituents. Overall, the pyridinylmethyl derivatives displayed toxic effects of higher frequency and severity than many other uracil derivatives. Furthermore, the N^1-monosubstituted 3-pyridinylmethly uracils were completely inactive, and in the few cases where 2-pyridinylmethyl derivatives were active (**9a**, **9b**, and **9e**), the activities were lower than that of their N^1-benzyl counterparts (**vi**, **iii**, and **v**, respectively). It is believed that limited passive diffusion across the BBB may be responsible for reducing the activity of these compounds, since the average Log P for all the pyridinylmethyl derivatives (~0.42) is well outside the ideal range for CNS drugs (1.5-2.7). In comparison, the various benzylated uracil derivatives from this thesis, which seem to display higher overall activity than the pyridinylmethyl uracils, have an average Log P (~1.76) within this ideal range.

It is interesting to note that the N^1,N^3-disubstituted pyridinylmethyl uracil derivative **11b** displayed a low level of activity, since all previously synthesized dibenzylated derivatives were completely inactive. This calls into question the earlier suggestion that N^1,N^3-disubstitution causes complete inactivation (observation 1b from section 2.2.2). Further insight as to whether or not N^3-H is required for anticonvulsant activity will be provided once the biological results for compounds **23** and **24** have been received.

Many of the substituted benzyl uracil derivatives (i.e., **14b**, **15a-d**) did exhibit comparable activity to benzylated derivatives **iii-vi** in the MES test, however, aside from **15d**, they were not nearly as active in the ScMET test. Therefore, an N^1-benzyl

substituent still appears to provide superior anticonvulsant activity. However, unsubstituted benzyl derivatives **iii-vi** displayed overall higher levels of neurotoxicity, suggesting that perhaps a substituted benzyl group could be found that permits optimal levels of both activity and toxicity.

Interestingly, neither of the N^1-benzylated derivatives **22a** or **22b** demonstrated any toxic effects. Although **22b** was completely inactive and **22a** was not ScMET active, **22a** did display slightly higher MES activity than **vi**, suggesting that Cl may be even more viable than Br as a C^5 uracil substituent. This is also corroborated by the increased MES activity of **12e** over **12a**, and the improved MES and ScMET activity of **15d** over **15a**. Further insight into this theory will be provided once the results for **21b** have been received.

Based on a comparison of the average molecular weights of the active (~274 g/mol) and inactive (~292 g/mol) uracil derivatives, it appears that a lower molecular weight may be beneficial for anticonvulsant activity. This is not an unreasonable conclusion, as molecules of lower molecular weight should more easily diffuse through the BBB. This could perhaps explain the higher activity of C^5-Cl derivatives over C^5-Br derivatives, although electronic and size differences may also play a role.

In summary, the general structure-activity trends described in section 2.2.2 of this thesis were, for the most part, still observed. However, the list of observations should be slightly modified to the following:

1) For substitutions at N^1 and N^3:

   a. Substitution at *either* N^1 or N^3 increases anticonvulsant activity, but N^3-substituted analogues typically display higher toxicity

   b. Concurrent substitution at *both* N^1 and N^3 appears to reduce activity

   c. Of all the N-substitutents tested, the benzyl group displays the most promising anticonvulsant activity, but various substituted benzyl groups (i.e., *m*-$CH_3C_6H_4CH_2$-, *m*-$BrC_6H_4CH_2$-, *p*-$FC_6H_4CH_2$-) that exhibit comparable activity have a better toxicological profile

2) For substitutions at C^5 and C^6:

   a. Substitution at C^6 is unfavourable: any substituent other than H typically increases toxicity and reduces biological activity

   b. Substitution at C^5 with moderately small substituents (such as CH_3, I, Br, and especially Cl) rather than larger groups (such as alkyl chains and rings) or smaller groups (such as H and F) improves biological activity

Chapter 6: Quantitative Structure-Activity Relationship Study

6.1   **QSAR Background Information**

A strictly observational SAR will identify molecular features that are necessary for biological activity and aid the medicinal chemist in the design of new analogues. A computational QSAR, on the other hand, permits the development of a statistical model that can be used to predict the biological activity of various analogues before they have been synthesized and tested.

The development of a QSAR model generally involves the following steps [102, 103, 104]:

1. Establish a training set:

A training set is a database of compounds with known biological activities. The most stable 3D structure of each compound is usually required to ensure that accurate molecular descriptors are assigned. In addition, the biological activity of each compound must be quantified for analysis. Ideally, this is done through the calculation of either half-maximal inhibitory concentrations (IC_{50}) or half-maximal effective concentrations (EC_{50})—respectively, the in vitro or in vivo concentrations of each active compound required to obtain 50% of the maximum effect.

2. Calculate molecular descriptors:

Numerical values (molecular descriptors) associated with specific molecular properties are assigned to each compound. These molecular descriptors can represent both the 2D properties (atom count, molecular weight, bond length, partial charge,

hydrophobicity, etc.) and the 3D properties (surface area, volume, shape, etc.) of the compound.

3. Model the relationship between the descriptors and biological activity:

A functional relationship between the molecular descriptors and biological activity can be achieved through a number of statistical analyses, including the Partial Least Squares (PLS) method or the Binary QSAR method. The PLS method employs a type of mathematical regression and allows for the prediction of a compound's degree of activity. The Binary QSAR method uses a Bayesian inference technique and allows for a binary (pass/fail) prediction of activity.

4. Validate the model using internal and external methods:

Internal validation is based on the ability of the model to predict the activities of compounds in the training set. The linear regression term (R^2) and the Leave-One-Out (LOO) cross-validated R^2 term (q^2) are usually used to gauge the internal accuracy of the model, with acceptable q^2 values being those above 0.60. Although low q^2 values are indicative of low predictivity, high q^2 values do not necessarily correlate with high predictive power. Therefore, external validation based on compounds outside of the training set is also required.

5. Use the QSAR model to predict activity:

An accurate QSAR model can be used to predict the activity of newly designed analogues. This will serve to guide the medicinal chemist in his or her decision as to which analogues are worthy of synthesis and experimental evaluation.

6.2   The Development of the PLS-12 Uracil QSAR Model

All computational methods were performed using MOE [55]. The atomic charges

and optimized geometries for all compounds were calculated using molecular mechanics

with the MMFF94s force field [105]. All energy minimizations were carried out in vacuo

using a gradient convergence criterion of 0.05 kcal/(Å•mol). All possible interactions

were enabled and the long range cut off was set to be between 8-10 Å.

The IC_{50} and EC_{50} values could not be determined for the uracil derivatives

synthesized in this thesis. Therefore, biological activity was instead quantified using an

arbitrary scale of 0-3 based on the MES test results from NIH, where 0 = no activity and

3 = a relatively high level of activity (see table 16 for determined activities).

Consequently, all uracils for which no MES data had yet been received could not be

included in any QSAR calculations.

A wide variety of both 2D and 3D molecular descriptors were empirically

calculated for all relevant compounds by means of the MOE QuaSAR-Descriptor

application. The QSAR function in MOE was then used to develop a PLS uracil QSAR

model using the 12 compounds bolded in table 16 as the training set. Fine-tuning of this

model was achieved by manually eliminating all descriptors with a relative importance

close to zero (≤ 0.0001) and sorting through those that remained one-by-one to determine

the combination of descriptors that yielded the highest q^2 value. For the resulting model

(PLS-12), $R^2 = 1.000$ and $q^2 = 0.943$.

External validation of the PLS-12 model was carried out using the N^1-

monosubstituted uracil derivatives synthesized for this thesis that were not included in the

training set, as well as the previously synthesized uracil derivatives **i-vii**. The

experimentally determined activities of each compound used in this QSAR study are

shown in table 16, along with the corresponding activities predicted by the PLS-12

model.

Table 16: Assigned and PLS-12 predicted activities for uracil derivatives (*Incorrect pass/fail prediction)

Compound	Experimental Activity	PLS-12 Predicted Activity
9a	**2**	**2.00**
9b	**1**	**1.00**
9d	0	-3.42
9e	**3**	**3.00**
9f	0	-5.86
10a	**0**	**0.00**
10b	0	-5.10
10c	0	-8.14
11a	0	-3.95
11b	**1**	**1.00**
*11c	0	4.76
*10d	0	0.84
12a	**1**	**1.00**
12b	2	2.04
12c	**0**	**0.00**
*12d	0	1.05
12e	3	0.44
13a	**0**	**0.00**
*13b	0	1.93
13c	0	-0.29
14a	0	-0.04
14b	**2**	**2.00**
*14c	1	-0.13
15a	**2**	**2.00**
15b	3	5.41
15c	**3**	**3.00**
16	0	-3.53
20	0	-0.26
*18	1	-3.38
19	0	-0.21
21a	2	2.36
22a	**3**	**3.00**
22b	0	-0.15
i	3	14.72
ii	3	13.70
iii	3	1.93
iv	3	4.05
v	3	0.40
vi	3	0.04
vii	2	0.63
viii	0	-18.99
ix	0	-6.37

The PLS-12 uracil QSAR model correlates molecular features to biological activity through the use of 12 descriptors. These descriptors, along with their relative level of importance within the model are shown in table 17:

Table 17: The descriptors from the PLS-12 QSAR model (*Distance matrix example shown in figure 22)

Descriptor Abbreviation	Descriptor	Relative Importance
2D Descriptors:		
• Weight	The molecular weight of the compound	0.127666
• weinerPath	Half the sum of all the distance matrix entries[*]	1.000000
3D Descriptors:		
• pmi	Principal moment of inertia	0.250903
• pmi1	First diagonal element of diagonalized moment of inertia tensor	0.327440
• pmi2	Second diagonal element of the diagonalized moment of inertia tensor	0.093430
• pmiY	y-component of the principal moment of inertia (external coordinates)	0.350482
• vsurf_HB2	Hydrogen-bond donor capacity	0.266939
• vsurf_D1	Hydrophobic volume	0.056088
• vsurf_W2	Hydrophilic volume	0.247751
• vsurf_Wp1	Polar volume	0.186540
• CASA+	Positive charge weighted surface area	0.797942
• CASA-	Negative charge weighted surface area	0.183277
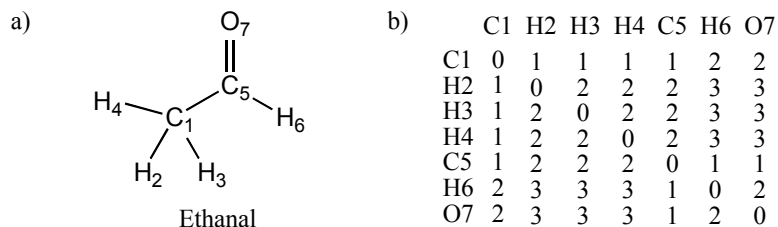
Figure 22: a) Numbered structure of ethanal and b) distance matrix for ethanal

6.3   **Discussion of Uracil QSAR Models**

The descriptors that dictate predictivity within the PLS-12 QSAR model can all
be rationalized in terms of pharmaceutical, pharmacokinetic, and pharmacodynamic
considerations. Weiner path is a measure of structural connectivity, and the descriptors
for principal moment of intertia (pmi, pmi1, pmi2, and pmiY) are measures of the
distribution of mass and overall shape of a molecule. These molecular properties are all
important for the proper binding of a molecule to its target receptor. The descriptors of
charge (CASA+ and CASA-), hydrophobicity (vsurf_HB2), hydrophilicity (vsurf_W2),
and hydrogen bonding capability (vsurf_HB2) are all also pharmacodynamically relevant,
particularly with regard to drug-receptor complementarity. These latter four descriptors,
as well as the descriptor of weight, are also all significant with respect to the successful
transport of a drug molecule through the bloodstream and across various lipid
membranes, such as the BBB. It is somewhat surprising that Log P was not identified as a
highly significant descriptor, since a pattern regarding Log P was recognized in section
6.4.2.2 of this thesis. However, since Log P is representative of the ratio between the
hydrophobicity and hydrophilicity, the relationship between Log P and biological activity
is likely still accounted for through a combination of the vsurf_HB2, v_surf W2, v-
surf_HB2, CASA+, and CASA- descriptors.

The PLS-12 model exhibited the highest level of predictivity out of the numerous
attempted models. Multiple binary QSAR studies and other PLS QSAR studies using
various different combinations of compounds for the training set were also attempted, but
their q^2 ranged from only 0.45-0.70. Furthermore, their predictive power for the activity
of uracils outside of their respective training sets was extremely low. The PLS-model, on
the other hand, demonstrated 100% internal accuracy and is capable of external

prediction on a pass/fail basis. Although the model is not capable of predicting the exact degree of activity on the arbitrarily defined scale of 0-3, it was able to correctly distinguish between active and inactive compounds in 24 out of the 30 uracils used for the test set. This translates to a pass/fail predictive accuracy of 80%, suggesting that the algorithm might be a useful tool for guiding further analogue synthesis.

The lack of predictive power for the actual degree of accuracy in the PLS-model could be attributed to a number of factors. Firstly, the method used to quantify uracil activity was inherently prone to significant error, since personal judgement was involved. Furthermore, measuring accuracy on an arbitrary scale using only whole integer numbers is a considerable oversimplification. A more reliable scale could be developed if biological evaluation employed an increased number of test subjects per concentration group. However, the calculation and use of EC_{50} values would be required to achieve the highest level of accuracy.

The general lack of predictive power demonstrated in all attempted uracil QSAR models may be unavoidable, as uracils likely exert their anticonvulsant effects via multiple modes of action, and β-amino acid metabolites may be partially responsible for the observed activity. However, the low predictive power of these models could also be attributed to the small amount of uracil data available, and improvement may be achieved in the future once a higher number of analogues have been synthesized and tested.

Chapter 7: Conclusion and Future Directions

7.1　　　　　　Conclusion and Future Directions: Project 1

A substructure search was conducted on a database of exogenous molecules to find those that exhibit drug-like properties and contain the sodium channel pharmacophore of phenytoin. A number of the compounds identified by this search were selected for evaluation in animal models of epilepsy at NIH, resulting in the identification of multiple molecular classes from which new anticonvulsant lead compounds could be derived. These molecular classes include the phenyl thiazolones, naphthalene acetamides, phenyl acetanilides, oxindoles, and isatins. Future work pertaining to this project includes the investigation of the anticonvulsant activity of analogues within each of these five molecular classes in an attempt to discover patentable lead compounds and eventually develop new anticonvulsant drug candidates.

7.2　　　　　　Conclusion and Future Directions: Project 2

Numerous substituted uracil derivatives were synthesized, 22 of which were novel. All uracil analogues were submitted for evaluation in animal models of epilepsy at NIH. Many were found to display very promising in vivo anticonvulsant activity in an array of seizure models, verifying their potential for the treatment of a broad range of seizure types, including those found in drug-resistant epilepsy. Furthermore, the overall neurotoxicity of uracil derivates in mice was demonstrated to be quite low, and the occurrence of other general side effects proved to be minimal. These findings, in conjunction with the assumed antiepileptogenic properties of the β-amino acid metabolites of uracils, suggest that uracil derivates show an immense capacity for the

development of an antiepileptic drug that overcomes all of the major downfalls of current epilepsy medications.

A predictive QSAR model was developed that is capable of distinguishing between active and inactive uracil derivatives with an accuracy of 80%. This model may prove to be a helpful tool for the future design of active uracil analogues.

Future analogue synthesis could proceed in a variety of different directions. Numerous substituted benzyl uracil derivates have not yet been explored, and are certainly worthy of investigation. The effects of various other phenyl bioisosteres (such as the naphthalenes, thiophenes, pyrroles, indoles) on anticonvulsant activity may also be useful to examine. Lastly, the improved biological profile of C^5-chloro substituted uracils suggests that the synthesis of additional uracils of this type is of particular interest.

Other future directions of this project should include the evaluation of all synthesized uracil derivatives in animal models of epileptogenesis, such as the spontaneous recurrent seizure (SRS) model [60] or the various neurotrauma models [106] of epilepsy. In addition, the metabolic breakdown of the various uracil derivatives should be investigated to verify the in vivo formation of β-amino acids. The anticonvulsant and antiepileptogenic activity of these β-amino acid metabolites should then be examined and compared to the results from their respective uracil precursors in order to determine the contribution of each to the anticonvulsant activity observed.

REFERENCES

1.   Fisher, R. S. Epileptic Seizures and Epilepsy: Definitions Proposed by the International League Against Epilepsy (ILAE) and the International Bureau for Epilepsy (IBE). *Epilepsia.* **2005***, 46*, 470.

2.   Nybakken, O. *Greek and Latin in Scientific Terminology*; Iowa State University Press, **1962**.

3.   Martini, F. H. *Fundamentals of Anatomy & Physiology*, 7th ed.; Pearson Education, Inc., San Francisco, CA, **2006**.

4.   Craig, D. I. Brain-Compatible Learning: Principles and Applications in Athletic Training. *J. Athl Training.* **2003***, 38*, 342.

5.   Elger, C. E. Epilepsy: A Comprehensive Textbook, Vol 1. *Arch. Neurol.* **2008***, 65*, 1676.

6.   Morano, G. N.; Seibyl, J. P. Technical Overview of Brain SPECT Imaging: Improving Acquisition and Processing of Data. *J. Nucl. Med. Technol.* **2003***, 31*, 191.

7.   Bortz, J. J. Neuropsychiatric and Memory Issues in Epilepsy. *Mayo Clin. Proc.* **2003***, 78*, 781.

8.   Niedermeyer, E. The *Epilepsies: Diagnosis and Management*; Urban & Schwarzenberg, Inc., Baltimore, Maryland, **1990**; 419.

9.   Browne, T.; Feldman, R. Eds. *Epilepsy Diagnosis and Management*; Little, Brown & Co., **1983**.

10.   Stys, P. K.; Waxman, S.G.; Ransom, B. R. Ionic Mechanisms of Anoxic Injury in Mammalian CNS White Matter: Role of Na Channels and Na ( )-Ca2 Exchanger. *J. Neurosci.* **1992***, 12*, 430.

11.   Mayer, S. A.; Claassen, J.; Mendelsohn, F.; Dennis, L. J.; Fitzsimmons, B. F. Refractory Status Epilepticus: Frequency, Risk Factors, and Impact on Outcome. *Arch. Neurol.* **2002***, 59*, 205.

12.   Towne, A. R.; Pellock, J. M.; Ko, D.; DeLorenzo, R. J. Determinants of Mortality in Status Epilepticus. *Epilepsia.* **1994***, 35*, 27.

13.   Jacobs, M. P.; Leblanc, G. G.; Brooks-Kayal, A.; Jensen, F. E.; Lowenstein, D. H.; Noebels, J. L.; Spencer, D. D.; Swann, J. W. Curing Epilepsy: Progress and Future Directions. *Epilepsy Behav.* **2009***, 14*, 438-445.

14. Bialer, M.; White, H. S. Key Factors in the Discovery and Development of New Antiepileptic Drugs. *Nat. Rev. Drug Discov.* **2010***, 9*, 68-82.

15. Scott, D. F. *The History of Epileptic Therapy: An Account of how Medication was Developed*; Parthenon Pub. Group, **1993**.

16. Gross, R. A Brief History of Epilepsy and its Therapy in the Western Hemisphere. *Epilepsy Res.* **1992***, 12*, 65.

17. Porter, R. J.; Rogawski, M. A. New Antiepileptic Drugs: From Serendipity to Rational Discovery. *Epilepsia.* **1992***, 33*, S1.

18. Brodie, M. J. Antiepileptic Drug Therapy the Story so Far. *Seizure.* **2010***, 19*, 650.

19. Bazil, C. W.; Pedley, T. A. Advances in the Medical Treatment of Epilepsy. *Annu. Rev. Med.* **1998***, 49*, 135-162.

20. Loscher, W. Current Status and Future Directions in the Pharmacotherapy of Epilepsy. *Trends Pharmacol. Sci.* **2002***, 23*, 113.

21. Shorvon, S. D.; Farmer, P. J. Epilepsy in Developing Countries: A Review of Epidemiological, Sociocultural, and Treatment Aspects. *Epilepsia.* **1988***, 29*, S36.

22. White, H. S. Preclinical Development of Antiepileptic Drugs: Past, Present, and Future Directions. *Epilepsia.* **2003***, 44*, 2.

23. Prunetti, P.; Perucca, E. New and Forthcoming Anti-Epileptic Drugs. *Curr. Opin. Neurol.* **2011***, 24*, 159.

24. Johannessen Landmark, C.; Patsalos, P. N. Drug Interactions Involving the New Second- and Third-Generation Antiepileptic Drugs. *Expert Rev. Neurother.* **2010***, 10*, 119-140.

25. LaRoche, S. M.; Helmers, S. L. The New Antiepileptic Drugs: Scientific Review. *JAMA (Chicago, Ill.).* **2004***, 291*, 605.

26. Pellock, J. M.; Carbamazepine Side Effects in Children and Adults. *Epilepsia*. **1987***, 28*, Suppl 3: S64-70

27. Benbadis, S. R.; Tatum, W. O.,4th. Advances in the Treatment of Epilepsy. *Am. Fam. Physician.* **2001***, 64*, 91-98.

28. Wermuth, C., Ed. *The Practice of Medicinal Chemistry*, 3rd ed.; Academic Press, **2008**.

29.   Weaver, D.; Nogrady, T. *Medicinal Chemistry: A Molecular and Biochemical Approach*; Oxford University Press, **2005**.

30.   Holtkamp, M.; Meierkord, H. Anticonvulsant, Antiepileptogenic, and Antiictogenic Pharmacostrategies. *Cell Mol. Life Sci.* **2007**, *64*, 2023-2041.

31.   Espinoza-Fonseca, L. M. The Benefits of the Multi-Target Approach in Drug Design and Discovery. *Bioorg. Med. Chem.* **2006**, *14*, 896-897.

32.   Meldrum, B. S.; Rogawski, M. A. Molecular Targets for Antiepileptic Drug Development. *Neurotherapeutics.* **2007**, *4*, 18-61.

33.   Wulff, H.; Zhorov, B. S. K+ Channel Modulators for the Treatment of Neurological Disorders and Autoimmune Diseases. *Chem. Rev.* **2008**, *108*, 1744-1773.

34.   Chebib, M.; Johnston, G. A. GABA-Activated Ligand Gated Ion Channels: Medicinal Chemistry and Molecular Biology. *J. Med. Chem.* **2000**, *43*, 1427-1447.

35.   Meldrum, B. S. Identification and Preclinical Testing of Novel Antiepileptic Compounds. *Epilepsia.* **1997**, *38*, Suppl 9, S7-15.

36.   Lima, L. M.; Barreiro, E. J. Bioisosterism: A Useful Strategy for Molecular Modification and Drug Design. *Curr. Med. Chem.* **2005**, *12*, 23-49.

37.   Lipinski, C. A.; Lombardo, F.; Dominy, B. W.; Feeney, P. J. Experimental and Computational Approaches to Estimate Solubility and Permeability in Drug Discovery and Development Settings. *Adv. Drug Deliv. Rev.* **2001**, *46*, 3-26.

38.   Lipinski, C. A. Lead- and Drug-Like Compounds: The Rule-of-Five Revolution. *Drug Discov. Today: Technologies.* **2004**, *1*, 337.

39.   Pajouhesh, H.; Lenz, G. R. Medicinal Chemical Properties of Successful Central Nervous System Drugs. *NeuroRx.* **2005**, *2*, 541-553.

40.   Stella, V. J. A Case for Prodrugs: Fosphenytoin. *Adv. Drug Deliv. Rev.* **1996**, *19*, 311.

41.   Striano, P.; Striano, S. New and Investigational Antiepileptic Drugs. *Expert Opin. Investig. Drugs.* **2009**, *18*, 1875-1884.

42.   Schachter, S. C. Currently Available Antiepileptic Drugs. *Neurotherapeutics.* **2007**, *4*, 4-11.

43. Sabers, A.; Gram, L. Newer Anticonvulsants: Comparative Review of Drug Interactions and Adverse Effects. *Drugs.* **2000***, 60*, 23-33.

44. Longo, L. P.; Johnson, B. Addiction: Part I. Benzodiazepines--Side Effects, Abuse Risk and Alternatives. *Am. Fam. Physician.* **2000***, 61*, 2121-2128.

45. Wheless, J. W.; Vazquez, B. Rufinamide: A Novel Broad-Spectrum Antiepileptic Drug. *Epilepsy Curr.* **2010***, 10*, 1-6.

46. Schmidt, D. Adverse Effects of Valproate. *Epilepsia.* **1984***, 25*, S44.

47. Lindhout, D.; Omtzigt, J. G. Teratogenic Effects of Antiepileptic Drugs: Implications for the Management of Epilepsy in Women of Childbearing Age. *Epilepsia.* **1994***, 35 Suppl 4*, S19-28.

48. Shackleton, D. P.; Kasteleijn-Nolst Trenite, D. G.; de Craen, A. J.; Vandenbroucke, J. P.; Westendorp, R. G. Living with Epilepsy: Long-Term Prognosis and Psychosocial Outcomes. *Neurology.* **2003***, 61*, 64-70.

49. Tao, J. X.; Qian, S.; Baldwin, M.; Chen, X. J.; Rose, S.; Ebersole, S. H.; Ebersole, J. S. SUDEP, Suspected Positional Airway Obstruction, and Hypoventilation in Postictal Coma. *Epilepsia.* **2010***, 51*, 2344-2347.

50. Sirven, J.; Whedon, B.; Caplan, D.; Liporace, J.; Glosser, D.; O'Dwyer, J.; Sperling, M. R. The Ketogenic Diet for Intractable Epilepsy in Adults: Preliminary Results. *Epilepsia.* **1999***, 40*, 1721-1726.

51. Kossoff, E. H.; Zupec-Kania, B. A.; Rho, J. M. Ketogenic Diets: An Update for Child Neurologists. *J. Child Neurol.* **2009***, 24*, 979-988.

52. Kemeny, A. A. Surgery for Epilepsy. *Seizure.* **2001***, 10*, 461.

53. Unverferth, K.; Engel, J.; Hofgen, N.; Rostock, A.; Gunther, R.; Lankau, H. J.; Menzer, M.; Rolfs, A.; Liebscher, J.; Muller, B.; Hofmann, H. J. Synthesis, Anticonvulsant Activity, and Structure-Activity Relationships of Sodium Channel Blocking 3-Aminopyrroles. *J. Med. Chem.* **1998***, 41*, 63-73.

54. Tasso, S. M. Pharmacophore Model for Antiepileptic Drugs Acting on Sodium Channels. *J. Mol. Model.* **2001***, 7*, 231.

55. *Molecular Operating Environment (MOE)*, 2010.10; Chemical Computing Group Inc., 1010 Sherbooke St. West, Suite #910, Montreal, QC, Canada, H3A 2R7, **2010**.

56. Reginald, G.; Grisham, C. *Biochemistry*, 4th ed.; Brooks/Cole, **2010**.

57.	Guillain, B. M. Design and Synthesis of Uracil Analogs as Anticonvulsant and Antiepileptogenic Active Prodrugs (MSc Thesis). Queen's University, **2000**.

58.	Tiedje, K. E.; Stevens, K.; Barnes, S.; Weaver, D. F. Beta-Alanine as a Small Molecule Neurotransmitter. *Neurochem. Int.* **2010**, *57*, 177-188.

59.	Hill, C. A.; Harris, R. C.; Kim, H. J.; Harris, B. D.; Sale, C.; Boobis, L. H.; Kim, C. K.; Wise, J. A. Influence of Beta-Alanine Supplementation on Skeletal Muscle Carnosine Concentrations and High Intensity Cycling Capacity. *Amino Acids.* **2007**, *32*, 225-233.

60.	Cavalheiro, E. A. The Pilocarpine Model of Epilepsy. *Ital. J. Neurol. Sci.* **1995**, *16*, 33.

61.	Tsuchiya, Y.; Tamura, T.; Fujii, M.; Ito, M. Keto-Enol Tautomer of Uracil and Thymine. *J. Phys. Chem.* **1988**, *92*, 1760.

62.	Tian, S. X. How Many Uracil Tautomers there are? Density Functional Studies of Stability Ordering of Tautomers. *Chem. Phys.* **1999**, *242*, 217.

63.	Kryachko, E. S. Theoretical Study of Tautomeric Forms of Uracil. 1. Relative Order of Stabilities and their Relation to Proton Affinities and Deprotonation Enthalpies. *J. Phys. Chem. A.* **2001**, *105*, 1288.

64.	Jonas, J. Nucleic acid components and their analogues. XVI. Dissociation Constant of Uracil, 6-Azauracil, 5-Azauracil and Related Compounds. *Coll. Czechoslov. Chem. Commun.* **1962**, *27*, 716.

65.	Davidson, D. The Preparation of Uracil from Urea. *J. Am. Chem. Soc.* **1926**, *48*, 2379.

66.	Paxson, F. L. *The Last American Frontier*; The Macmillan Company, **1910**.

67.	Bergmann, W. Researches on Pyrimidines. CXXXII. A New Synthesis of Thymine. *J. Am. Chem. Soc.* **1933**, *55*, 1733.

68.	Beckwith, A. L. J. Oxidative Cyclization of Diamides by Phenyliodoso Acetate. *Aust. J. Chem. , 43*, 451.

69.	Maruyama, T. Halogenation of Pyrimidine 6-O-Cyclonucleosides. *J. Org. Chem.* **1983**, *48*, 2719.

70.	Tee, O. S. Mechanisms of Bromination of Uracil Derivatives. 6. Cytosine and N-Substituted Derivatives. *J. Org. Chem.* **1982**, *47*, 1018.

71. Longley, D. B.; Harkin, D. P.; Johnston, P. G. 5-Fluorouracil: Mechanisms of Action and Clinical Strategies. *Nat. Rev. Cancer.* **2003***, 3*, 330-338.

72. Hronowski, L. J. J. Synthesis of Cyclopentane Analogs of 5-Fluorouracil Nucleosides. *Can. J. Chem.* **1992***, 70*, 1162.

73. Barton, D. H.; Hesse, R. H.; To, H. T.; Pechet, M. M. A Convenient Synthesis of 5-Fluorouracil. *J. Org. Chem.* **1972***, 37*, 329-330.

74. Visser, G. W. M. Mechanism and Stereochemistry of the Fluorination of Uracil and Cytosine using Fluorine and Acetyl Hypofluorite. *J. Org. Chem.* **1986***, 51*, 1466.

75. Johnson, T. B. Researches on Pyrimidines. LXXXVII. Alkylation of 5-Amino-Uracil. *J. Am. Chem. Soc.* **1919***, 41*, 782.

76. Itahara, T. Nitration of Aromatic Heterocycles with Palladium (II) Acetate and Sodium Nitrite. *Bull. Chem. Soc. Jpn.* **1983***, 56*, 2171.

77. Huang, G. F. Nitration of Pyrimidine Bases and Nucleotides by Nitronium Tetrafluoroborate. Synthesis of 5-Nitro-2'-Deoxyuridine. *J. Org. Chem.* **1977***, 42*, 3821.

78. Andres, P. A New Synthesis of 5-Trifluoromethyluracil. *J. Fluorine Chem.* **1996***, 77*, 93.

79. Baker, B. R.; Rzeszotarski, W. Irreversible Enzyme Inhibitors. CIV. Inhibitors of Thymidine Phosphorylase. 8. further Studies on Hydrophobic Bonding with 6-Substituted Uracils. *J. Med. Chem.* **1967***, 10*, 1109-1113.

80. Baker, B. R. Nonclassical Antimetabolites XVIII. Simulation of 5′‐phosphoribosyl Binding II. ω‐uracil Alkanoic Acids Related to 2′‐deoxyuridylate. *J. Pharm. Sci.* **1965***, 54*, 25.

81. Baker, B. R. Nonclassical Antimetabolites. XXVI. Inhibitors of Thymidine Kinase. II. 1, 2 Inhibition by Functionalized 1-Alkyluracils. *J. Med. Chem.* **1966***, 9*, 73.

82. Wu, F. Benzhydryl as an Efficient Selective Nitrogen Protecting Group for Uracils. *J. Org. Chem.* **2004***, 69*, 9307.

83. Cruickshank, K. A. The Benzoylation of Uracil and Thymine. *Tetrahedron Lett.* **1984***, 25*, 681.

84. Zhang, Z. L. The Benzoylation of 6-Methyluracil and 5-Nitro-6-Methyluracil. *Chinese Chem. Lett.* **2005***, 16*, 287.

85. Romeo, G. Synthesis of N, O-Homonucleosides with High Conformational Freedom. *Arkivoc.* **2009***, 8*, 168.

86. Jayakanthan, K. Stereoselective Synthesis of 4'-Selenonucleosides using the Pummerer Glycosylation Reaction. *Carbohydr. Res.* **2008***, 343*, 1790.

87. Jarowicki, K. Protecting Groups. *Contemp. Org. Synth.* **1997***, 4*, 454.

88. Edstrom, E. D. Development of Methylthiomethyl (MTM) Protection for N1 of Pyrrolo [2, 3-d] Pyrimidin-2, 4-Diones. *Tetrahedron Lett.* **1996***, 37*, 759.

89. Guillain, B. M. Synthesis and Three-Dimensional Quantitative Structure-Activity Relationship Studies of Uracil-Based Molecules as Potential Antiepileptic Active Prodrugs (PhD Thesis). Dalhousie University, **2006**.

90. Zhang, Z.; Zhou, S.; Wang, X.; Wang, H.; Chen, Y.; Liu, J. Tetra-n-Butylammonium Hydroxide: An Efficient Catalyst for N-Alkylation of Pyrimidines and Purines. *Chem. Res. Chinese U.* **2006***, 22*, 451.

91. Suwinski, J. Salts of 5-Substituted Uracils with 1, 8-Diazabicyclo [5.4. 0]-Undec-7-Ene: Convenient Reagents for Nucleophilic Addition and Substitution Reactions. *Synthesis.* **2001**, 225.

92. Boncel, S. Michael Versus Retro-Michael Reaction in the Regioselective Synthesis of N-1 and N-3 Uracil Adducts. *Tetrahedron.* **2010**.

93. Privat, E. A Proposed Mechanism for the Mutagenicity of 5-formyluracil. *Mut. Res.* **1996**, 354, 151-156.

94. Ding, J. C. Crystal Structure of 5-Fluoro-1-Benzyluracil,(C6H5) CH2 (C4N2H2FO2). *Z Krist. New Cryst. St.* **2006***, 221*, 83.

95. Jones, T. R. Azafluorenes Containing Two Bridgehead Nitrogen Atoms. *J. Chem. Soc. Perk. T. 1.* **1987**, 2585.

96. Baker, B. R.; Kelley, J. L. Irreversible Enzyme Inhibitors. CLXX. Inhibition of FUDR Phosphorylase from Walker 256 Rat Tumor by 1-Substituted Uracils. *J. Med. Chem.* **1970***, 13*, 458-461.

97. Novikov, M. S. Synthesis of 5-(Arylamino)-1-Benzyluracils. *Chem. Heterocycl. Comp.* **2005***, 41*, 766.

98.   Kundu, N. G.; Schmitz, S. A. N-Alkylated Derivatives of 5-Fluorouracil. *J. Pharm. Sci.* **1982***, 71*, 935-938.

99.   Stables, J. P.; Kupferberg, H. J. The NIH Anticonvulsant Drug Development (ADD) Program: Preclinical Anticonvulsant Screening Project. In *Molecular and Cellular Targets for Anti-Epileptic Drugs*; John Libbey & Company Ltd., 1997; 191.

100.   Smith, M.; Wilcox, K. S.; White, H. S. Discovery of Antiepileptic Drugs. *Neurotherapeutics.* **2007***, 4*, 12-17.

101.   Siddiqui, N. An Updated Review: Emerging Anticonvulsants. *IJPBA*, **2010**, 1, *5*, 404-415

102.   Vilar, S.; Cozza, G.; Moro, S. Medicinal Chemistry and the Molecular Operating Environment (MOE): Application of QSAR and Molecular Docking to Drug Discovery. *Curr. Top. Med. Chem.* **2008***, 8*, 1555-1572.

103.   Labute, P. Binary QSAR: A New Method for the Determination of Quantitative Structure Activity Relationships. *Pac. Symp. Biocomput.* **1999**, 444-455.

104.   Tropsha, A. The Importance of being Earnest: Validation is the Absolute Essential for Successful Application and Interpretation of QSPR Models. *QSAR Comb. Sci.* **2003***, 22*, 69.

105.   Halgren, T. A. MMFF VI. MMFF94s Option for Energy Minimization Studies. *J. Computat. Chem.* **1999***, 20*, 720.

106.   Pitkanen, A.; McIntosh, T. Animal Models of Post-Traumatic Epilepsy. *J. Neurotrauma.* **2006***, 23*, 241.

Experimental:

<u>Data Collection</u>

A colourless-block crystal of $C_{11}H_9N_2O_2Cl$ having approximate dimensions of 0.34 x 0.29 x 0.21 mm was mounted on a glass fiber. All measurements were made on a Rigaku RAXIS RAPID imaging plate area detector with graphite monochromated Mo-Kα radiation.

Indexing was performed from 4 oscillations that were exposed for 180 seconds. The crystal-to-detector distance was 127.40 mm.

Cell constants and an orientation matrix for data collection corresponded to a primitive triclinic cell with dimensions:

$a = 7.1536(3)$ Å $\alpha = 82.24(2)^o$
$b = 8.9287$ Å $\beta = 74.508(17)^o$
$c = 9.2335(2)$ Å $\gamma = 67.181(15)^o$
$V = 523.53(2)$ Å^3

For Z = 2 and F.W. = 236.66, the calculated density is 1.501 g/cm^3. Based on a statistical analysis of intensity distribution, and the successful solution and refinement of the structure, the space group was determined to be:

P-1 (#2)

The data were collected at a temperature of 26 ± 1^oC to a maximum 2θ value of 71.6^o. A total of 79 oscillation images were collected. A sweep of data was done using ω oscillations from 35.0 to 95.0^o in 5.0^o steps. The exposure rate was 168.0 [sec./^{o}]. The detector swing angle was -0.11^o. A second sweep was performed using ω oscillations from 42.5 to 132.5^o in 5.0^o steps. The exposure rate was 168.0 [sec./^{o}]. The detector swing angle was -0.11^o. Another sweep was performed using ω oscillations from 37.0 to 105.0^o in 5.0^o steps. The exposure rate was 168.0 [sec./^{o}]. The detector swing angle was -0.11^o. Another sweep was performed using ω oscillations from 20.0 to 200.0^o in 5.0^o steps. The exposure rate was 168.0 [sec./^{o}]. The detector swing angle was -0.11^o. The crystal-to-detector distance was 127.40 mm. Readout was performed in the 0.100 mm pixel mode.

<u>Data Reduction</u>

Of the 12998 reflections that were collected, 4048 were unique (R_{int} = 0.022); equivalent reflections were merged.

The linear absorption coefficient, μ, for Mo-Kα radiation is 3.488 cm^{-1}. An empirical absorption correction was applied which resulted in transmission factors ranging from 0.854 to 0.929. The data were corrected for Lorentz and polarization effects.

<u>Structure Solution and Refinement</u>

The structure was solved by direct methods[1] and expanded using Fourier techniques[2]. The non-hydrogen atoms were refined anisotropically. Hydrogen atoms were refined isotropically. The final cycle of full-matrix least-squares refinement[3] on F was based on 1989 observed reflections (I > 3.00σ(I)) and 145 variable parameters and converged (largest parameter shift was 0.00 times its esd) with unweighted and weighted agreement factors of:

$$R = \Sigma \, ||Fo| - |Fc|| \, / \, \Sigma \, |Fo| = 0.0336$$

$$R_W = [\, \Sigma \, w \, (|Fo| - |Fc|)^2 \, / \, \Sigma \, w \, Fo^2]^{1/2} = 0.0420$$

The standard deviation of an observation of unit weight[4] was 1.05. A Robust-resistant weighting scheme was used[5]. Plots of $\Sigma \, w \, (|Fo| - |Fc|)^2$ versus |Fo|, reflection order in data collection, sin θ/λ and various classes of indices showed no unusual trends. The maximum and minimum peaks on the final difference Fourier map corresponded to 0.22 and -0.24 e$^-$/Å^3, respectively.

Neutral atom scattering factors were taken from Cromer and Waber[6]. Anomalous dispersion effects were included in Fcalc[7]; the values for Δf' and Δf" were those of Creagh and McAuley[8]. The values for the mass attenuation coefficients are those of Creagh and Hubbell[9]. All calculations were performed using the CrystalStructure[10,11] crystallographic software package.

References:

(1) <u>SHELX97</u>: Sheldrick, G.M. (1997).

(2) <u>DIRDIF99</u>: Beurskens, P.T., Admiraal, G., Beurskens, G., Bosman, W.P., de Gelder, R., Israel, R. and Smits, J.M.M.(1999). The DIRDIF-99 program system, Technical Report of the Crystallography Laboratory, University of Nijmegen, The Netherlands.

(3) Least Squares function minimized:

$\Sigma w(|F_O|-|F_C|)^2$ where w = Least Squares weights.

(4) Standard deviation of an observation of unit weight:

$$[\Sigma w(|F_O|-|F_C|)^2/(N_O-N_V)]^{1/2}$$

where: N_O = number of observations
N_V = number of variables

(5) Carruthers, J.R. and Watkin, D.J. (1979), Acta Cryst, A35, 698-699

(6) Cromer, D. T. & Waber, J. T.; "International Tables for X-ray Crystallography", Vol. IV, The Kynoch Press, Birmingham, England, Table 2.2 A (1974).

(7) Ibers, J. A. & Hamilton, W. C.; Acta Crystallogr., 17, 781 (1964).

(8) Creagh, D. C. & McAuley, W.J .; "International Tables for Crystallography", Vol C, (A.J.C. Wilson, ed.), Kluwer Academic Publishers, Boston, Table 4.2.6.8, pages 219-222 (1992).

(9) Creagh, D. C. & Hubbell, J.H..; "International Tables for Crystallography", Vol C, (A.J.C. Wilson, ed.), Kluwer Academic Publishers, Boston, Table 4.2.4.3, pages 200-206 (1992).

(10) CrystalStructure 3.8: Crystal Structure Analysis Package, Rigaku and Rigaku Americas (2000-2007). 9009 New Trails Dr. The Woodlands TX 77381 USA.

(11) CRYSTALS Issue 11: Carruthers, J.R., Rollett,J.S., Betteridge, P.W., Kinna, D., Pearce, L., Larsen, A., and Gabe, E. Chemical Crystallography Laboratory, Oxford, UK. (1999)

Experimental Details:

A. Crystal Data

Empirical Formula	$C_{11}H_9N_2O_2Cl$
Formula Weight	236.66
Crystal Color, Habit	colourless, block
Crystal Dimensions	0.34 X 0.29 X 0.21 mm
Crystal System	triclinic
Lattice Type	Primitive
Indexing Images	4 oscillations @ 180.0 seconds
Detector Position	127.40 mm
Pixel Size	0.100 mm
Lattice Parameters	$a = 7.1536(3)$ Å
	$b = 8.9287$ Å
	$c = 9.2335(2)$ Å
	$\alpha = 82.24(2)$ º
	$\beta = 74.508(17)$ º
	$\gamma = 67.181(15)$ º
	$V = 523.53(2)$ Å^3
Space Group	P-1 (#2)
Z value	2
D_{calc}	1.501 g/cm^3
F_{000}	244.00
μ(MoKα)	3.488 cm^{-1}

B. Intensity Measurements

Diffractometer	Rigaku RAXIS-UNKNOWN
Radiation	MoKα (λ = 0.71070 Å) graphite monochromated
Data Images	79 exposures
ω oscillation Range	35.0 - 95.0°
Exposure Rate	168.0 sec./°
ω oscillation Range	42.5 - 132.5°
Exposure Rate	168.0 sec./°
ω oscillation Range	37.0 - 105.0°
Exposure Rate	168.0 sec./°
ω oscillation Range	20.0 - 200.0°
Exposure Rate	168.0 sec./°
Detector Position	127.40 mm
Pixel Size	0.100 mm
$2\theta_{max}$	71.6°
No. of Reflections Measured	Total: 12998 Unique: 4044 (R_{int} = 0.022)
Corrections	Lorentz-polarization Absorption (trans. factors: 0.854 - 0.929)

C. Structure Solution and Refinement

Structure Solution	Direct Methods (SHELX97)
Refinement	Full-matrix least-squares on F
Function Minimized	Σ w $(|Fo| - |Fc|)^2$
Least Squares Weights parameters	Chebychev polynomial with 3
	4.8679,3.7115,3.2359,
$2\theta_{max}$ cutoff	53.0^o
Anomalous Dispersion	All non-hydrogen atoms
No. Observations (I>3.00σ(I))	1989
No. Variables	145
Reflection/Parameter Ratio	13.72
Residuals: R (I>3.00σ(I))	0.0336
Residuals: Rw (I>3.00σ(I))	0.0420
Goodness of Fit Indicator	1.047
Max Shift/Error in Final Cycle	0.000
Maximum peak in Final Diff. Map	0.22 e$^-$/Å^3
Minimum peak in Final Diff. Map	-0.24 e$^-$/Å^3

Table 1. Atomic coordinates and B_{iso}/B_{eq}

atom	x	y	z	B_{eq}
Cl1	0.13965(5)	1.21621(3)	0.43137(4)	4.589(8)
O1	0.32986(17)	0.90277(13)	0.26738(10)	5.06(2)
O2	0.46734(14)	0.56563(10)	0.67258(9)	4.047(17)
N1	0.39175(14)	0.73744(11)	0.47307(10)	3.372(18)
N2	0.32123(15)	0.83764(11)	0.70934(10)	3.330(17)
C1	0.31970(17)	0.88923(14)	0.40134(13)	3.43(2)
C2	0.23689(16)	1.02140(13)	0.50449(13)	3.28(2)
C3	0.23971(17)	0.99274(13)	0.65053(13)	3.40(2)
C4	0.39746(16)	0.70438(13)	0.62119(12)	3.196(19)
C5	0.33607(18)	0.80990(14)	0.86731(12)	3.59(2)
C6	0.17458(17)	0.74943(12)	0.96818(11)	3.31(2)
C7	-0.0237(2)	0.79666(16)	0.94532(14)	4.19(2)
C8	-0.1669(2)	0.7375(2)	1.04295(18)	5.33(3)
C9	-0.1109(2)	0.6331(2)	1.16221(19)	5.76(3)
C10	0.0841(2)	0.58953(17)	1.18704(17)	5.25(3)
C11	0.2276(2)	0.64671(15)	1.09024(14)	4.14(2)

$B_{eq} = 8/3 \ \pi^2(U_{11}(aa^*)^2 + U_{22}(bb^*)^2 + U_{33}(cc^*)^2 + 2U_{12}(aa^*bb^*)\cos \gamma + 2U_{13}(aa^*cc^*)\cos \beta + 2U_{23}(bb^*cc^*)\cos \alpha)$

Table 2. Atomic coordinates and B $_{iso}$ involving hydrogens/B_{eq}

atom	x	y	z	B_{eq}
H1	0.4376	0.6555	0.4227	4.36
H2	0.1860	1.0820	0.7147	4.06
H3	0.4706	0.7318	0.8709	4.38
H4	0.3197	0.9097	0.9041	4.35
H5	-0.0624	0.8690	0.8637	5.04
H6	-0.3032	0.7692	1.0275	6.52
H7	-0.2088	0.5915	1.2272	6.85
H8	0.1210	0.5200	1.2708	5.85
H9	0.3635	0.6159	1.1065	4.73

$B_{eq} = 8/3 \ \pi^2(U_{11}(aa^*)^2 + U_{22}(bb^*)^2 + U_{33}(cc^*)^2 + 2U_{12}(aa^*bb^*)\cos \gamma + 2U_{13}(aa^*cc^*)\cos \beta + 2U_{23}(bb^*cc^*)\cos \alpha)$

Table 3. Anisotropic displacement parameters

Atom	U_{11}	U_{22}	U_{33}	U_{12}	U_{13}	U_{23}
Cl1	0.0656(2)	0.03669(18)	0.0661(2)	-0.01429(14)	-0.01919(15)	-0.01139(13)
O1	0.0799(6)	0.0560(5)	0.0433(4)	-0.0106(4)	-0.0170(4)	0.0020(3)
O2	0.0667(5)	0.0332(4)	0.0483(4)	-0.0095(3)	-0.0181(3)	-0.0013(3)
N1	0.0478(4)	0.0344(4)	0.0404(4)	-0.0090(3)	-0.0090(3)	-0.0051(3)
N2	0.0509(4)	0.0337(4)	0.0398(4)	-0.0129(3)	-0.0108(3)	-0.0022(3)
C1	0.0410(4)	0.0417(5)	0.0430(5)	-0.0118(4)	-0.0094(4)	0.0021(4)
C2	0.0390(4)	0.0332(4)	0.0495(5)	-0.0124(3)	-0.0095(4)	0.0037(4)
C3	0.0465(5)	0.0326(5)	0.0475(5)	-0.0129(4)	-0.0089(4)	-0.0028(4)
C4	0.0418(4)	0.0340(4)	0.0424(5)	-0.0105(3)	-0.0096(3)	-0.0018(3)
C5	0.0531(5)	0.0423(5)	0.0431(5)	-0.0160(4)	-0.0161(4)	-0.0036(4)
C6	0.0508(5)	0.0340(4)	0.0385(5)	-0.0106(4)	-0.0117(4)	-0.0065(3)
C7	0.0539(6)	0.0566(7)	0.0483(6)	-0.0149(5)	-0.0154(4)	-0.0103(5)
C8	0.0564(7)	0.0789(9)	0.0723(9)	-0.0285(6)	-0.0042(6)	-0.0310(7)
C9	0.0869(10)	0.0597(8)	0.0684(8)	-0.0402(7)	0.0170(7)	-0.0203(6)
C10	0.0855(9)	0.0434(6)	0.0560(7)	-0.0191(6)	-0.0014(6)	0.0009(5)
C11	0.0614(6)	0.0409(5)	0.0468(5)	-0.0096(4)	-0.0141(4)	-0.0002(4)

The general temperature factor expression: $\exp(-2\pi^2(a^{*2}U_{11}h^2 + b^{*2}U_{22}k^2 + c^{*2}U_{33}l^2 + 2a^*b^*U_{12}hk + 2a^*c^*U_{13}hl + 2b^*c^*U_{23}kl))$

Table 4. Bond lengths (Å)

atom	atom	distance	atom	atom	distance
Cl(1)	C(2)	1.7206(10)	O(1)	C(1)	1.2117(15)
O(2)	C(4)	1.2237(12)	N(1)	C(1)	1.3926(14)
N(1)	C(4)	1.3678(14)	N(2)	C(3)	1.3757(13)
N(2)	C(4)	1.3772(14)	N(2)	C(5)	1.4714(14)
C(1)	C(2)	1.4527(16)	C(2)	C(3)	1.3422(17)
C(5)	C(6)	1.5056(17)	C(6)	C(7)	1.3806(19)
C(6)	C(11)	1.3909(15)	C(7)	C(8)	1.392(2)
C(8)	C(9)	1.382(2)	C(9)	C(10)	1.370(2)
C(10)	C(11)	1.381(2)			

Table 5. Bond lengths involving hydrogens (Å)

atom	atom	distance	atom	atom	distance
N(1)	H(1)	0.827	C(3)	H(2)	0.950
C(5)	H(3)	0.950	C(5)	H(4)	0.950
C(7)	H(5)	0.951	C(8)	H(6)	0.949
C(9)	H(7)	0.951	C(10)	H(8)	0.951
C(11)	H(9)	0.950			

Table 6. Bond angles (º)

atom	atom	atom	angle	atom	atom	atom	angle
C(1)	N(1)	C(4)	127.72(9)	C(3)	N(2)	C(4)	121.12(9)
C(3)	N(2)	C(5)	120.78(9)	C(4)	N(2)	C(5)	118.07(8)
O(1)	C(1)	N(1)	121.43(11)	O(1)	C(1)	C(2)	126.22(10)
N(1)	C(1)	C(2)	112.34(9)	Cl(1)	C(2)	C(1)	117.38(8)
Cl(1)	C(2)	C(3)	121.34(9)	C(1)	C(2)	C(3)	121.27(9)
N(2)	C(3)	C(2)	121.76(10)	O(2)	C(4)	N(1)	122.46(10)
O(2)	C(4)	N(2)	121.80(10)	N(1)	C(4)	N(2)	115.73(8)
N(2)	C(5)	C(6)	113.89(11)	C(5)	C(6)	C(7)	122.05(9)
C(5)	C(6)	C(11)	118.14(11)	C(7)	C(6)	C(11)	119.78(11)
C(6)	C(7)	C(8)	119.46(11)	C(7)	C(8)	C(9)	120.16(15)
C(8)	C(9)	C(10)	120.35(16)	C(9)	C(10)	C(11)	119.88(14)
C(6)	C(11)	C(10)	120.33(14)				

Table 7. Bond angles involving hydrogens (º)

atom	atom	atom	angle	atom	atom	atom	angle
C(1)	N(1)	H(1)	118.4	C(4)	N(1)	H(1)	113.8
N(2)	C(3)	H(2)	119.1	C(2)	C(3)	H(2)	119.1
N(2)	C(5)	H(3)	108.3	N(2)	C(5)	H(4)	108.3
C(6)	C(5)	H(3)	108.5	C(6)	C(5)	H(4)	108.4
H(3)	C(5)	H(4)	109.4	C(6)	C(7)	H(5)	120.4
C(8)	C(7)	H(5)	120.2	C(7)	C(8)	H(6)	119.8
C(9)	C(8)	H(6)	120.0	C(8)	C(9)	H(7)	119.6
C(10)	C(9)	H(7)	120.0	C(9)	C(10)	H(8)	120.2
C(11)	C(10)	H(8)	119.9	C(6)	C(11)	H(9)	119.5
C(10)	C(11)	H(9)	120.1				

Table 8. Torsion Angles(º)

atom1	atom2	atom3	atom4	angle	atom1	atom2	atom3	atom4	angle
C(1)	N(1)	C(4)	O(2)	-178.86(12)	C(1)	N(1)	C(4)	N(2)	0.51(18)
C(4)	N(1)	C(1)	O(1)	177.30(13)	C(4)	N(1)	C(1)	C(2)	-2.26(18)
C(3)	N(2)	C(4)	O(2)	-178.81(12)	C(3)	N(2)	C(4)	N(1)	1.81(17)
C(4)	N(2)	C(3)	C(2)	-2.17(19)	C(3)	N(2)	C(5)	C(6)	104.69(12)
C(5)	N(2)	C(3)	C(2)	175.68(11)	C(4)	N(2)	C(5)	C(6)	-77.39(12)
C(5)	N(2)	C(4)	O(2)	3.28(18)	C(5)	N(2)	C(4)	N(1)	-176.09(10)
O(1)	C(1)	C(2)	Cl(1)	1.12(19)	O(1)	C(1)	C(2)	C(3)	-177.68(14)
N(1)	C(1)	C(2)	Cl(1)	-179.35(8)	N(1)	C(1)	C(2)	C(3)	1.85(17)
Cl(1)	C(2)	C(3)	N(2)	-178.58(9)	C(1)	C(2)	C(3)	N(2)	0.17(19)
N(2)	C(5)	C(6)	C(7)	-33.39(14)	N(2)	C(5)	C(6)	C(11)	148.55(10)
C(5)	C(6)	C(7)	C(8)	-179.58(13)	C(5)	C(6)	C(11)	C(10)	179.24(12)
C(7)	C(6)	C(11)	C(10)	1.14(19)	C(11)	C(6)	C(7)	C(8)	-1.55(19)
C(6)	C(7)	C(8)	C(9)	0.4(2)	C(7)	C(8)	C(9)	C(10)	1.3(2)
C(8)	C(9)	C(10)	C(11)	-1.7(2)	C(9)	C(10)	C(11)	C(6)	0.5(2)

The sign is positive if when looking from atom 2 to atom 3 a clock-wise motion of atom 1 would superimpose it on atom 4.

Table 9. Distances beyond the asymmetric unit out to 3.60 Å

atom	atom	distance	atom	atom	distance
Cl(1)	O(1)	3.0110(11)	Cl(1)	N(1)[1]	3.5337(10)
Cl(1)	N(2)[2]	3.5842(10)	Cl(1)	C(1)	2.7149(11)
Cl(1)	C(3)	2.6767(11)	Cl(1)	C(4)[2]	3.5458(13)
O(1)	Cl(1)	3.0110(11)	O(1)	N(1)	2.2733(12)
O(1)	C(2)	2.3789(15)	O(1)	C(3)	3.5671(15)
O(1)	C(4)	3.5583(14)	O(1)	C(7)[1]	3.4889(15)
O(1)	C(8)[3]	3.4861(15)	O(1)	C(11)[4]	3.374(2)
O(2)	O(2)[5]	3.3966(12)	O(2)	N(1)	2.2727(11)
O(2)	N(1)[5]	2.8792(13)	O(2)	N(2)	2.2738(12)
O(2)	C(1)	3.5818(13)	O(2)	C(3)	3.5195(13)
O(2)	C(4)[5]	3.5582(14)	O(2)	C(5)	2.7276(15)
O(2)	C(6)	3.1652(11)	O(2)	C(9)[6]	3.561(2)
O(2)	C(10)[7]	3.491(2)	O(2)	C(11)[7]	3.3730(16)
N(1)	Cl(1)[1]	3.5337(10)	N(1)	O(1)	2.2733(12)
N(1)	O(2)	2.2727(11)	N(1)	O(2)[5]	2.8792(13)
N(1)	N(2)	2.3245(13)	N(1)	C(2)	2.3639(13)
N(1)	C(3)	2.6828(15)	N(2)	Cl(1)[2]	3.5842(10)
N(2)	O(2)	2.2738(12)	N(2)	N(1)	2.3245(13)
N(2)	C(1)	2.8212(15)	N(2)	C(2)	2.3744(14)
N(2)	C(6)	2.4953(13)	N(2)	C(7)	2.9296(15)
C(1)	Cl(1)	2.7149(11)	C(1)	O(2)	3.5818(13)
C(1)	N(2)	2.8212(15)	C(1)	C(3)	2.4364(17)
C(1)	C(3)[2]	3.5927(19)	C(1)	C(4)	2.4781(15)
C(2)	O(1)	2.3789(15)	C(2)	N(1)	2.3639(13)
C(2)	N(2)	2.3744(14)	C(2)	C(2)[1]	3.5781(18)
C(2)	C(3)[2]	3.5921(16)	C(2)	C(4)	2.7944(14)
C(3)	Cl(1)	2.6767(11)	C(3)	O(1)	3.5671(15)
C(3)	O(2)	3.5195(13)	C(3)	N(1)	2.6828(15)
C(3)	C(1)	2.4364(17)	C(3)	C(1)[2]	3.5927(19)
C(3)	C(2)[2]	3.5921(16)	C(3)	C(4)	2.3973(15)
C(3)	C(5)	2.4757(15)	C(3)	C(6)	3.4459(14)
C(3)	C(7)	3.5436(17)	C(4)	Cl(1)[2]	3.5458(13)
C(4)	O(1)	3.5583(14)	C(4)	O(2)[5]	3.5582(14)
C(4)	C(1)	2.4781(15)	C(4)	C(2)	2.7944(14)
C(4)	C(3)	2.3973(15)	C(4)	C(5)	2.4431(16)
C(4)	C(6)	3.1766(13)	C(4)	C(7)	3.5547(14)
C(5)	O(2)	2.7276(15)	C(5)	C(3)	2.4757(15)
C(5)	C(4)	2.4431(16)	C(5)	C(7)	2.526(2)
C(5)	C(11)	2.4853(16)	C(6)	O(2)	3.1652(11)
C(6)	N(2)	2.4953(13)	C(6)	C(3)	3.4459(14)
C(6)	C(4)	3.1766(13)	C(6)	C(8)	2.395(2)
C(6)	C(9)	2.766(2)	C(6)	C(10)	2.4042(17)
C(7)	O(1)[1]	3.4889(15)	C(7)	N(2)	2.9296(15)
C(7)	C(3)	3.5436(17)	C(7)	C(4)	3.5547(14)
C(7)	C(5)	2.526(2)	C(7)	C(9)	2.405(2)
C(7)	C(10)	2.7741(19)	C(7)	C(11)	2.3976(19)
C(8)	O(1)[8]	3.4861(15)	C(8)	C(6)	2.395(2)
C(8)	C(10)	2.388(2)	C(8)	C(11)	2.756(2)
C(9)	O(2)[6]	3.561(2)	C(9)	C(6)	2.766(2)
C(9)	C(7)	2.405(2)	C(9)	C(11)	2.380(2)
C(10)	O(2)[7]	3.491(2)	C(10)	C(6)	2.4042(17)
C(10)	C(7)	2.7741(19)	C(10)	C(8)	2.388(2)

Table 9. Distances beyond the asymmetric unit out to 3.60 Å (continued)

atom	atom	distance	atom	atom	distance
C(11)	O(1)[9]	3.374(2)	C(11)	O(2)[7]	3.3730(16)
C(11)	C(5)	2.4853(16)	C(11)	C(7)	2.3976(19)
C(11)	C(8)	2.756(2)	C(11)	C(9)	2.380(2)

Symmetry Operators:

(1) -X,-Y+2,-Z+1   (2) -X+1,-Y+2,-Z+1
(3) X+1,Y,Z-1   (4) X,Y,Z-1
(5) -X+1,-Y+1,-Z+1   (6) -X,-Y+1,-Z+2
(7) -X+1,-Y+1,-Z+2   (8) X-1,Y,Z+1
(9) X,Y,Z+1

Table 10. Distances beyond the asymmetric unit out to 3.60 Å involving hydrogens

atom	atom	distance	atom	atom	distance
Cl(1)	H(2)	2.775	Cl(1)	H(3)[1]	3.504
Cl(1)	H(5)[2]	3.161	Cl(1)	H(8)[3]	2.883
Cl(1)	H(8)[4]	3.492	O(1)	H(1)	2.438
O(1)	H(2)[2]	3.599	O(1)	H(2)[1]	3.566
O(1)	H(4)[5]	3.366	O(1)	H(4)[1]	3.466
O(1)	H(5)[2]	2.612	O(1)	H(6)[6]	2.898
O(1)	H(7)[6]	3.356	O(1)	H(9)[5]	3.031
O(2)	H(1)	2.375	O(2)	H(1)[7]	2.060
O(2)	H(3)	2.517	O(2)	H(7)[8]	2.645
O(2)	H(8)[9]	2.916	O(2)	H(9)[9]	2.675
N(1)	H(1)[7]	3.334	N(1)	H(7)[6]	3.076
N(2)	H(1)	3.046	N(2)	H(2)	2.016
N(2)	H(3)	1.987	N(2)	H(4)	1.986
N(2)	H(5)	2.658	C(1)	H(1)	1.929
C(1)	H(2)	3.292	C(1)	H(2)[1]	3.511
C(1)	H(5)[2]	3.454	C(1)	H(7)[6]	3.511
C(2)	H(1)	3.123	C(2)	H(2)	1.987
C(3)	H(1)	3.509	C(3)	H(3)	3.135
C(3)	H(4)	2.506	C(3)	H(5)	2.959
C(4)	H(1)	1.863	C(4)	H(1)[7]	3.006
C(4)	H(2)	3.246	C(4)	H(3)	2.558
C(4)	H(4)	3.197	C(4)	H(5)	3.346
C(4)	H(7)[8]	3.394	C(4)	H(8)[9]	3.581
C(5)	H(2)	2.627	C(5)	H(5)	2.699
C(5)	H(6)[10]	3.185	C(5)	H(9)	2.618
C(5)	H(9)[9]	3.581	C(6)	H(2)	3.537
C(6)	H(2)[4]	3.411	C(6)	H(3)	2.019
C(6)	H(4)	2.018	C(6)	H(5)	2.034
C(6)	H(6)	3.252	C(6)	H(8)	3.262
C(6)	H(9)	2.035	C(7)	H(2)[4]	3.220
C(7)	H(3)	3.245	C(7)	H(4)	2.918
C(7)	H(4)[4]	2.898	C(7)	H(6)	2.038
C(7)	H(7)	3.261	C(7)	H(7)[8]	3.595
C(7)	H(9)	3.253	C(8)	H(2)[4]	2.874

Table 10. Distances beyond the asymmetric unit out to 3.60 Å involving hydrogens (continued)

atom	atom	distance	atom	atom	distance
C(8)	H(3)[11]	3.403	C(8)	H(4)[4]	2.969
C(8)	H(5)	2.042	C(8)	H(7)	2.029
C(8)	H(8)	3.247	C(9)	H(1)[12]	3.426
C(9)	H(2)[4]	2.728	C(9)	H(5)	3.263
C(9)	H(6)	2.031	C(9)	H(8)	2.023
C(9)	H(9)	3.239	C(10)	H(2)[4]	2.923
C(10)	H(3)[9]	3.329	C(10)	H(6)	3.243
C(10)	H(6)[8]	3.577	C(10)	H(7)	2.021
C(10)	H(9)	2.031	C(11)	H(2)[4]	3.261
C(11)	H(3)	2.535	C(11)	H(3)[9]	3.262
C(11)	H(4)	2.899	C(11)	H(5)	3.259
C(11)	H(7)	3.241	C(11)	H(8)	2.030
C(11)	H(9)[9]	3.216	H(1)	O(1)	2.438
H(1)	O(2)	2.375	H(1)	O(2)[7]	2.060
H(1)	N(1)[7]	3.334	H(1)	N(2)	3.046
H(1)	C(1)	1.929	H(1)	C(2)	3.123
H(1)	C(3)	3.509	H(1)	C(4)	1.863
H(1)	C(4)[7]	3.006	H(1)	C(9)[6]	3.426
H(1)	H(1)[7]	2.869	H(1)	H(7)[6]	2.589
H(1)	H(8)[5]	3.584	H(1)	H(9)[5]	3.191
H(2)	Cl(1)	2.775	H(2)	O(1)[2]	3.599
H(2)	O(1)[1]	3.566	H(2)	N(2)	2.016
H(2)	C(1)	3.292	H(2)	C(1)[1]	3.511
H(2)	C(2)	1.987	H(2)	C(4)	3.246
H(2)	C(5)	2.627	H(2)	C(6)	3.537
H(2)	C(6)[4]	3.411	H(2)	C(7)[4]	3.220
H(2)	C(8)[4]	2.874	H(2)	C(9)[4]	2.728
H(2)	C(10)[4]	2.923	H(2)	C(11)[4]	3.261
H(2)	H(3)	3.379	H(2)	H(4)	2.317
H(2)	H(5)	3.046	H(2)	H(6)[4]	3.305
H(2)	H(7)[4]	3.106	H(2)	H(8)[4]	3.374
H(3)	Cl(1)[1]	3.504	H(3)	O(2)	2.517
H(3)	N(2)	1.987	H(3)	C(3)	3.135
H(3)	C(4)	2.558	H(3)	C(6)	2.019
H(3)	C(7)	3.245	H(3)	C(8)[10]	3.403
H(3)	C(10)[9]	3.329	H(3)	C(11)	2.535
H(3)	C(11)[9]	3.262	H(3)	H(2)	3.379
H(3)	H(4)	1.551	H(3)	H(5)	3.540
H(3)	H(6)[10]	2.573	H(3)	H(8)[9]	2.993
H(3)	H(9)	2.347	H(3)	H(9)[9]	2.861
H(4)	O(1)[13]	3.366	H(4)	O(1)[1]	3.466
H(4)	N(2)	1.986	H(4)	C(3)	2.506
H(4)	C(4)	3.197	H(4)	C(6)	2.018
H(4)	C(7)	2.918	H(4)	C(7)[4]	2.898
H(4)	C(8)[4]	2.969	H(4)	C(11)	2.899
H(4)	H(2)	2.317	H(4)	H(3)	1.551
H(4)	H(5)	3.016	H(4)	H(5)[4]	2.847
H(4)	H(6)[10]	2.963	H(4)	H(6)[4]	2.970
H(4)	H(9)	2.971	H(5)	Cl(1)[2]	3.161
H(5)	O(1)[2]	2.612	H(5)	N(2)	2.658
H(5)	C(1)[2]	3.454	H(5)	C(3)	2.959

Table 10. Distances beyond the asymmetric unit out to 3.60 Å involving hydrogens (continued)

atom	atom	distance	atom	atom	distance
H(5)	C(4)	3.346	H(5)	C(5)	2.699
H(5)	C(6)	2.034	H(5)	C(8)	2.042
H(5)	C(9)	3.263	H(5)	C(11)	3.259
H(5)	H(2)	3.046	H(5)	H(3)	3.540
H(5)	H(4)	3.016	H(5)	H(4)[4]	2.847
H(5)	H(6)	2.342	H(6)	O(1)[12]	2.898
H(6)	C(5)[11]	3.185	H(6)	C(6)	3.252
H(6)	C(7)	2.038	H(6)	C(9)	2.031
H(6)	C(10)	3.243	H(6)	C(10)[8]	3.577
H(6)	H(2)[4]	3.305	H(6)	H(3)[11]	2.573
H(6)	H(4)[11]	2.963	H(6)	H(4)[4]	2.970
H(6)	H(5)	2.342	H(6)	H(7)	2.328
H(6)	H(9)[11]	3.070	H(7)	O(1)[12]	3.356
H(7)	O(2)[8]	2.645	H(7)	N(1)[12]	3.076
H(7)	C(1)[12]	3.511	H(7)	C(4)[8]	3.394
H(7)	C(7)	3.261	H(7)	C(7)[8]	3.595
H(7)	C(8)	2.029	H(7)	C(10)	2.021
H(7)	C(11)	3.241	H(7)	H(1)[12]	2.589
H(7)	H(2)[4]	3.106	H(7)	H(6)	2.328
H(7)	H(8)	2.324	H(7)	H(9)[11]	3.448
H(8)	Cl(1)[14]	2.883	H(8)	Cl(1)[4]	3.492
H(8)	O(2)[9]	2.916	H(8)	C(4)[9]	3.581
H(8)	C(6)	3.262	H(8)	C(8)	3.247
H(8)	C(9)	2.023	H(8)	C(11)	2.030
H(8)	H(1)[13]	3.584	H(8)	H(2)[4]	3.374
H(8)	H(3)[9]	2.993	H(8)	H(7)	2.324
H(8)	H(9)	2.332	H(9)	O(1)[13]	3.031
H(9)	O(2)[9]	2.675	H(9)	C(5)	2.618
H(9)	C(5)[9]	3.581	H(9)	C(6)	2.035
H(9)	C(7)	3.253	H(9)	C(9)	3.239
H(9)	C(10)	2.031	H(9)	C(11)[9]	3.216
H(9)	H(1)[13]	3.191	H(9)	H(3)	2.347
H(9)	H(3)[9]	2.861	H(9)	H(4)	2.971
H(9)	H(6)[10]	3.070	H(9)	H(7)[10]	3.448
H(9)	H(8)	2.332	H(9)	H(9)[9]	2.806

Symmetry Operators:

(1) -X+1,-Y+2,-Z+1   (2) -X,-Y+2,-Z+1
(3) X,Y+1,Z-1   (4) -X,-Y+2,-Z+2
(5) X,Y,Z-1   (6) X+1,Y,Z-1
(7) -X+1,-Y+1,-Z+1   (8) -X,-Y+1,-Z+2
(9) -X+1,-Y+1,-Z+2   (10) X+1,Y,Z
(11) X-1,Y,Z   (12) X-1,Y,Z+1
(13) X,Y,Z+1   (14) X,Y-1,Z+1

APPENDIX B: X-ray Crystallographic Data for **vi**

Experimental:

Data Collection

A colourless block crystal of $C_{11}H_9BrN_2O_2$ having approximate dimensions of 0.37 x 0.22 x 0.18 mm was mounted on a glass fiber. All measurements were made on a Rigaku RAXIS RAPID imaging plate area detector with graphite monochromated Mo-Kα radiation.

Indexing was performed from 4 oscillations that were exposed for 180 seconds. The crystal-to-detector distance was 127.40 mm.

Cell constants and an orientation matrix for data collection corresponded to a primitive triclinic cell with dimensions:

a = 7.2155(6) Å α = 85.32(2)^o
b = 8.9425 Å β = 75.075(18)^o
c = 9.3584(2) Å γ = 67.150(20)^o
V = 537.57(5) Å^3

For Z = 2 and F.W. = 281.11, the calculated density is 1.737 g/cm^3. Based on a statistical analysis of intensity distribution, and the successful solution and refinement of the structure, the space group was determined to be:

P-1 (#2)

The data were collected at a temperature of 23 $\pm$ 1°C to a maximum 2θ value of 71.3^o. A total of 86 oscillation images were collected. A sweep of data was done using ω oscillations from 160.0 to 190.0^o in 5.0^o steps. The exposure rate was 180.0 [sec./^{o}]. The detector swing angle was -0.07^o. A second sweep was performed using ω oscillations from 20.0 to 170.0^o in 5.0^o steps. The exposure rate was 180.0 [sec./^{o}]. The detector swing angle was -0.07^o. Another sweep was performed using ω oscillations from 39.0 to 115.0^o in 5.0^o steps. The exposure rate was 180.0 [sec./^{o}]. The detector swing angle was -0.07^o. Another sweep was performed using ω oscillations from 20.0 to 197.0^o in 5.0^o steps. The exposure rate was 180.0 [sec./^{o}]. The detector swing angle was -0.07^o. The crystal-to-detector distance was 127.40 mm. Readout was performed in the 0.100 mm pixel mode.

Data Reduction

Of the 14604 reflections that were collected, 4179 were unique (R_{int} = 0.035); equivalent reflections were merged.

The linear absorption coefficient, μ, for Mo-Kα radiation is 38.195 cm^{-1}. An empirical absorption correction was applied which resulted in transmission factors ranging from 0.199 to 0.503. The data were corrected for Lorentz and polarization effects. A correction for secondary extinction[1] was applied (coefficient = 19.035000).

Structure Solution and Refinement

The structure was solved by direct methods[2] and expanded using Fourier techniques[3]. The non-hydrogen atoms were refined anisotropically. Hydrogen atoms were refined isotropically. The final cycle of full-matrix least-squares refinement[4] on F was based on 2018 observed reflections ($I > 3.00\sigma(I)$) and 146 variable parameters and converged (largest parameter shift was 0.00 times its esd) with unweighted and weighted agreement factors of:

$$R = \Sigma \, ||Fo| - |Fc|| \, / \, \Sigma \, |Fo| = 0.0254$$

$$R_W = [\, \Sigma \, w \, (|Fo| - |Fc|)^2 \, / \, \Sigma \, w \, Fo^2]^{1/2} = 0.0315$$

The standard deviation of an observation of unit weight[5] was 1.05. A Robust-resistant weighting scheme was used[6]. Plots of $\Sigma \, w \, (|Fo| - |Fc|)^2$ versus $|Fo|$, reflection order in data collection, $\sin \theta/\lambda$ and various classes of indices showed no unusual trends. The maximum and minimum peaks on the final difference Fourier map corresponded to 0.31 and -0.47 e$^-$/Å^3, respectively.

Neutral atom scattering factors were taken from Cromer and Waber[7]. Anomalous dispersion effects were included in Fcalc[8]; the values for $\Delta f'$ and $\Delta f''$ were those of Creagh and McAuley[9]. The values for the mass attenuation coefficients are those of Creagh and Hubbell[10]. All calculations were performed using the CrystalStructure[11,12] crystallographic software package.

References:

(1) Larson, A.C. (1970), Crystallographic Computing, 291-294. F.R. Ahmed, ed. Munksgaard, Copenhagen (equation 22, with V replaced by the cell volume).

(2) SHELX97: Sheldrick, G.M. (1997).

(3) <u>DIRDIF99</u>: Beurskens, P.T., Admiraal, G., Beurskens, G., Bosman, W.P., de Gelder, R., Israel, R. and Smits, J.M.M.(1999). The DIRDIF-99 program system, Technical Report of the Crystallography Laboratory, University of Nijmegen, The Netherlands.

(4) Least Squares function minimized:

$$\Sigma w(|F_O|-|F_C|)^2 \quad \text{where w = Least Squares weights.}$$

(5) Standard deviation of an observation of unit weight:

$$[\Sigma w(|F_O|-|F_C|)^2/(N_O-N_V)]^{1/2}$$

where: N_O = number of observations
N_V = number of variables

(6) Carruthers, J.R. and Watkin, D.J. (1979), Acta Cryst, A35, 698-699

(7) Cromer, D. T. & Waber, J. T.; "International Tables for X-ray Crystallography", Vol. IV, The Kynoch Press, Birmingham, England, Table 2.2 A (1974).

(8) Ibers, J. A. & Hamilton, W. C.; Acta Crystallogr., 17, 781 (1964).

(9) Creagh, D. C. & McAuley, W.J .; "International Tables for Crystallography", Vol C, (A.J.C. Wilson, ed.), Kluwer Academic Publishers, Boston, Table 4.2.6.8, pages 219-222 (1992).

(10) Creagh, D. C. & Hubbell, J.H..; "International Tables for Crystallography", Vol C, (A.J.C. Wilson, ed.), Kluwer Academic Publishers, Boston, Table 4.2.4.3, pages 200-206 (1992).

(11) <u>CrystalStructure 3.8</u>: Crystal Structure Analysis Package, Rigaku and Rigaku Americas (2000-2007). 9009 New Trails Dr. The Woodlands TX 77381 USA.

(12) <u>CRYSTALS Issue 11</u>: Carruthers, J.R., Rollett,J.S., Betteridge, P.W., Kinna, D., Pearce, L., Larsen, A., and Gabe, E. Chemical Crystallography Laboratory, Oxford, UK. (1999)

Experimental Details:

A. Crystal Data

Empirical Formula	$C_{11}H_9BrN_2O_2$
Formula Weight	281.11
Crystal Color, Habit	colourless, block
Crystal Dimensions	0.37 X 0.22 X 0.18 mm
Crystal System	triclinic
Lattice Type	Primitive
Indexing Images	4 oscillations @ 180.0 seconds
Detector Position	127.40 mm
Pixel Size	0.100 mm
Lattice Parameters	$a = 7.2155(6)$ Å
	$b = 8.9425$ Å
	$c = 9.3584(2)$ Å
	$\alpha = 85.32(2)\ ^o$
	$\beta = 75.075(18)\ ^o$
	$\gamma = 67.150(20)\ ^o$
	$V = 537.57(9)$ Å^3
Space Group	P-1 (#2)
Z value	2
D_{calc}	1.737 g/cm^3
F_{000}	280.00
$\mu(MoK\alpha)$	38.195 cm^{-1}

B. Intensity Measurements

Diffractometer	Rigaku RAXIS-RAPID
Radiation	MoKα (λ = 0.71070 Å) graphite monochromated
Data Images	86 exposures
ω oscillation Range	160.0 - 190.0°
Exposure Rate	180.0 sec./°
ω oscillation Range	20.0 - 170.0°
Exposure Rate	180.0 sec./°
ω oscillation Range	39.0 - 115.0°
Exposure Rate	180.0 sec./°
ω oscillation Range	20.0 - 197.0°
Exposure Rate	180.0 sec./°
Detector Position	127.40 mm
Pixel Size	0.100 mm
$2\theta_{max}$	71.3°
No. of Reflections Measured	Total: 14604 Unique: 4177 (R_{int} = 0.035)
Corrections	Lorentz-polarization Absorption (trans. factors: 0.199 - 0.503) Secondary Extinction (coefficient: 1.90350e+001)

C. Structure Solution and Refinement

Structure Solution	Direct Methods (SHELX97)
Refinement	Full-matrix least-squares on F
Function Minimized	$\Sigma\ w\ (|Fo| - |Fc|)^2$
Least Squares Weights parameters	Chebychev polynomial with 3
	6.8770,0.4106,5.4337,
$2\theta_{max}$ cutoff	53.0^o
Anomalous Dispersion	All non-hydrogen atoms
No. Observations (I>3.00σ(I))	2018
No. Variables	146
Reflection/Parameter Ratio	13.82
Residuals: R (I>3.00σ(I))	0.0254
Residuals: Rw (I>3.00σ(I))	0.0315
Goodness of Fit Indicator	1.052
Max Shift/Error in Final Cycle	0.000
Maximum peak in Final Diff. Map	0.31 e$^-$/Å^3
Minimum peak in Final Diff. Map	-0.47 e$^-$/Å^3

Table 1. Atomic coordinates and B_{iso}/B_{eq}

atom	x	y	z	B_{eq}
Br1	0.13192(3)	0.73041(2)	1.06826(2)	4.217(5)
O1	0.2702(2)	0.3981(2)	1.22439(16)	4.95(3)
O2	0.4743(2)	0.06328(16)	0.82557(15)	3.95(2)
N1	0.3744(2)	0.23426(18)	1.02218(16)	3.24(2)
N2	0.3486(2)	0.33486(18)	0.78833(16)	3.16(2)
C1	0.2932(2)	0.3855(2)	1.09245(19)	3.26(3)
C2	0.2436(2)	0.5179(2)	0.9900(2)	3.18(3)
C3	0.2711(2)	0.4900(2)	0.84592(19)	3.24(3)
C4	0.4041(2)	0.2018(2)	0.87582(18)	3.05(3)
C5	0.3613(2)	0.3069(2)	0.63239(19)	3.41(3)
C6	0.5792(2)	0.2512(2)	0.53496(18)	3.17(3)
C7	0.7272(3)	0.3020(2)	0.5592(2)	4.00(4)
C8	0.9264(3)	0.2466(3)	0.4643(2)	5.17(5)
C9	0.9738(4)	0.1425(3)	0.3467(2)	5.71(5)
C10	0.8239(4)	0.0961(2)	0.3214(2)	5.33(5)
C11	0.6279(3)	0.1493(2)	0.4147(2)	4.15(4)

$B_{eq} = 8/3 \ \pi^2(U_{11}(aa^*)^2 + U_{22}(bb^*)^2 + U_{33}(cc^*)^2 + 2U_{12}(aa^*bb^*)\cos \gamma + 2U_{13}(aa^*cc^*)\cos \beta + 2U_{23}(bb^*cc^*)\cos \alpha)$

Table 2. Atomic coordinates and B_{iso} involving hydrogens/B_{eq}

atom	x	y	z	B_{eq}
H1	0.4198	0.1553	1.0847	3.88
H2	0.2362	0.5796	0.7822	3.77
H3	0.2788	0.4054	0.5949	4.07
H4	0.3074	0.2261	0.6286	4.06
H5	0.6937	0.3740	0.6395	4.89
H6	1.0291	0.2803	0.4806	6.20
H7	1.1097	0.1032	0.2835	5.76
H8	0.8558	0.0268	0.2392	5.65
H9	0.5253	0.1163	0.3969	4.92

$B_{eq} = 8/3 \ \pi^2(U_{11}(aa^*)^2 + U_{22}(bb^*)^2 + U_{33}(cc^*)^2 + 2U_{12}(aa^*bb^*)\cos \gamma + 2U_{13}(aa^*cc^*)\cos \beta + 2U_{23}(bb^*cc^*)\cos \alpha)$

Table 3. Anisotropic displacement parameters

atom	U_{11}	U_{22}	U_{33}	U_{12}	U_{13}	U_{23}
Br1	0.05559(14)	0.03821(13)	0.05905(14)	-0.01173(9)	-0.00738(9)	-0.01238(8)
O1	0.0931(11)	0.0549(8)	0.0383(6)	-0.0281(8)	-0.0123(7)	-0.0031(5)
O2	0.0696(8)	0.0331(6)	0.0428(6)	-0.0141(5)	-0.0149(5)	0.0003(5)
N1	0.0491(7)	0.0359(7)	0.0365(6)	-0.0153(6)	-0.0099(5)	0.0033(5)
N2	0.0472(7)	0.0338(7)	0.0350(6)	-0.0116(5)	-0.0093(5)	0.0009(5)
C1	0.0452(8)	0.0413(8)	0.0367(7)	-0.0179(7)	-0.0054(6)	-0.0030(6)
C2	0.0364(7)	0.0348(8)	0.0456(8)	-0.0120(6)	-0.0041(6)	-0.0050(6)
C3	0.0411(8)	0.0336(8)	0.0434(8)	-0.0109(6)	-0.0075(6)	0.0019(6)
C4	0.0431(8)	0.0338(8)	0.0366(7)	-0.0132(6)	-0.0085(6)	0.0011(6)
C5	0.0522(9)	0.0392(8)	0.0370(8)	-0.0139(7)	-0.0150(6)	0.0015(6)
C6	0.0521(8)	0.0329(7)	0.0329(7)	-0.0127(6)	-0.0131(6)	0.0048(6)
C7	0.0601(10)	0.0549(10)	0.0403(8)	-0.0228(9)	-0.0181(7)	0.0074(7)
C8	0.0549(11)	0.0780(15)	0.0630(12)	-0.0259(10)	-0.0203(10)	0.0254(11)
C9	0.0610(12)	0.0581(13)	0.0616(13)	-0.0010(10)	0.0060(10)	0.0174(10)
C10	0.0850(16)	0.0435(10)	0.0497(11)	-0.0126(10)	0.0070(10)	-0.0039(8)
C11	0.0743(12)	0.0398(9)	0.0410(8)	-0.0209(8)	-0.0107(8)	-0.0008(7)

The general temperature factor expression: $\exp(-2\pi^2(a*^2U_{11}h^2 + b*^2U_{22}k^2 + c*^2U_{33}l^2 + 2a*b*U_{12}hk + 2a*c*U_{13}hl + 2b*c*U_{23}kl))$

Table 4. Bond lengths (Å)

atom	atom	distance	atom	atom	distance
Br(1)	C(2)	1.8796(17)	O(1)	C(1)	1.211(2)
O(2)	C(4)	1.223(2)	N(1)	C(1)	1.392(2)
N(1)	C(4)	1.368(2)	N(2)	C(3)	1.376(2)
N(2)	C(4)	1.374(2)	N(2)	C(5)	1.474(2)
C(1)	C(2)	1.453(2)	C(2)	C(3)	1.341(2)
C(5)	C(6)	1.510(2)	C(6)	C(7)	1.384(3)
C(6)	C(11)	1.391(2)	C(7)	C(8)	1.400(2)
C(8)	C(9)	1.386(4)	C(9)	C(10)	1.377(4)
C(10)	C(11)	1.378(3)			

Table 5. Bond lengths involving hydrogens (Å)

atom	atom	distance	atom	atom	distance
N(1)	H(1)	0.894	C(3)	H(2)	0.950
C(5)	H(3)	0.950	C(5)	H(4)	0.951
C(7)	H(5)	0.950	C(8)	H(6)	0.950
C(9)	H(7)	0.950	C(10)	H(8)	0.950
C(11)	H(9)	0.951			

Table 6. Bond angles (º)

atom	atom	atom	angle	atom	atom	atom	angle
C(1)	N(1)	C(4)	127.70(14)	C(3)	N(2)	C(4)	121.30(15)
C(3)	N(2)	C(5)	120.68(14)	C(4)	N(2)	C(5)	117.90(15)
O(1)	C(1)	N(1)	121.33(16)	O(1)	C(1)	C(2)	126.46(17)
N(1)	C(1)	C(2)	112.20(15)	Br(1)	C(2)	C(1)	117.32(13)
Br(1)	C(2)	C(3)	121.15(13)	C(1)	C(2)	C(3)	121.51(16)
N(2)	C(3)	C(2)	121.50(15)	O(2)	C(4)	N(1)	122.41(15)
O(2)	C(4)	N(2)	121.83(16)	N(1)	C(4)	N(2)	115.75(14)
N(2)	C(5)	C(6)	113.70(17)	C(5)	C(6)	C(7)	122.26(16)
C(5)	C(6)	C(11)	117.9(2)	C(7)	C(6)	C(11)	119.83(17)
C(6)	C(7)	C(8)	119.5(2)	C(7)	C(8)	C(9)	120.0(2)
C(8)	C(9)	C(10)	120.0(2)	C(9)	C(10)	C(11)	120.3(2)
C(6)	C(11)	C(10)	120.3(2)				

Table 7. Bond angles involving hydrogens (º)

atom	atom	atom	angle	atom	atom	atom	angle
C(1)	N(1)	H(1)	110.5	C(4)	N(1)	H(1)	121.5
N(2)	C(3)	H(2)	119.3	C(2)	C(3)	H(2)	119.2
N(2)	C(5)	H(3)	108.4	N(2)	C(5)	H(4)	108.3
C(6)	C(5)	H(3)	108.5	C(6)	C(5)	H(4)	108.4
H(3)	C(5)	H(4)	109.4	C(6)	C(7)	H(5)	120.2
C(8)	C(7)	H(5)	120.3	C(7)	C(8)	H(6)	120.0
C(9)	C(8)	H(6)	120.0	C(8)	C(9)	H(7)	120.0
C(10)	C(9)	H(7)	120.0	C(9)	C(10)	H(8)	119.8
C(11)	C(10)	H(8)	119.9	C(6)	C(11)	H(9)	119.8
C(10)	C(11)	H(9)	119.9				

Table 8. Torsion Angles(º)

atom1	atom2	atom3	atom4	angle	atom1	atom2	atom3	atom4	angle
C(1)	N(1)	C(4)	O(2)	-178.9(2)	C(1)	N(1)	C(4)	N(2)	0.7(3)
C(4)	N(1)	C(1)	O(1)	178.2(2)	C(4)	N(1)	C(1)	C(2)	-1.8(2)
C(3)	N(2)	C(4)	O(2)	-179.54(19)	C(3)	N(2)	C(4)	N(1)	0.9(2)
C(4)	N(2)	C(3)	C(2)	-1.0(2)	C(3)	N(2)	C(5)	C(6)	106.16(19)
C(5)	N(2)	C(3)	C(2)	174.87(18)	C(4)	N(2)	C(5)	C(6)	-77.8(2)
C(5)	N(2)	C(4)	O(2)	4.5(2)	C(5)	N(2)	C(4)	N(1)	-175.11(17)
O(1)	C(1)	C(2)	Br(1)	-0.1(2)	O(1)	C(1)	C(2)	C(3)	-178.4(2)
N(1)	C(1)	C(2)	Br(1)	179.93(13)	N(1)	C(1)	C(2)	C(3)	1.6(2)
Br(1)	C(2)	C(3)	N(2)	-178.59(14)	C(1)	C(2)	C(3)	N(2)	-0.4(3)
N(2)	C(5)	C(6)	C(7)	-32.9(2)	N(2)	C(5)	C(6)	C(11)	149.04(16)
C(5)	C(6)	C(7)	C(8)	-179.69(18)	C(5)	C(6)	C(11)	C(10)	179.41(17)
C(7)	C(6)	C(11)	C(10)	1.3(2)	C(11)	C(6)	C(7)	C(8)	-1.7(2)
C(6)	C(7)	C(8)	C(9)	0.4(3)	C(7)	C(8)	C(9)	C(10)	1.3(3)
C(8)	C(9)	C(10)	C(11)	-1.7(3)	C(9)	C(10)	C(11)	C(6)	0.4(3)

The sign is positive if when looking from atom 2 to atom 3 a clock-wise motion of atom 1 would superimpose it on atom 4.

Table 9. Distances beyond the asymmetric unit out to 3.60 Å

atom	atom	distance	atom	atom	distance
Br(1)	O(1)	3.1144(15)	Br(1)	N(1)[1)]	3.5752(18)
Br(1)	C(1)	2.8550(18)	Br(1)	C(3)	2.8171(17)
Br(1)	C(4)[2)]	3.5757(19)	O(1)	Br(1)	3.1144(15)
O(1)	N(1)	2.271(2)	O(1)	C(2)	2.381(2)
O(1)	C(3)	3.569(2)	O(1)	C(4)	3.557(2)
O(1)	C(7)[1)]	3.498(3)	O(1)	C(8)[3)]	3.504(3)
O(1)	C(11)[4)]	3.471(2)	O(2)	O(2)[5)]	3.431(2)
O(2)	N(1)	2.272(2)	O(2)	N(1)[5)]	2.8685(19)
O(2)	N(2)	2.2707(19)	O(2)	C(1)	3.580(2)
O(2)	C(3)	3.518(2)	O(2)	C(4)[5)]	3.573(2)
O(2)	C(5)	2.723(2)	O(2)	C(6)	3.158(2)
O(2)	C(10)[6)]	3.574(3)	O(2)	C(11)[6)]	3.443(3)
N(1)	Br(1)[1)]	3.5752(18)	N(1)	O(1)	2.271(2)
N(1)	O(2)	2.272(2)	N(1)	O(2)[5)]	2.8685(19)
N(1)	N(2)	2.322(2)	N(1)	C(2)	2.361(2)
N(1)	C(3)	2.684(2)	N(2)	O(2)	2.2707(19)
N(2)	N(1)	2.322(2)	N(2)	C(1)	2.820(2)
N(2)	C(2)	2.370(2)	N(2)	C(6)	2.498(2)
N(2)	C(7)	2.934(2)	C(1)	Br(1)	2.8550(18)
C(1)	O(2)	3.580(2)	C(1)	N(2)	2.820(2)
C(1)	C(3)	2.438(2)	C(1)	C(4)	2.478(2)
C(2)	O(1)	2.381(2)	C(2)	N(1)	2.361(2)
C(2)	N(2)	2.370(2)	C(2)	C(4)	2.790(2)
C(3)	Br(1)	2.8171(17)	C(3)	O(1)	3.569(2)
C(3)	O(2)	3.518(2)	C(3)	N(1)	2.684(2)
C(3)	C(1)	2.438(2)	C(3)	C(4)	2.397(2)
C(3)	C(5)	2.477(2)	C(3)	C(6)	3.459(2)
C(3)	C(7)	3.571(2)	C(4)	Br(1)[2)]	3.5757(19)
C(4)	O(1)	3.557(2)	C(4)	O(2)[5)]	3.573(2)
C(4)	C(1)	2.478(2)	C(4)	C(2)	2.790(2)
C(4)	C(3)	2.397(2)	C(4)	C(5)	2.440(2)
C(4)	C(6)	3.177(2)	C(4)	C(7)	3.557(2)
C(5)	O(2)	2.723(2)	C(5)	C(3)	2.477(2)
C(5)	C(4)	2.440(2)	C(5)	C(7)	2.535(3)
C(5)	C(11)	2.486(2)	C(6)	O(2)	3.158(2)
C(6)	N(2)	2.498(2)	C(6)	C(3)	3.459(2)
C(6)	C(4)	3.177(2)	C(6)	C(8)	2.405(3)
C(6)	C(9)	2.775(2)	C(6)	C(10)	2.402(2)
C(7)	O(1)[1)]	3.498(3)	C(7)	N(2)	2.934(2)
C(7)	C(3)	3.571(2)	C(7)	C(4)	3.557(2)
C(7)	C(5)	2.535(3)	C(7)	C(9)	2.413(2)
C(7)	C(10)	2.775(3)	C(7)	C(11)	2.401(3)
C(8)	O(1)[7)]	3.504(3)	C(8)	C(6)	2.405(3)
C(8)	C(10)	2.393(4)	C(8)	C(11)	2.765(4)
C(9)	C(6)	2.775(2)	C(9)	C(7)	2.413(2)
C(9)	C(11)	2.389(3)	C(10)	O(2)[6)]	3.574(3)
C(10)	C(6)	2.402(2)	C(10)	C(7)	2.775(3)
C(10)	C(8)	2.393(4)	C(11)	O(1)[8)]	3.471(2)
C(11)	O(2)[6)]	3.443(3)	C(11)	C(5)	2.486(2)
C(11)	C(7)	2.401(3)	C(11)	C(8)	2.765(4)
C(11)	C(9)	2.389(3)			

Symmetry Operators:

(1) -X+1,-Y+1,-Z+2   (2) -X,-Y+1,-Z+2
(3) X-1,Y,Z+1   (4) X,Y,Z+1
(5) -X+1,-Y,-Z+2   (6) -X+1,-Y,-Z+1
(7) X+1,Y,Z-1   (8) X,Y,Z-1

Table 10. Distances beyond the asymmetric unit out to 3.60 Å involving hydrogens

atom	atom	distance	atom	atom	distance
Br(1)	H(2)	2.884	Br(1)	H(4)[1]	3.583
Br(1)	H(5)[2]	3.221	Br(1)	H(8)[3]	2.916
Br(1)	H(8)[4]	3.464	O(1)	H(1)	2.347
O(1)	H(2)[1]	3.597	O(1)	H(3)[5]	3.491
O(1)	H(5)[2]	2.617	O(1)	H(6)[6]	2.958
O(1)	H(7)[6]	3.226	O(1)	H(9)[5]	3.100
O(2)	H(1)	2.509	O(2)	H(1)[7]	2.003
O(2)	H(4)	2.512	O(2)	H(7)[8]	2.733
O(2)	H(8)[9]	3.001	O(2)	H(9)[9]	2.730
N(1)	H(1)[7]	3.335	N(1)	H(7)[6]	3.141
N(2)	H(1)	3.146	N(2)	H(2)	2.019
N(2)	H(3)	1.991	N(2)	H(4)	1.990
N(2)	H(5)	2.660	C(1)	H(1)	1.900
C(1)	H(2)	3.294	C(1)	H(2)[1]	3.590
C(1)	H(5)[2]	3.476	C(1)	H(7)[6]	3.459
C(2)	H(1)	3.135	C(2)	H(2)	1.986
C(3)	H(1)	3.571	C(3)	H(3)	2.506
C(3)	H(4)	3.131	C(3)	H(5)	2.991
C(4)	H(1)	1.988	C(4)	H(1)[7]	2.974
C(4)	H(2)	3.246	C(4)	H(3)	3.195
C(4)	H(4)	2.553	C(4)	H(5)	3.346
C(4)	H(7)[8]	3.537	C(5)	H(2)	2.631
C(5)	H(5)	2.707	C(5)	H(6)[10]	3.173
C(5)	H(9)	2.620	C(5)	H(9)[9]	3.566
C(6)	H(2)	3.552	C(6)	H(2)[4]	3.416
C(6)	H(3)	2.023	C(6)	H(4)	2.022
C(6)	H(5)	2.035	C(6)	H(6)	3.263
C(6)	H(8)	3.259	C(6)	H(9)	2.038
C(7)	H(2)[4]	3.260	C(7)	H(3)	2.933
C(7)	H(3)[4]	2.873	C(7)	H(4)	3.251
C(7)	H(6)	2.048	C(7)	H(7)	3.272
C(7)	H(9)	3.258	C(8)	H(2)[4]	2.916
C(8)	H(3)[4]	2.958	C(8)	H(4)[11]	3.420
C(8)	H(5)	2.051	C(8)	H(7)	2.035
C(8)	H(8)	3.250	C(9)	H(1)[12]	3.543
C(9)	H(2)[4]	2.730	C(9)	H(5)	3.272
C(9)	H(6)	2.035	C(9)	H(8)	2.025
C(9)	H(9)	3.246	C(10)	H(2)[4]	2.885
C(10)	H(4)[9]	3.330	C(10)	H(6)	3.250
C(10)	H(7)	2.026	C(10)	H(9)	2.027
C(11)	H(2)[4]	3.228	C(11)	H(3)	2.897
C(11)	H(4)	2.536	C(11)	H(4)[9]	3.250

Table 10. Distances beyond the asymmetric unit out to 3.60 Å involving hydrogens (continued)

atom	atom	distance	atom	atom	distance
C(11)	H(5)	3.261	C(11)	H(7)	3.246
C(11)	H(8)	2.027	C(11)	H(9)[9]	3.213
H(1)	O(1)	2.347	H(1)	O(2)	2.509
H(1)	O(2)[7]	2.003	H(1)	N(1)[7]	3.335
H(1)	N(2)	3.146	H(1)	C(1)	1.900
H(1)	C(2)	3.135	H(1)	C(3)	3.571
H(1)	C(4)	1.988	H(1)	C(4)[7]	2.974
H(1)	C(9)[6]	3.543	H(1)	H(1)[7]	2.973
H(1)	H(7)[6]	2.685	H(1)	H(8)[5]	3.546
H(1)	H(9)[5]	3.165	H(2)	Br(1)	2.884
H(2)	O(1)[1]	3.597	H(2)	N(2)	2.019
H(2)	C(1)	3.294	H(2)	C(1)[1]	3.590
H(2)	C(2)	1.986	H(2)	C(4)	3.246
H(2)	C(5)	2.631	H(2)	C(6)	3.552
H(2)	C(6)[4]	3.416	H(2)	C(7)[4]	3.260
H(2)	C(8)[4]	2.916	H(2)	C(9)[4]	2.730
H(2)	C(10)[4]	2.885	H(2)	C(11)[4]	3.228
H(2)	H(3)	2.321	H(2)	H(4)	3.379
H(2)	H(5)	3.079	H(2)	H(6)[4]	3.368
H(2)	H(7)[4]	3.108	H(2)	H(8)[4]	3.318
H(3)	O(1)[13]	3.491	H(3)	N(2)	1.991
H(3)	C(3)	2.506	H(3)	C(4)	3.195
H(3)	C(6)	2.023	H(3)	C(7)	2.933
H(3)	C(7)[4]	2.873	H(3)	C(8)[4]	2.958
H(3)	C(11)	2.897	H(3)	H(2)	2.321
H(3)	H(4)	1.551	H(3)	H(5)	3.031
H(3)	H(5)[4]	2.849	H(3)	H(6)[10]	2.897
H(3)	H(6)[4]	2.995	H(3)	H(9)	2.965
H(4)	Br(1)[1]	3.583	H(4)	O(2)	2.512
H(4)	N(2)	1.990	H(4)	C(3)	3.131
H(4)	C(4)	2.553	H(4)	C(6)	2.022
H(4)	C(7)	3.251	H(4)	C(8)[10]	3.420
H(4)	C(10)[9]	3.330	H(4)	C(11)	2.536
H(4)	C(11)[9]	3.250	H(4)	H(2)	3.379
H(4)	H(3)	1.551	H(4)	H(5)	3.544
H(4)	H(6)[10]	2.599	H(4)	H(8)[9]	2.982
H(4)	H(9)	2.351	H(4)	H(9)[9]	2.827
H(5)	Br(1)[2]	3.221	H(5)	O(1)[2]	2.617
H(5)	N(2)	2.660	H(5)	C(1)[2]	3.476
H(5)	C(3)	2.991	H(5)	C(4)	3.346
H(5)	C(5)	2.707	H(5)	C(6)	2.035
H(5)	C(8)	2.051	H(5)	C(9)	3.272
H(5)	C(11)	3.261	H(5)	H(2)	3.079
H(5)	H(3)	3.031	H(5)	H(3)[4]	2.849
H(5)	H(4)	3.544	H(5)	H(6)	2.355
H(6)	O(1)[12]	2.958	H(6)	C(5)[11]	3.173
H(6)	C(6)	3.263	H(6)	C(7)	2.048
H(6)	C(9)	2.035	H(6)	C(10)	3.250
H(6)	H(2)[4]	3.368	H(6)	H(3)[11]	2.897
H(6)	H(3)[4]	2.995	H(6)	H(4)[11]	2.599
H(6)	H(5)	2.355	H(6)	H(7)	2.336

Table 10. Distances beyond the asymmetric unit out to 3.60 Å involving hydrogens (continued)

atom	atom	distance	atom	atom	distance
H(6)	H(9)[11]	3.201	H(7)	O(1)[12]	3.226
H(7)	O(2)[8]	2.733	H(7)	N(1)[12]	3.141
H(7)	C(1)[12]	3.459	H(7)	C(4)[8]	3.537
H(7)	C(7)	3.272	H(7)	C(8)	2.035
H(7)	C(10)	2.026	H(7)	C(11)	3.246
H(7)	H(1)[12]	2.685	H(7)	H(2)[4]	3.108
H(7)	H(6)	2.336	H(7)	H(8)	2.324
H(7)	H(9)[11]	3.474	H(8)	Br(1)[14]	2.916
H(8)	Br(1)[4]	3.464	H(8)	O(2)[9]	3.001
H(8)	C(6)	3.259	H(8)	C(8)	3.250
H(8)	C(9)	2.025	H(8)	C(11)	2.027
H(8)	H(1)[13]	3.546	H(8)	H(2)[4]	3.318
H(8)	H(4)[9]	2.982	H(8)	H(7)	2.324
H(8)	H(9)	2.325	H(9)	O(1)[13]	3.100
H(9)	O(2)[9]	2.730	H(9)	C(5)	2.620
H(9)	C(5)[9]	3.566	H(9)	C(6)	2.038
H(9)	C(7)	3.258	H(9)	C(9)	3.246
H(9)	C(10)	2.027	H(9)	C(11)[9]	3.213
H(9)	H(1)[13]	3.165	H(9)	H(3)	2.965
H(9)	H(4)	2.351	H(9)	H(4)[9]	2.827
H(9)	H(6)[10]	3.201	H(9)	H(7)[10]	3.474
H(9)	H(8)	2.325	H(9)	H(9)[9]	2.785

Symmetry Operators:

(1) -X,-Y+1,-Z+2
(2) -X+1,-Y+1,-Z+2
(3) X-1,Y+1,Z+1
(4) -X+1,-Y+1,-Z+1
(5) X,Y,Z+1
(6) X-1,Y,Z+1
(7) -X+1,-Y,-Z+2
(8) -X+2,-Y,-Z+1
(9) -X+1,-Y,-Z+1
(10) X-1,Y,Z
(11) X+1,Y,Z
(12) X+1,Y,Z-1
(13) X,Y,Z-1
(14) X+1,Y-1,Z-1